5-2016

The effects of ball interactions on the dynamic behavior of a ball balancer rotating at speeds above the translational resonant frequency of the system.

Gregory A. Dedow
University of Louisville

THE EFFECTS OF BALL INTERACTIONS ON THE DYNAMIC BEHAVIOR OF A BALL BALANCER ROTATING AT SPEEDS ABOVE THE TRANSLATIONAL RESONANT FREQUENCY OF THE SYSTEM

By

Gregory A. Dedow
B.S. Mechanical Engineering, University of Michigan, 2012

A Thesis
Submitted to the Faculty of the
University of Louisville
J.B. Speed School of Engineering
as Partial Fulfillment of the Requirements
for the Professional Degree

Master of Science in Mechanical Engineering

Department of Mechanical Engineering
University of Louisville
Louisville, KY

May 2016

THE EFFECTS OF BALL INTERACTIONS ON THE DYNAMIC BEHAVIOR OF A BALL BALANCER ROTATING AT SPEEDS ABOVE THE TRANSLATIONAL RESONANT FREQUENCY OF THE SYSTEM

By

Gregory A. Dedow
B.S. Mechanical Engineering, University of Michigan, 2012

A Thesis Approved On

April 11, 2016

by the following Thesis Committee:

Thesis Director
Dr. Kevin Murphy

Dr. Bruce Alphenaar

Dr. Christopher Richards

ACKNOWLEDGMENTS

I would like to thank Dr. Bruce Alphenaar, Dr. Kevin Murphy and Dr. Chris Richards for their support in reviewing this thesis material. I would like to especially thank Dr. Kevin Murphy for being my thesis advisor and helping tremendously in the development of this numerical model.

I would also like to thank Paul Davis and Quentin Pollett for being great consulting resources regarding the fundamentals of rotor-dynamics and ball balancer applications.

I would like to thank Tim Oconnell for his support in deciding to complete the challenging task of a Master's Thesis.

Lastly, I would like to thank Leanne Gali and my family Claire, Lauren and Mark Dedow for supporting me in everything I do.

ABSTRACT

THE EFFECTS OF BALL INTERACTIONS ON THE DYNAMIC BEHAVIOR OF A BALL BALANCER ROTATING AT SPEEDS ABOVE THE TRANSLATIONAL RESONANT FREQUENCY OF THE SYSTEM

Gregory A. Dedow

April 11, 2016

Many applications are inherently rotational in nature. These applications range from industrial products to consumer products. As seen in a traditional frequency response plot, the motion of a rotating imbalance does not approach zero as the forcing frequency is increased. Unlike a traditional forced mass spring oscillator, the motion of the rotating imbalance approaches some non-zero value. To account for this residual motion, some systems utilize a balancing device to reduce this motion. These balancing devices can be passive or active, depending on the design considerations. This paper will focus on the traditional, passive ball-type balancer due to its simplicity and extensive use in application. This paper derives the equations of motion for a vertically oriented ball-type balancing system. Due to the high non-linearity of these equations, a fourth order Runge-Kutta numerical integration method is used. The ball balancer equations of motion contain the proper physics needed for full operation such that the ball balancer can translate horizontally, vertically and rotate angularly in the presence of gravity. Acceleration terms are included such that a wide range of operating conditions can be tested. Additionally, n number of balls are present, which are affected by rolling friction and viscous fluid drag.

Unlike many numerical models published in the past, the ball-to-ball interactions are not neglected within this model. These interactions include collisions, and train formations and separations. An application of the method presented by (Henon 1982) is utilized where the equations of motion are altered such that an exact integration step can be solved. This is based on the need for a displacement step (collision) or a force step (separation).

Although the model presented can accommodate n number of balls, only a maximum ball count of two is considered. It is shown how the behavior of the balls affect the motion response of the ball balancer at rotational velocities above the translational resonance of the system. It is seen that a critical transition is reached; the operating point at which the ball balancer becomes effective at offsetting an eccentric mass. It is also seen that ball balancer displacement decreases until a point of saturation, after which ball balancer displacement increases. Also for the two

ball case, it is shown that the spatial characteristics of the balls do affect steady state motion. The angle that separates two contacting balls alters the center of gravity of the train of balls such that the balancing capacity of the system is reduced. Although this effect is shown to be small for a two ball case, the balancing capacity is further reduced as the angle between two contacting balls becomes larger.

TABLE OF CONTENTS

PAGE

APPROVAL PAGE ii

ACKNOWLEDGMENTS iii

ABSTRACT iv

LIST OF FIGURES x

I. BACKGROUND OF PROBLEM 1

A. Problem Overview 1

B. Literature Overview 2

C. Explanation of Novelty of Ball Balancer Model 6

II. REVIEW OF KINEMATIC MOTION 9

A. Introduction 9

B. The Mass Spring Oscillator 9

C. Free Motion of the Mass Spring Oscillator System 12

1. Critically Damped Motion 12

2. Over Damped Motion 13

3. Under Damped Motion 14

D. Forced Motion of the Mass Spring Oscillator System 16

1. External Forcing Frequency Equals Natural Frequency 17

2. External Forcing Frequency Greater Than Natural Frequency 18

E. Extension to a Rotating Imbalance System 19

1. Imbalance Rotates at Frequency Equal to Natural Frequency 21

2. Imbalance Rotates at Frequency Greater Than Natural Frequency 22

III. COLLISION AND SEPARATION CAPTURE TECHNIQUE 24

A. Introduction 24

B. Poincaré Mapping 24

C. State Variable Transformation 26

D. Collision Capture Technique 26

E. Separation Capture Technique 27

IV. COLLISION CAPTURE VALIDATION 29

A. Introduction 29

B. Explanation of Collision Technique 29

1. Collision With a Stationary Wall 30

2. Collision Between Two Masses 32

V. SEPARATION CAPTURE VALIDATION 36

A. Introduction 36

B. Explanation of Separation Technique 36

1. Two Masses with the Same Initial Conditions 37

2. Two Masses Develop a Grazing Condition 39

VI. EQUATIONS OF MOTION OF THE BALL BALANCER MODEL 42

A. Introduction 42

B. Simplified Reference Frames 42

C. Velocity of Points O', P_1 and P_j 44

D. Kinetic Energy Terms 46

E. Potential Energy Terms 47

F. Non-Conservative Forces 48

G. Lagrangian Energy Approach 48

H. Final Equations of Motion - Second Order 49

1. Ball Balancer Motion in the Horizontal Direction 49

2. Ball Balancer Motion in the Vertical Direction 50

3. Angular Motion of Ball 1 and jth Ball 50

I. Train Equation Derivation 51

J. Final Equations of Motion - Third Order 54

1. Ball Balancer Motion in the Horizontal Direction 55

2. Ball Balancer Motion in the Vertical Direction 55

3. Angular Motion of Ball 1 and jth Ball 56

VII. VELOCITY TRANSFORMATION AFTER A COLLISION 57

A. Introduction 57

B. Velocity Transformation 57

1. Impulses Acting on the Balls 58

2. Impulses Acting on the Ball Balancer 60

3. Coefficient of Restitution 61
4. Impulses Due to Additional Balls in Colliding Train 62
5. Impulses Due to Additional Balls Not in Colliding Train 63
6. Impulses Due to External Forces On the Ball Balancer 63
7. Angular Impulses due to Rolling Friction Acting on Balls 64
8. Angular Impulses due to Rolling Friction Acting on the Ball Balancer . . 64
9. Impulses Due to Interaction Forces Between Balls in a Train 65
C. Final Conservation of Momentum Analysis 65
D. Discussion on Collisions Between Trains 65

VIII. BALL BALANCER MODEL VALIDATION 69
A. Introduction 69
B. One Degree of Freedom Systems 69
1. Ball Balancer Motion 69
2. Ball Motion 71
3. Ball Balancer Center of Gravity Rotational Motion 73
C. Collisions and Separations 75
1. Two Balls Colliding 76
2. Two Balls Separating 78
3. Ten Balls Colliding 80

IX. STEADY STATE ANALYSIS 84
A. Introduction 84
B. Steady State Bifurcation 84
1. Zone One - $\dot{\phi} < 0.34\omega_n$ 85
2. Zone Two - $0.34\omega_n \leq \dot{\phi} < 0.75\omega_n$ 86
3. Zone Three - $0.75\omega_n \leq \dot{\phi} < 1.11\omega_n$ 87
4. Zone Four - $\dot{\phi} \geq 1.11\omega_n$ 88
C. Ball Balancer Maximum Motion Analysis 90
1. Effect of Eccentric Mass on Ball Balancer Motion with PM Assumption . 90
2. Effect of Eccentric Mass on Ball Balancer Motion with FR Assumption . 96
3. Effect of Eccentric Mass on Ball Balancer Motion with Different Ball Radii 98

X. CONCLUSIONS 100

XI. RECOMMENDATIONS 102

REFERENCES 103

APPENDIX - NOMENCLATURE 105

CURRICULUM VITA 114

LIST OF FIGURES

FIGURE		PAGE
1	A Time Error is Introduced by Neglecting the Physical Nature of the Balls	7
2	A Free Body Diagram of a Mass Spring Oscillator	10
3	The Displacement (a) and Velocity (b) of a Critically Damped Mass Spring System	13
4	The Displacement (a) and Velocity (b) of an Over Damped Mass Spring System	14
5	The Displacement (a) and Velocity (b) of an Under Damped Mass Spring System	16
6	The Displacement Response (a) and Phase Angle (b) of a Mass Spring System	17
7	The Displacement (a) and Velocity (b) of a Forced, Under Damped Mass Spring System at the Natural Frequency	18
8	The Displacement (a) and Velocity (b) of a Forced, Under Damped Mass Spring System at Five Times the Natural Frequency	19
9	A Free Body Diagram of a Horizontally Oriented Rotating Imbalance	19
10	The Displacement Response (a) and Phase Angle (b) of a Rotating Imbalance System	21
11	The Displacement (a) and Velocity (b) of a Rotating Imbalance System at the Natural Frequency	22
12	The Displacement (a) and Velocity (b) of a Rotating Imbalance System at Five Times the Natural Frequency	23
13	Schematic of a Poincaré Section Taken at Some Location in the $\tilde{z}$ Direction	25
14	Schematic of a Contacting Two Mass System	27
15	Schematic of a Mass Colliding with a Stationary Wall	29
16	When a Collision is Detected, the Solver Takes a Time Step Backwards, then a Displacement Step to the Point of Collision	31
17	The Displacement (a) and Velocity (b) of the Mass Colliding with a Stationary Wall	31
18	A Zoomed In View of the Displacement of the Mass Colliding with a Stationary Wall	32
19	Schematic of a Two Mass Collision	33
20	The Displacement (a) and Velocity (b) of the Two Masses Colliding	34
21	A Zoomed In View of the Displacement of the Two Masses Colliding	34
22	Schematic of Two Masses Separating	37

23 The Displacement (a), Velocity (b) and Interaction Force (c) for the Two Masses in the Same Initial Conditions Case. The Solid Line Denotes Mass One and the Dotted Line Denotes Mass Two. The Thick Line in (a) and (b) Denotes the Region where the Masses are Touching 38
24 A Zoomed In View of the Interaction Force Between the Two Masses when the Separation Occurs 39
25 The Displacement (a), Velocity (b) and Interaction Force (c) for the Two Masses in the Grazing Condition Case. The Solid Line Denotes Mass One and the Dotted Line Denotes Mass Two. The Thick Line in (a) and (b) Denotes the Region where the Masses are Touching 40
26 A Zoomed In View of the Interaction Force Between the Two Masses when the Separation Occurs 41
27 Schematic (a) and Schematic (b) Show the Reference Frames Used to Simplify the Ball Balancer Model 44
28 A Free Body Diagram of a Train of Three Balls 52
29 The Collision Angle is a Function of the Ball Radius and the Ball Balancer Radius . 52
30 The Velocities of the Balls Before the Collision are Purely Angular (a). The Velocities of the Balls After the Collision are both Angular and Radial (b) 57
31 The Velocities for Each Ball Must be Rewritten in the N-T Reference Frame 58
32 The Experimental Result of One Ball Colliding with a Train 66
33 The Experimental Result of Two Balls Colliding with a Train 67
34 The Momentum of Each Colliding Ball Propagates Through the Train of Balls . . . 68
35 The Displacement (a), Velocity (b) and Acceleration (c) of the Ball Balancer Model and the Traditional Horizontal Mass Spring System Produce the Same Results . . . 70
36 The Displacement (a), Velocity (b) and Acceleration (c) of the Ball Balancer Model and the Traditional Vertical Mass Spring System Produce the Same Results 71
37 The Displacement (a), Velocity (b) and Acceleration (c) of the Ball Balancer Model and the Traditional Pendulum Produce the Same Results 72
38 The Displacement (a), Velocity (b) and Acceleration (c) of the Ball Balancer Model and the Traditional Horizontal Rotating Imbalance Produce the Same Results 74
39 The Displacement (a), Velocity (b) and Acceleration (c) of the Ball Balancer Model and the Traditional Vertical Rotating Imbalance Produce the Same Results 75
40 The Initial Starting Positions of the Two Balls Inside the Ball Balancer 77
41 The Total Energy in the System During the Simulation (a) and the Absolute Value of the Error in Energy During the Simulation (b) 77

42 The Displacement (a), Velocity (b) and Ball Locations (c) of the Ball Balancer Model. The Solid Line in (a) and (b) Represents the Horizontal Ball Balancer Motion, the Dashed Line Represents the Vertical Ball Balancer Motion 78
43 The Initial Starting Positions of the Two Balls Inside the Ball Balancer 79
44 The Total Energy in the System During the Simulation (a) and the Absolute Value of the Error in Energy During the Simulation (b) 79
45 The Displacement (a), Velocity (b) and Ball Location (c) of the Ball Balancer Model. The Solid Line in (a) and (b) Represents the Horizontal Ball Balancer Motion, the Dashed Line Represents the Vertical Ball Balancer Motion 80
46 The Initial Starting Positions of the Ten Balls Inside the Ball Balancer 81
47 The Total Energy in the System During the Simulation (a) and the Absolute Value of the Error in Energy During the Simulation (b) 81
48 The Displacement (a), Velocity (b) and Acceleration (c) of the Ball Balancer Model. The Solid Line Represents the Horizontal Ball Balancer Motion, the Dashed Line Represents the Vertical Ball Balancer Motion 82
49 Steady State Bifurcation Plots for the Horizontal (a) and Vertical (b) Ball Balancer Motion with 0.05 lbs of Eccentric Mass and One Ball 85
50 Horizontal Ball Balancer and Ball Motion for Ball Balancer Velocity Located in Zone One 86
51 Horizontal Ball Balancer and Ball Motion for Ball Balancer Velocity Located in Zone Two 87
52 Horizontal Ball Balancer and Ball Motion for Ball Balancer Velocity Located in Zone Three 88
53 Horizontal Ball Balancer and Ball Motion for Ball Balancer Velocity Located in Zone Four 89
54 The Maximum Horizontal Ball Balancer Motion as a Function of Eccentric Mass for Ball Balancer Rotational Velocities of $1.5\omega_n$ (a), $2.0\omega_n$ (b) and $2.5\omega_n$ (c) using the PM assumption 91
55 The One Ball Motion Before (a) and After (b) the Critical Transition is Reached with a Ball Balancer Rotational Velocity of $2.0\omega_n$ 92
56 The One Ball Motion with a Ball Balancer Rotational Velocity of $1.5\omega_n$ (a), $2.0\omega_n$ (b) and $2.5\omega_n$ (c) 93
57 The Two Ball Motion with a Ball Balancer Rotational Velocity of $1.5\omega_n$ with an Eccentric Mass Below the Critical Transition 94

58 The Two Ball Motion Before (a) and After (b) the Critical Transition is Reached with a Ball Balancer Rotational Velocity of $2.0\omega_n$ 94
59 The Two Ball Motion with a Ball Balancer Rotational Velocity of $1.5\omega_n$ (a), $2.0\omega_n$ (b) and $2.5\omega_n$ (c) 96
60 The Maximum Horizontal Ball Balancer Motion as a Function of Eccentric Mass for Ball Balancer Rotational Velocities of $1.5\omega_n$ (a), $2.0\omega_n$ (b) and $2.5\omega_n$ (c) using the FR assumption 97
61 The Angle that Separates the Balls in the Two Ball Case when the PM Assumption is Used (a) and when the FR Assumption is Used (b) with a Ball Balancer Rotational Velocity of $2.5\omega_n$ and $\frac{m_e}{m_{P_i}} = 4$ 98
62 The Maximum Ball Balancer Motion as a Function of Eccentric Mass for a Ball Balancer Rotational Velocity of $2.5\omega_n$ using the FR assumption (a). A Zoomed In View of the Maximum Ball Balance Motion for the Three Cases (b) 99

I. BACKGROUND OF PROBLEM

A. Problem Overview

From industrial applications like turbo machinery and power generation, to consumer products like washing machines, computer disc drives and tires, rotational applications are everywhere. Designing a rotational system can be somewhat difficult; the operating conditions, motion envelope and rotational forces must all be considered to ensure adequate machine life and adequate spin performance. All rotational systems have some degree of unbalance; there is no such thing as a perfectly balanced rotor, only in theory. This unbalance comes from inherent manufacturing defects or variable unbalances over the life of the system. To account for this unbalance, some systems use an additional balancing device to ensure that the effects of the unbalance are within the design limits of the system. These balancing devices range from those that are passive and involve a ring of steel balls, pendulums or even fluid, to those that are active and involve electronic control and feedback control systems (Zhou and Shi 2001). Balancing devices are needed to reduce the motion envelope of the spinning body and keep constraint forces from being higher than the structural limits of the system. From a practical perspective, passive balancers tend to be more economical since cost is much lower than active systems (Thearle 1961). In addition, passive balancers are an interesting device since no exterior control system is needed; solely the rotor-dynamics allows for balancing to be achieved. For this reason, this paper will focus on the passive mechanism for automatic balancing. This paper will derive the equations of motion that describe a passive balancing device that uses spheres as balancing masses. The spheres are suspended in a viscous fluid such that the angular motion of the balls is coupled to the rotational and translational motion of the balancer. The balls play a vital role in the behavior of the balancer. The balls are the mechanism for balancing; if one understands the ball behavior better, one understands the balancer behavior better. For this reason, unlike many models that have been published in the past, the physical size of the balls will be taken into account. This not only means accounting for the diameter of the balls, but also accounting for the interactions that the balls have with each other. This includes the collisions and train separations. This next level of modeling will allow a deeper glimpse into the behavior of a ball balancer.

B. Literature Overview

Many have completed studies and observed the behavior of ball balancers throughout the years, whether through experiments or through numerical models. All of these efforts were in hopes to establish something new about the behavior of the system interactions of the ball balancer.

Thearle was one of the first to study the practicality of an automatic balancer. He performed studies on different types of dynamic balancers that ranged from pendulum balancers to ball balancers. He found that ball balancers were much easier to use than pendulum balancers and offered a much more economical solution. As time went on, the complexity of the ball balancer model progressed to include more complicated models and deeper investigations into the behavior of a ball balancer. A single rotor ball balancer was studied significantly to begin the development process. Many studies were performed that ranged from those regarding the stability behavior of the ball balancer, transient behavior of the ball balancer and even the effect that various physical parameters had on the total ball balancer behavior. Green, Champneys and Friswell studied the transient behavior of a single ball balancer and how the system behavior was affected by the system eigenvalues (Green, Champneys, and Friswell 2006). Rajalingham and Bhat studied the response of a ball balancer system that incorporated a residual imbalance located on the end of a flexible shaft (Rajalingham and Bhat 2006). It was found that the system was very non-linear and stabilized to either a steady-state configuration or settled down to a limit-cycle vibration depending on the parameters of the test. Green, Champneys and Lieven investigated the behavior of a horizontally oriented rotor spinning at a constant angular speed with two balls (Green, Champneys, and Lieven 2006). The regions of stability were calculated utilizing a bifurcation analysis at steady state. Green et al. used the same ball balancer model as in (Green, Champneys, and Lieven 2006), but studied the stability behavior when the ball count was increased to three and four balls (Green et al. 2008). A similar steady state bifurcation analysis was performed. Gorbenko studied the behavior of a horizontally oriented ball balancer spinning at a constant angular speed with n number of balls (Gorbenko 2003). Specifically, the lower speed threshold at which a stable solution could be achieved was studied. A numerical study was used to determine the lowest speed threshold given a set of physical parameters, and also to determine the lowest speed threshold when varying those physical parameters. Ehyaei and Moghaddam investigated the behavior of a horizontally oriented ball balancer spinning at a constant angular speed mounted on a flexible shaft with two balancing balls (Ehyaei and Moghaddam 2009). A Stodola-Green rotor model was used instead of the traditional Jeffcott rotor model. A stability analysis was performed on the linearized equations using the Roth-Hurwitz

criteria. It was determined that stability can only be achieved when the system parameters are within a certain stability region and that the rotating speed must be greater than the first natural frequency. In addition, the simulation output showed that the viscous fluid drag on the balls and the translational ball balancer damping are essential for balancing. Kim, Lee and Chung created a model that accounted for the translational and rotational motion of the ball balancer in three dimensional space. (Kim, Lee, and Chung 2005). It was concluded that the two dimensional, in-plane model is sufficient at predicting the behavior of the ball balancer, whereas the out-of-plane motion contributes very little to the total motion of the ball balancer. Although the rotational component made little contribution on total motion, it was recommended that the translational, as well as the rotational resonant frequencies be considered when selecting operating speeds of the ball balancer. Lu and Tien investigated three types of ball motions, termed pure-oscillatory, pure-rotary and compound rotary periodic motion (Lu and Tien 2012). The study presented included a numerical model as well as an experimental setup to show the development of these three ball motions. Kim and Chung studied the effect that the rotational resonant frequency had on the behavior of the ball balancer (Kim and Chung 2002). The research recommended that the ball balancer not operate near the rotational resonant frequency, as well as the translational resonant frequency if the best ball balancer performance is wanted by the designer. Chao, Huang and Sung studied a horizontally oriented ball balancer that utilized Euler angles to model a ball balancer that was non-planar in space (Chao, Huang, and Sung 2003). The model showed that even with a non-planar ball balancer, sufficient balance could be achieved, as long as the ball balancer was installed below the imbalance plane, in the case where the imbalance plane was offset vertically from the ball balancer. Chung developed a horizontally oriented ball balancer model and analyzed the time response data using a numerical model implementing polar coordinates (Chung 1999). The investigation involved the stability behavior based on several different system parameters which included system damping, ball mass and mass eccentricity. It was discovered that, based on the selection of certain parameters, balancing may not be possible at speeds above the critical velocity. Rajalingham, Bhat and Rakheja studied the behavior of a rotor mounted to a vertical, flexible shaft with no external damping (Rajalingham, Bhat, and Rakheja 1998). It was observed that there were regions of stability and instability above and below the critical speed, which depended on the relative amounts of eccentric mass, ball mass and groove radius.

To further increase the complexity of the ball balancer model and to learn more about practical implementation of ball balancers, studies began observing the behavior of the two plane ball balancer. Rodrigues et al. studied a two plane ball balancer, but included additional degrees of freedom; the angular rotations about the vertical and horizontal axes (Rodrigues et al. 2008).

The first non-linear bifurcation analysis was completed for a two plane ball balancer. The team of Rodrigues et al. also observed the behavior of two horizontally oriented ball balancers, spinning at a constant angular speed with four total balls, two balls for each rotor (Rodrigues et al. 2011b). A bifurcation analysis and an investigation into the effect of anisotropic supports were presented with this model. Insight was gathered into device asymmetry, which included differing ball masses and a short analysis on rotor acceleration. The findings from the numerical studies were compared to experimental methods by using a table-top ball balancer rig (Rodrigues et al. 2011a). Sperling et al. investigated the behavior of two horizontally oriented ball balancers spinning at a constant angular speed (Sperling et al. 2002). The two-plane system had five degrees of freedom, only neglecting the axial translation of the ball balancer. The system utilized four balancing balls, two balls for each rotor. The model involved two unbalances that could be modified in magnitude, and their radial and axial locations. Several physical factors of the model were observed, which were centered around system damping. The study was able to show the "Sommerfeld effect", an event in which the balls stall in the absolute reference frame while the ball balancer continues to spin.

Many researches also began investigating ball balancer behavior due to newly studied physical parameters. These parameters were centered around the various physical aspects of the model which included suspension supports, ball rolling friction, gravity and rotor acceleration to name a few. Chan, Sung and Chao investigated the effect of non-linear springs on the behavior of a ball balancer (Chan, Sung, and Chao 2011). It was found that a non-linear suspension affected the end stability positions of the balls. It was also observed that the end stability diagrams were slightly different due to the non-linearity of the ball balancer supports. Sung et al. investigated how the magnitude, frequency and phase of an external force affected the position of the balls in a ball balancer (Sung et al. 2013). The results of the model determined that the ball positions were not affected by the external force unless that external force was at the resonant frequency of the system. It was also discovered that the rolling friction acting between the balls and the ball balancer was enough to hold the balls in place even when an external force was imparted on the system. Chung derived the equations of motion of a vertically oriented ball balancer in which gravity and rotor acceleration were included (Chung 2004). It was determined that a ball balancer could still properly function and balance an eccentricity even in the presence of gravity. An investigation into rotor acceleration recommended that accelerations be as smooth as possible so as to not disrupt the ball locations. Huang studied the behavior of a horizontally oriented ball balancer spinning at a constant angular speed and commented on the effect that rolling friction had on the equilibrium location of the balls (Huang 2008). It was found that the balancing balls may not fully reach their ideal balancing position in the presence of rolling

friction. To counteract this behavior, a method was proposed which involved using a series of decelerations and accelerations to perturb the location of the balls such that a more stable ball location may be occupied. Yang et al. investigated the behavior of a horizontally oriented disk spinning at both a speed lower than the natural frequency and higher than the natural frequency while including two balls (Yang et al. 2005). The impact of rolling friction on the end whirling radius of the rotor when at steady state was studied. The results showed that a high friction coefficient increased the variability in stability location of the balls. Chan, Sung and Chao also investigated the effect that rolling friction had on the settling position of the balls (Chan, Sung, and Chao 2012). It was found that the rolling friction between the ball and the ball balancer was the main reason for residual vibrations even at speeds above the critical velocity. Huang and Chao investigated the behavior of a horizontally oriented ball balancer spinning at a constant angular speed with one ball while observing the runway eccentricity, rolling resistance and ball viscous drag force (Huang and Chao 2002). Rajalingham and Rakheja investigated the effect a ball balancer had on the suppression of vibration in hand-held power tools (Rajalingham and Rakheja 1998). Namely the effect that rolling friction had on the stability position of the balls. Although others have studied rolling friction, it was concluded that rolling friction decreased the unstable operating region of the ball balancer, which increased the stable speed range of the ball balancer. Bykov studied a horizontally oriented ball balancer and compared the ball balancer behavior when an orthotropic shaft was used instead of a traditional isotropic shaft (Bykov 2013). It was discovered that the stability region for an orthotropic shaft is narrower than that of an isotropic shaft. In addition, the orthotropic shaft had much greater motion amplitudes when accelerating through the critical speed region.

Along with the investigation of physical parameters of the ball balancer model, more novel ideas began to surface that addressed several of the limitations of the ball balancer. Sohn et al. studied the stability behavior of a pendulum balancer (Sohn et al. 2007). Hwang and Chung studied a horizontally oriented ball balancer with two raceways to reduce the occurrence of collisions (Hwang and Chung 1999). The two race ways reduced the ball-to-ball interactions which were intended to rule out the ball interaction effect on overall ball balancer behavior. Blanco-Ortega et al. studied the behavior of a horizontally oriented disk spinning at a constant speed with two balancing masses able to move radially and tangentially by a control mechanism (Blanco-Ortega et al. 2008). Kim and Na investigated the transient response of a ball balancer using a five ball system (Kim and Na 2013). A novel ball balancer concept was introduced where springs were placed between balls such that the balls would remain separated at low speeds and were allowed to pack together at high speeds. This concept was shown to lower the overall motion of the ball balancer compared to the typical no-spring counterpart. Lu

and Wang developed and derived the equations of motion for a new type of balancer, called a "ball-rod-spring" balancer (Lu and Wang 2011). The main purpose of the new model was to give the balls an additional component of motion in the radial direction. It was shown that this extra degree of freedom increased the stable region of the ball balancer and could reduce the total motion of the ball balancer.

As with all research, the intent is to push the development of the ball balancer model forward and to prove or disprove the necessary inclusion of various characteristics. Multiple balls, multiples planes of balls, different suspension systems, environmental factors, etc. have all been studied with great success. However, one element has not been studied intensely that many have overlooked to narrow their investigatory focus. This element is the ball-to-ball interactions. A clear assumption is typically made that the balls are assumed to be point masses and, although constrained to the same fixed radius, can pass through one another, thus disregarding any ball-to-ball interactions. Some have been able to make a case that collisions are unlikely due to the design of the ball balancer model (Hwang and Chung 1999), but most make an assumption. This assumption is that the collisions are perfectly elastic, completely conserving energy and thus, can be neglected. From a development stand-point, this seems like an adequate assumption since the ball balancer model will be less complicated neglecting the collisions. Additionally, neglecting collisions seems reasonable if the diameter of a ball is small compared to the diameter of the ball balancer. However, the assumption begins to break down if the diameter of the balls are not small compared to the size of the ball balancer or if there are many balls within the ball balancer. Although the models presented in the previous works are indeed correct, the comparison to the physical world may not always be correct. This is where the work presented in this paper breaks new ground in the development of ball balancer knowledge.

C. Explanation of Novelty of Ball Balancer Model

Assuming that the balls in the ball balancer are in fact perfect spheres, the center of mass and the geometric center of the sphere lie at the same point in space. However, the outer surface of the sphere lies at some fixed radius away from the center. All the interactions that a ball will have with an adjacent ball occur at the surface of the sphere, not at the center. So the negligence of collisions may be correct with respect to conservation of energy, but the physicality of the assumption does not hold. In reality, the balls interact with one another at the surface of each ball. So when two balls should collide with each other and instead pass through one another, not only is this non-physical, error is introduced into the model. Ultimately, this error is manifested in an error in time. Due to the numerical method needed to solve the equations of motion for this problem, a model using a collision assumption will deviate from the actual

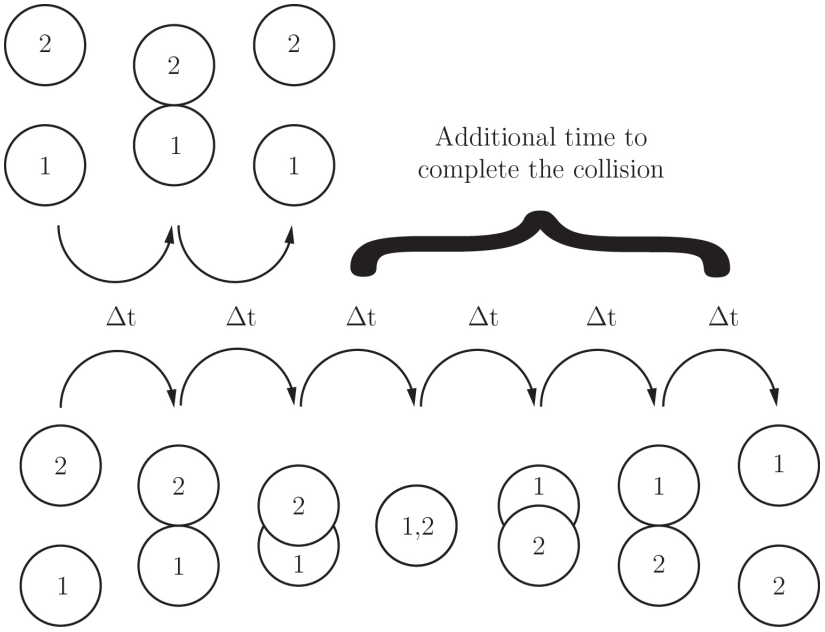

FIGURE 1 – A Time Error is Introduced by Neglecting the Physical Nature of the Balls

behavior of the system. To further explain, the time error introduced by this assumption is shown pictorially in Figure 1.

If collisions are neglected, the model begins to deviate from reality after the very first collision. There is a time error associated with how long it takes the balls to fully pass through each other. The error in time is approximately equal to Equation 1 where r_i is the radius of ball i and $\dot{\beta}_1$ is the relative velocity between the two balls,

$$\Delta t_e \approx \frac{r_1 + r_2}{\left|\dot{\beta}_1\right|} \tag{1}$$

Due to the discretization nature needed to solve the equations of motion, this error alters the initial conditions of the problem for the time step following the collision, resulting in non-physical behavior from that point forward. Additionally, the ball balancer equations of motion are highly non-linear, thus the behavior of the system is highly dependent on the initial conditions for each integration step. A small difference in initial conditions may cause a large change in behavior of the system.

This paper recognizes the fact that collisions are an unavoidable occurrence of a ball balancer. Given that the number of balls is sufficient and a collision does occur, the event of a collision presents a discontinuity into the ball balancer behavior. To show the effect of ball-to-ball interactions on the system behavior of the ball balancer, this paper will present a comparison to the steady state behavior of a system that includes these interactions and a system that does not include these interactions. The intent of this paper is to study the effect that the finite spatial

characteristics of the balls have on total ball balancer motion and behavior. Additionally, the intent of this model is to design a tool that can be used to more effectively design a ball balancer that is optimum for a set of working conditions.

This paper assumes that the ball balancer balls are in fact spherical and possess some finite diameter. Additionally, this papers includes a discretized integration method using a fourth order Runge-Kutta method that captures any ball-to-ball interaction exactly using the computational method outlined by (Henon 1982). From experimental observations of ball balancers, this model also captures the separation and formation of a train of balls. This is done by utilizing the equation-altering method outlined by (Dedow and Murphy 2016). The model uses a hybrid solving method, which can switch between a traditional time integration step or perform a displacement or force integration step depending on the need for a collision or separation, respectively. This model also applies a system level momentum analysis to determine the velocities of the ball balancer and balls after a collision. Additionally, this model includes rolling friction and the rotational inertial characteristics of the balls. Note that the model that will be presented in this paper contains many elements of the physics that are in play with the ball balancer system. The capabilities of this model are vast; hopefully more work and research will be performed using a similar model with similar capabilities. Despite this, only a small amount of the capabilities of this model will actually be covered in this paper. The presented material is only the surface of what can be discovered about the behavior of a ball balancer using this model.

II. REVIEW OF KINEMATIC MOTION

A. Introduction

Before an analysis can begin to observe the complex motion of a ball balancer, it is worth taking the time to revisit the simple and fundamental principles that govern kinematic motion and vibration theory. Focus will first be placed on the motion and behavior of an ideal mass spring oscillator since it is the most widely used and well know model for introductory dynamics. The exact solutions for the motion of the mass spring model are known and the physics is very well studied. After that, an extension to a rotating imbalance will be made that will give an introductory glimpse into how a ball balancer behaves.

B. The Mass Spring Oscillator

An ideal mass spring oscillator can be explained by the summation of four forces: the inertial forces due to the mass, the damping forces due to the damper, the potential forces due to the spring and the external forces due to external excitations. These four forces combine and interact in such a way that kinematic phenomena develop within this particular system. To start, it is assumed that the mass is only allowed to move in one coordinate direction (in this case the horizontal direction). The force acting on the mass due to the damper and the spring are $c_1\dot{x}_1$ and k_1x_1, respectively, where c_1 is the damping constant of the damper and k_1 is the spring constant of the spring. Figure 2 shows the free body diagram for the mass spring system. First, imagine that the mass moves in the positive direction. When the mass moves to the right, the damping force and the spring force act in the negative direction to oppose the motion of the mass. On the other hand, as the mass moves in the negative direction, the damping force and the spring force act in the positive direction to oppose the motion of the mass. The force opposition to the motion of the mass is seen in the equations of motions. The equation of motion for a one degree of freedom, mass spring oscillator can easily be written and is seen in Equation 2,

$$m_1\ddot{x}_1 = -c_1\dot{x}_1 - k_1x_1 + F_{EXT} \tag{2}$$

There can also be an external force applied to the mass, this is seen by the force F_{EXT}. Note that the force F_{EXT} can be any magnitude, direction or shape (impulse, step, sinusoidal, etc.). For simplicity, the force is assumed to be sinusoidal in shape and has the form, $F_{EXT} =$

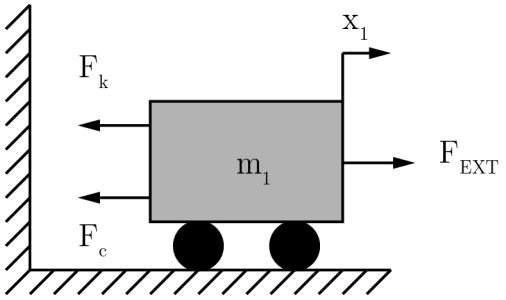

FIGURE 2 – A Free Body Diagram of a Mass Spring Oscillator

$F_{AMP} \sin(\omega_f + \gamma)$.

The one mass spring system can be simplified further by clearing the acceleration term and defining two new parameters, ω_{n_1} and ζ_1, which are defined as the natural frequency and the damping ratio, respectively. The natural frequency and the damping ratio are defined by the equations below,

$$\omega_{n_1} = \frac{k_1}{m_1} \qquad\qquad \zeta_1 = \frac{c_1}{2\sqrt{m_1 k_1}}$$

Substituting these variables into the original equation, the differential equation for the one mass system now becomes,

$$\ddot{x}_1 = -2\zeta_1 \omega_{n_1} \dot{x}_1 - {\omega_{n_1}}^2 x_1 + \frac{F_{EXT}}{m_1} \tag{3}$$

Equation 3 is the traditional equation for the one degree of freedom, mass spring oscillator. This equation can also be written in first order form by declaring two new variables u_1 and u_2 such that the equation can be written in matrix form, $\dot{\mathbf{x}} = \mathbf{A}\mathbf{x}$, where the boldface denotes a matrix. The differential equations for the one mass system in first order form are shown in Equations 4 and 5,

$$\dot{u}_1 = u_2 \tag{4}$$

$$\dot{u}_2 = -2\zeta_1 \omega_{n_1} u_2 - {\omega_{n_1}}^2 u_1 + \frac{F_{EXT}}{m_1} \tag{5}$$

The first order form helps to write the equations of motion for the one degree of freedom system in matrix form as seen in Equation 6. Matrix form is simply a way to organize the equations and will be very useful when the equations of motion for a system become more complex,

$$\left\{ \begin{array}{c} \dot{u}_1 \\ \dot{u}_2 \end{array} \right\} = \left[\begin{array}{cc} 0 & 1 \\ -{\omega_{n_1}}^2 & -2\zeta_1 \omega_{n_1} \end{array} \right] \left\{ \begin{array}{c} u_1 \\ u_2 \end{array} \right\} + \left[\begin{array}{c} 0 \\ \frac{F_{EXT}}{m_1} \end{array} \right] \tag{6}$$

The system behavior depends on the relative values of the damping ratio and natural frequency, along with the interaction of the external force. In the case where there is no external

force acting on the system, the response is said to be "free" or "unforced". In this case, the value of the forcing function equals zero, such that the original equation of motion becomes what is seen in Equation 7,

$$\begin{Bmatrix} \dot{u}_1 \\ \dot{u}_2 \end{Bmatrix} = \begin{bmatrix} 0 & 1 \\ -{\omega_{n_1}}^2 & -2\zeta_1\omega_{n_1} \end{bmatrix} \begin{Bmatrix} u_1 \\ u_2 \end{Bmatrix} \tag{7}$$

Referring to the second order equation written in Equation 3, the solution to the differential equation can be assumed to be some type of exponential defined by $x_1(t) = e^{\lambda t}$. The derivatives $x_1, \dot{x}_1$ and $\ddot{x}_1$ can be substituted into the original differential equation by taking the appropriate derivatives of $x_1(t)$. Making the proper substitutions and canceling out $e^{\lambda t}$ from both sides of the equation, the original equation of motion can be simplified to Equation 8 below,

$$\lambda^2 + 2\zeta_1\omega_{n_1}\lambda + {\omega_{n_1}}^2 = 0 \tag{8}$$

Finally, λ can be solved using the quadratic formula. The final expression for λ is shown in Equation 9,

$$\lambda = -\zeta_1\omega_{n_1} \pm \omega_{n_1}\sqrt{{\zeta_1}^2 - 1} \tag{9}$$

The two values of λ are the roots of the system and are computed from this equation by the addition and subtraction of the two terms in the expression. There are specifically three scenarios that develop from the values of λ that have high importance. The first is when the roots of the system are complex conjugates, caused when the damping ratio is a value less than one, but greater than zero. This system is characterized as under damped. The second is when the roots of the system are both equal and negative, caused when the damping ratio is equal to one. This system is characterized as critically damped. The third is when the roots of the system are both real and unequal, caused when the damping ratio is greater than one. This system is characterized as over damped. The next section details the response of the system under these three damping conditions. The initial conditions for the displacement of the mass and the velocity of the mass in all the following case studies are $x_1(0) = x_{1_0}$ and $\dot{x}_1(0) = \dot{x}_{1_0}$, respectively. The displacement and velocity for the mass spring oscillator in the free motion test cases are non-dimensionalized according to the following equations where the superscript asterisk denotes a non-dimensional term,

$$x_1^* = \frac{x_1}{x_{1_0}} \qquad\qquad \dot{x}_1^* = \frac{\dot{x}_1}{x_{1_0}\omega_{n_1}}$$

The displacement and velocity for the mass spring oscillator in the forced motion test cases are non-dimensionalized according to the following equations,

$$x_1^* = x_1 \frac{k_1}{F_{AMP}} \qquad \dot{x}_1^* = \dot{x}_1 \frac{k_1}{F_{AMP}\omega_{n_1}}$$

C. Free Motion of the Mass Spring Oscillator System

Generally speaking, the motion of the mass spring system can be broken down into two types of motion: free and forced. Free motion is characterized by the absence of an external force acting on the mass ($F_{EXT} = 0$). The differential equation for the free motion of the mass was previously shown in Equation 7. Forced motion is characterized by the presence of an external force acting on the mass ($F_{EXT} \neq 0$). The free motion of the system will be analyzed first. An analysis regarding the forced motion of the system will follow.

1. Critically Damped Motion

Critically damped motion is characterized by two equal and negative roots. The system is also characterized by a response in which the displacement amplitude decreases to zero, with no oscillations. The closed-form solution for the motion of the mass in the critically damped case is widely known and can be written as shown in Equations 10 and 11, where the constants A and B are found from the initial conditions of the problem. These solutions can be found in any undergraduate dynamics textbook and were derived by solving the differential equations of motion of the mass spring system to obtain a closed form solution,

$$x_1(t) = Ae^{-\zeta_1\omega_{n_1}t} + Bte^{-\zeta_1\omega_{n_1}t} \tag{10}$$

$$\dot{x}_1(t) = -A\zeta_1\omega_{n_1}e^{-\zeta_1\omega_{n_1}t} + Be^{-\zeta_1\omega_{n_1}t}(1 - \zeta_1\omega_{n_1}t), \tag{11}$$

where

$$A = x_{1_0} \qquad B = \dot{x}_{1_0} + x_{1_0}\zeta_1\omega_{n_1}$$

As said before, the typical response of a critically damped system is a response in which the displacement amplitude quickly decreases to zero with no oscillations. The physical parameters of this test case were selected such that $\zeta_1 = 1.0$ and $\omega_{n_1} = 1$ rad/s. The displacement and velocity responses can be plotted to observe the behavior of the critically damped system. These are plotted in Figure 3a and Figure 3b.

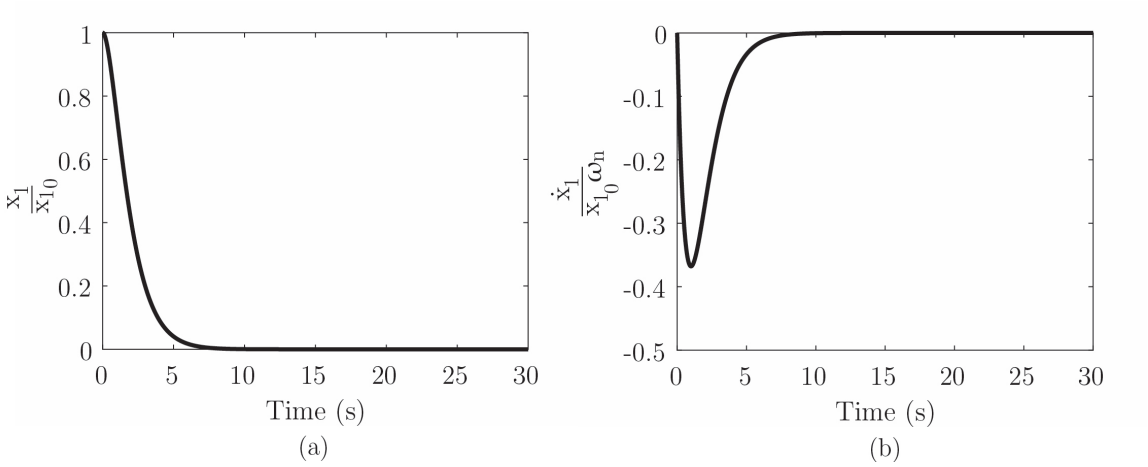

FIGURE 3 – The Displacement (a) and Velocity (b) of a Critically Damped Mass Spring System

From Figure 3, it can be seen that the displacement of the mass decreases very quickly back to its equilibrium position with no oscillations. It can also be seen that the velocity of the mass exhibits a similar behavior. The displacement and velocity responses are simply phase shifted due to their relationship with one another. A critically damped system is typically not found in practicality since it is difficult to ensure ζ_1 is exactly equal to one. Most of the time, the system will be slightly under damped or over damped even if the critically damped case is desired. Nonetheless, this is a classification of motion that should be understood.

2. Over Damped Motion

Over damped is characterized by when the system has two different real roots, and when the damping ratio equals a value greater than one. This system is also characterized by a response in which the displacement amplitude decreases to zero with no oscillations, but at a slower rate than the critically damped system. The closed-from solution to the motion of the mass in the over damped case is widely known and can be written as shown below in Equations 12 and 13, where the constants A and B are found from the initial conditions of the problem and $\lambda_{1,2}$ are the two roots of the system. These solutions can be found in any undergraduate dynamics textbook and were derived by solving the differential equations of motion of the mass spring system to obtain a closed form solution,

$$x_1(t) = Ae^{\lambda_1 t} + Be^{\lambda_2 t} \tag{12}$$

$$\dot{x}_1(t) = A\lambda_1 e^{\lambda_1 t} + B\lambda_2 e^{\lambda_2 t}, \tag{13}$$

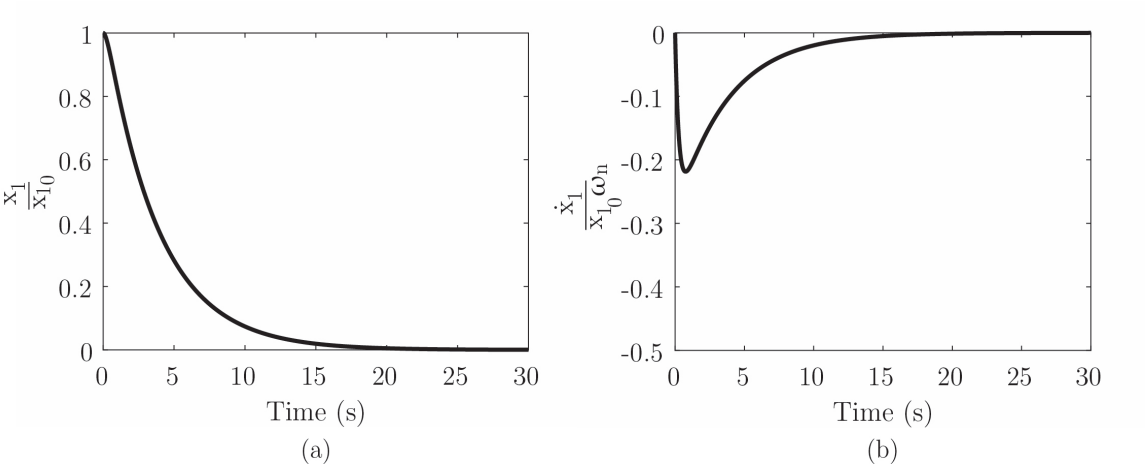

FIGURE 4 – The Displacement (a) and Velocity (b) of an Over Damped Mass Spring System

where

$$A = x_{1_0} - \frac{\dot{x}_{1_0} - \lambda_1 x_{1_0}}{\lambda_2 - \lambda_1} \qquad B = \frac{\dot{x}_{1_0} - \lambda_1 x_{1_0}}{\lambda_2 - \lambda_1}$$

As said before, the typical response of an over damped system is one in which the displacement amplitude decreases to zero with no oscillations, but at a slower rate than the critically damped system. The physical parameters of this test case were selected such that $\zeta_1 = 2.0$ and $\omega_{n_1} = 1$ rad/s. The displacement and velocity response can be plotted to observe the free response of the over damped system. These are plotted in Figure 4a and Figure 4b.

From Figure 4, it can be seen that the displacement of the mass decreases once released and decreases with no oscillations. Unlike the critically damped case, the rate at which the displacement decreases for the over damped case is slower than the rate for the critically damped case. This can be proven by comparing the maximum velocity of the mass in both the critically damped and over damped cases. The magnitude of the maximum velocity of the critically damped case ($\dot{x}_1^* = 0.37$) is higher than the velocity of the over damped case ($\dot{x}_1^* = 0.22$). The mass moves slower to the equilibrium position when over damped. Unlike the critically damped system, an over damped system is somewhat more frequently seen in normal use. Thus, it is a classification of motion that should definitely be understood.

3. Under Damped Motion

Lastly, under damped motion is characterized by when the system has two complex roots; when the damping ratio equals a value less than one, but greater than zero. This system is also characterized by oscillations at the natural frequency that exponentially decay over time. This response is similar to a ball bouncing on the floor. The ball bounces at a natural frequency,

based on the mass and stiffness of the ball. Assuming that energy is lost every bounce, the amplitude of the ball decreases over time until the height of the ball is essentially zero.

In this case, a new parameter must be defined and is called the "damped frequency". The damped frequency relates the natural frequency to the damping ratio and accounts for the shift in the resonant frequency due to the presence of damping. The damped frequency is defined below,

$$\omega_d = \omega_{n_1}\sqrt{1-\zeta_1}$$

The closed-form solution to the motion of the mass in the under damped case is widely known and can be written as shown in Equations 14 and 15, where the constants A and B are found from the initial conditions of the problem. These solutions can be found in any undergraduate dynamics textbook and were derived by solving the differential equations of motion of the mass spring system to obtain a closed form solution,

$$x_1(t) = e^{-\zeta_1\omega_{n_1}t}[A\cos(\omega_d t) + B\sin(\omega_d t)] \tag{14}$$

$$\dot{x}_1(t) = -Ae^{-\zeta_1\omega_{n_1}t}[\omega_d\sin(\omega_d t)+\zeta_1\omega_{n_1}\cos(\omega_d t)]+Be^{-\zeta_1\omega_{n_1}t}[\omega_d\cos(\omega_d t)-\zeta_1\omega_{n_1}\sin(\omega_d t)], \tag{15}$$

where

$$A = x_{1_0} \qquad\qquad B = \frac{\dot{x}_{1_0} + x_{1_0}\zeta_1\omega_{n_1}}{\omega_d}$$

As said before, the typical response of an under damped system is a diminishing sinusoid, which is seen by the multiplication of a decreasing exponential and a sinusoidal response. The physical parameters of this test case were selected such that $\zeta_1 = 0.2$, $\omega_{n_1} = 1$ rad/s and $\omega_d = 0.77$ rad/s. The displacement and velocity response can be plotted to observe the behavior of the free response of the under damped system. These are plotted in Figure 5a and Figure 5b.

From Figure 5, it can be seen that the displacement of the mass does in fact oscillate with a decaying sinusoid. The frequency of oscillation is defined by the damped natural frequency of the system, ω_d. As time goes on, energy is lost through the damper, thus the height of each successive oscillation decays. The rate of this decay of the sinusoid is defined by the product between the damping ratio and the natural frequency, $\zeta_1\omega_{n_1}$. Likewise, it can be seen that the velocity of the mass also shows the same decaying and oscillatory behavior. The displacement and velocity response are simply phase shifted due to their relationship with one another. The under damped system is the most common type of damping that is seen most engineering uses. Even more interesting than the oscillatory motion of the under damped motion is when the under damped system is under the influence of an external force. This behavior will be discussed in the next section.

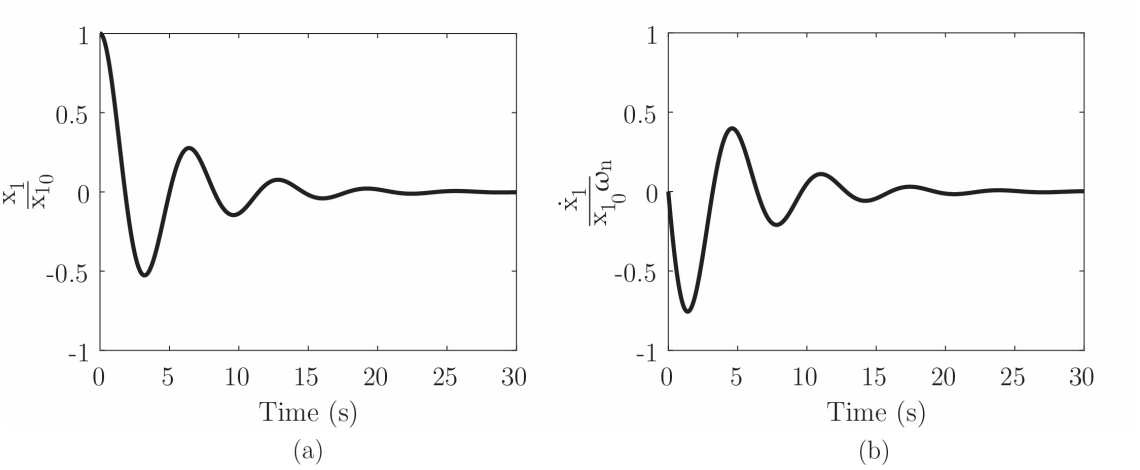

FIGURE 5 – The Displacement (a) and Velocity (b) of an Under Damped Mass Spring System

D. Forced Motion of the Mass Spring Oscillator System

Unlike the unforced system, a forced system is characterized by when the external force acting on the system is non-zero. This external force can be any variety of functions, but the most common are an impulse, step and sinusoidal input. For simplicity, only the sinusoidal input will be analyzed since the external force acting on the ball balancer is sinusoidal in nature.

Assuming that the external force input is equal to $F_{EXT} = F_{AMP}\sin(\omega_f t + \gamma)$, where F_{AMP} is the amplitude of the forcing function, ω_f is the frequency of the forcing function and γ is the phase shift, the differential equation for the motion of the mass can be rewritten as seen below,

$$\dot{u}_1 = u_2 \tag{16}$$

$$\dot{u}_2 = -2\zeta_1\omega_{n_1}u_2 - \omega_{n_1}^2 u_1 + \frac{F_{AMP}\sin(\omega_f t + \gamma)}{m_1} \tag{17}$$

For the following analyses, the case where the mass is under damped ($\zeta_1 < 1.0$) will be considered for simplicity. The same parameters that were used in the free motion, under damped case are used again. The under damped case is solely being considered here because it is where the most interesting interactions occur and the most useful observations can be made about the motion of the mass. To illustrate the motion of the mass excited by the external force, a resonant diagram can be created that shows the maximum motion of the mass at different forcing frequencies. The following resonant diagram only applies to motion at steady state after all transient behavior has been damped out. The resonant behavior of the system is seen in Figure 6.

As can be seen near the natural frequency of the system, a resonant phenomena occurs. The displacement of the mass increases to a maximum value near the natural frequency of the

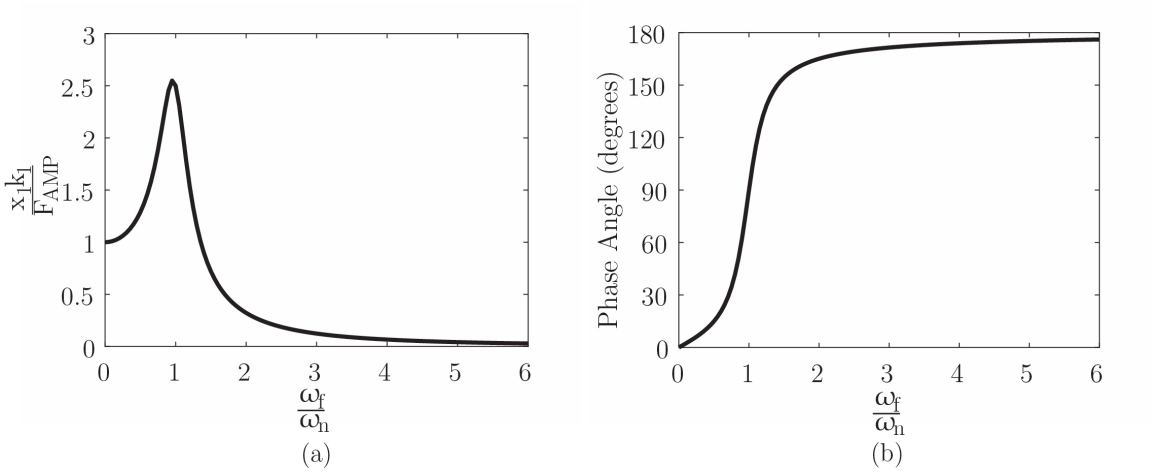

FIGURE 6 – The Displacement Response (a) and Phase Angle (b) of a Mass Spring System

system. The maximum value does not occur exactly at the natural frequency; the damping within the system shifts the location of the maximum displacement. Resonance occurs because of the unique relationship between the mass and stiffness of the system, as well as the external forcing frequency that acts on system. In addition, the phase angle between the location of the eccentric mass and the mass displacement shifts to 180 degrees out of phase as the rotational frequency increases beyond the natural frequency. It can also be seen that at forcing frequencies above the natural frequency, the motion of the mass decays to zero. To explain this further, two cases will be presented. The first will be when the forcing frequency is equal to the natural frequency of the system. The second will be when the forcing frequency is equal to five times the natural frequency of the system.

1. External Forcing Frequency Equals Natural Frequency

The closed-from solution for the motion of the mass in the forced, under damped case is widely known and can be written as seen in Equations 18 and 19, where the constants A, B, C and D are found from the initial conditions of the problem. Again, these solutions can be found in any undergraduate dynamics textbook and were derived by solving the differential equations of motion of the mass spring system to obtain a closed form solution,

$$x_1(t) = Ae^{-\zeta_1 \omega_{n_1} t} \sin(\omega_d t + C) + B\cos(\omega_f t - D) \tag{18}$$

$$\dot{x}_1(t) = Ae^{-\zeta_1 \omega_{n_1} t}[\omega_d \cos(\omega_d t + C) - \zeta_1 \omega_{n_1} \sin(\omega_d t + C)] - B\omega_f \sin(\omega_f t - D) \tag{19}$$

where

$$A = \frac{x_{1_0} - B\cos(D)}{\sin(C)} \qquad B = \frac{F_{AMP}}{\sqrt{(\omega_{n_1}^2 - \omega_f^2)^2 + (2\zeta_1 \omega_{n_1} \omega_f)^2}}$$

$$C = \tan^{-1}\left[\frac{\omega_d(x_{1_0} - B\cos(D))}{\dot{x}_{1_0} + \zeta_1\omega_{n_1}(x_{1_0} - B\cos(D))}\right] \qquad D = \tan^{-1}\left[\frac{2\zeta_1\omega_{n_1}\omega_f}{\omega_{n_1}^2 - \omega_f^2}\right]$$

The typical response of an under damped system with a force acting at the system natural frequency is a response in which the amplitude is stable, but increases to a maximum with an oscillatory behavior. The displacement and velocity responses are plotted in Figure 7a and 7b which show the behavior of the under damped and forced system,

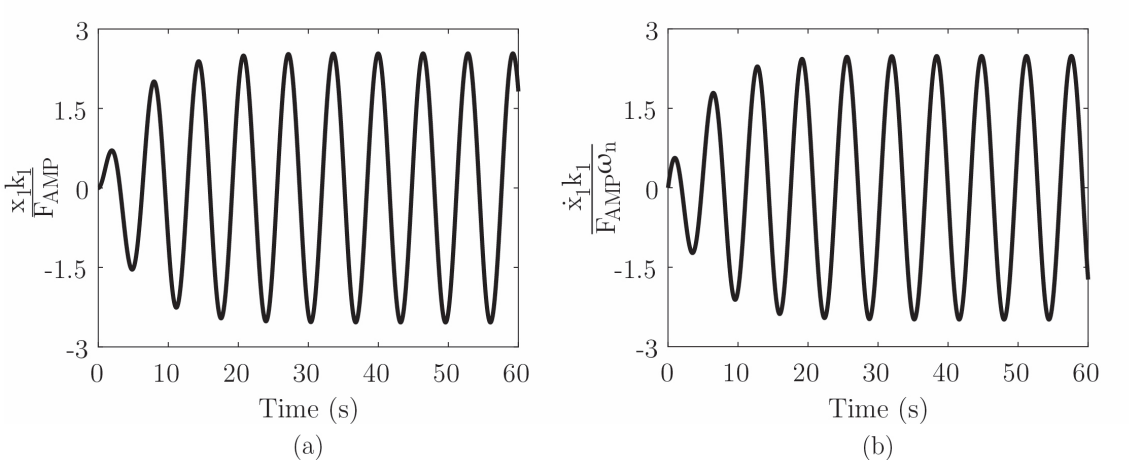

FIGURE 7 – The Displacement (a) and Velocity (b) of a Forced, Under Damped Mass Spring System at the Natural Frequency

It can be seen that if the input forcing function operates at the natural frequency of the free system, the motion is stable with larger amplitudes than other frequencies. The displacement and velocity of the mass grow to a maximum when steady state is achieved.

2. External Forcing Frequency Greater Than Natural Frequency

The typical response of an under damped system with a force acting at some frequency greater than the natural frequency is a response in which the amplitude is stable but smaller than when the excitation frequency equals the natural frequency. The displacement and velocity response can be plotted to observe the behavior of the under damped and forced system. These are plotted in Figure 8a and 8b, respectively. Note that this test case has an excitation frequency equal to five times the natural frequency of the system.

It can be seen that if the input forcing function operates at a higher frequency than the natural frequency of the free system, the motion is stable, but the displacement magnitude begins to approach zero. As the forcing frequency increases, the inertial characteristics of the system begin to dominate such that the displacement of the mass ultimately becomes unaffected by the external force.

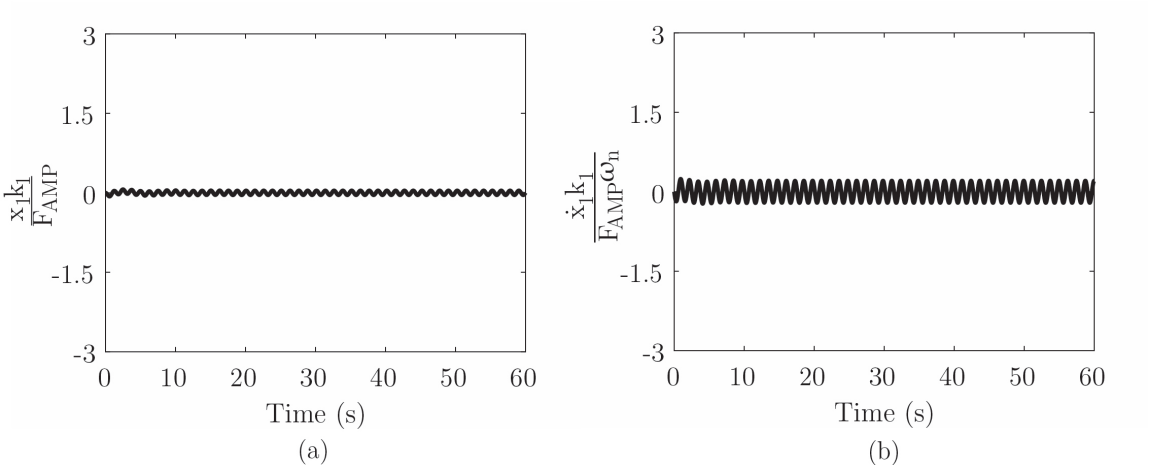

FIGURE 8 – The Displacement (a) and Velocity (b) of a Forced, Under Damped Mass Spring System at Five Times the Natural Frequency

E. Extension to a Rotating Imbalance System

In addition to the mass spring oscillator, a more relevant model to study is the one degree of freedom rotating imbalance. Although slightly more complicated, the rotating imbalance problem is much more applicable to the ball balancer problem. An eccentric mass rotates at some predetermined rotational speed, inputting a sinusoidal external forcing function into the system. The fundamental difference between the rotating imbalance model and the ball balancer model is the absence of balls. Nonetheless, this will serve as a perfect model to study before more complex behavior is observed.

A free body diagram of the rotating imbalance is shown in Figure 9 where e is the distance from the center of rotation to the eccentric mass and m_e is the eccentric mass.

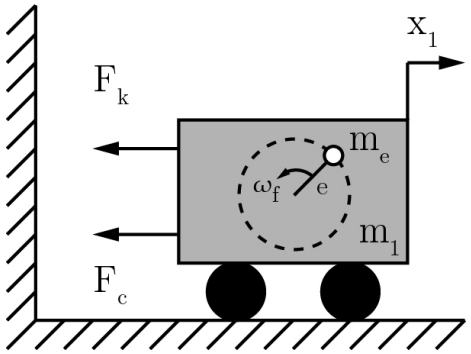

FIGURE 9 – A Free Body Diagram of a Horizontally Oriented Rotating Imbalance

The equations of motion for a rotating imbalance operating in the horizontal direction

are shown in Equations 20 and 21 below in first order form,

$$\dot{u}_1 = u_2 \tag{20}$$

$$\dot{u}_2 = -\frac{k_1}{m_1}u_1 - \frac{c_1}{m_1}u_2 + \frac{m_e}{m_1}e\omega_f^2 \sin(\omega_f t) \tag{21}$$

A forced system is characterized by when the external force on the system is non-zero, thus this system is in fact a forced system. As can be seen in Equations 20 and 21, the external force is sinusoidal in nature, but the nature of the external force is different than seen with the forced mass spring system. This difference is that the motion of the eccentric mass and the mass are coupled together. The rotating imbalance model has been well studied and a closed form solution exist for the motion of the mass. The exact closed form solution for the rotating imbalance problem is given below in Equations 22 and 23,

$$x_1(t) = A\sin\left(\omega_f t - \gamma\right) \tag{22}$$

$$\dot{x}_1(t) = A\omega_f \cos\left(\omega_f t - \gamma\right), \tag{23}$$

where

$$A = \frac{m_e e\omega_f^2}{\sqrt{\left(k_1 - m_e\omega_f^2\right)^2 + \left(c_1\omega_f\right)^2}} \qquad \gamma = \tan^{-1}\left(\frac{c_1\omega_f}{k_1 - m_1\omega_f^2}\right)$$

For the following analyses, the case where the mass is under damped ($\zeta_1 = 0.2$) will be considered for simplicity. The same parameters that were used in the under damped case for the one mass spring oscillator are used, with the addition of $e = 0.10$ ft and the ratio of of $\frac{m_e}{m_1} = 0.01$. Note that in the following study, the displacement and velocity of the rotating imbalance are non-dimensionalized according to the following equations,

$$x_1^* = \left(\frac{m_1}{m_e}\right)\frac{x_1}{e} \qquad \dot{x}_1^* = \left(\frac{m_1}{m_e}\right)\frac{x_1}{e\omega_{n_1}}$$

To illustrate the motion of the mass excited by the rotating imbalance, a resonant diagram can be created that shows the maximum motion of the mass at different frequencies of rotation. Since the equations defining the motion of the rotating imbalance are written for the steady state region, the following resonant diagram only applies to motion at steady state; all transient behavior has been damped out. The resonant behavior of the system is seen in Figure 10.

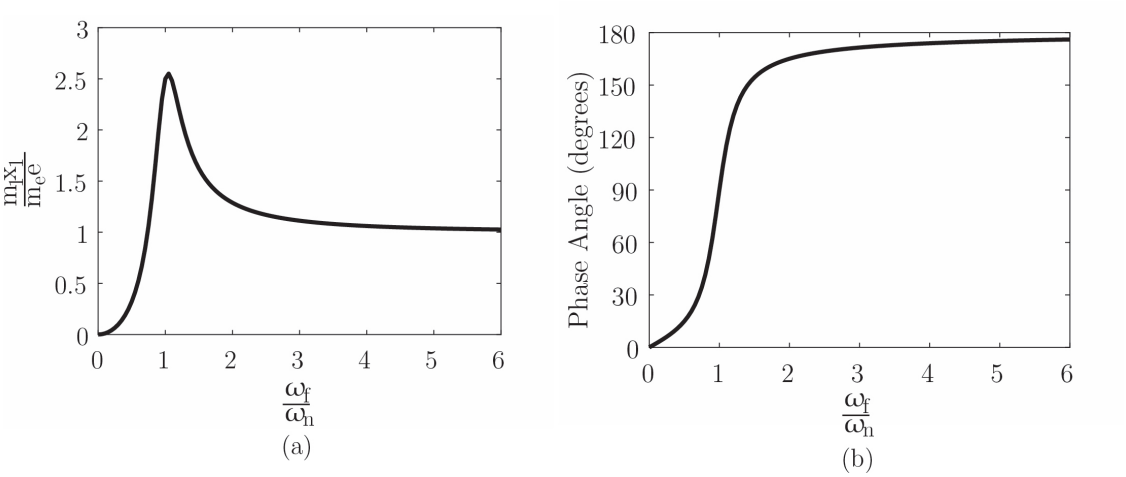

FIGURE 10 – The Displacement Response (a) and Phase Angle (b) of a Rotating Imbalance System

As can be seen near the resonant frequency of the system, a resonance phenomena occurs similar to what was seen in the single mass spring oscillator. The displacement of the mass increases to a maximum value near the natural frequency of the system. The maximum value does not occur exactly at the natural frequency; the damping within the system shifts the location of the maximum displacement. Resonance occurs because of the unique relationship between the mass and stiffness of the system, as well as the external forcing frequency that acts on system. In addition, the phase angle between the location of the eccentric mass and the mass displacement shifts to 180 degrees out of phase as the rotational frequency increases. Unlike the mass spring oscillator, even at frequencies above the natural frequency of the system, the motion of the rotating imbalance system is not zero; there is an offset in displacement due to the rotational nature of the system where F_{EXT} is a function of $m_e\omega_f^2$. To explain this further, two cases will be presented. The first will be with the rotating imbalance operating at a frequency equal to the natural frequency of the system. The second will be with the rotating imbalance operating at a frequency equal to five times the natural frequency of the system.

1. Imbalance Rotates at Frequency Equal to Natural Frequency

The typical response of an under damped system with an eccentric mass rotating at the natural frequency is a response in which the amplitude is larger than that of other frequencies, but oscillatory in nature. The displacement and velocity response are plotted in Figure 11a and 11b, respectively.

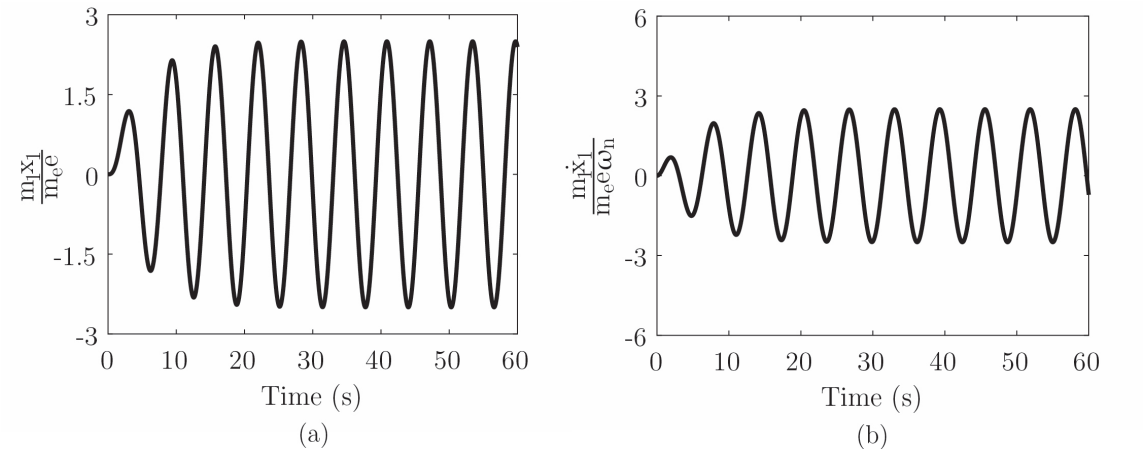

FIGURE 11 – The Displacement (a) and Velocity (b) of a Rotating Imbalance System at the Natural Frequency

It can be seen that if the eccentric mass rotates at a frequency equal to the natural frequency of the free system, the motion is stable and oscillatory. The displacement and velocity reach a steady state value as the transient motion is damped out. The response of the mass at this condition is interesting, but even more interesting behavior occurs when the eccentric mass rotates at a frequency larger than the natural frequency.

2. Imbalance Rotates at Frequency Greater Than Natural Frequency

The typical response of an under damped system with an eccentric mass rotating at some frequency greater than the natural frequency is similar to that when the eccentric mass rotates at the natural frequency. The displacement and velocity response can be plotted to observe the behavior of the system. These are plotted in Figure 12a and 12b, respectively. Note that this test case has a rotational frequency equal to five times the natural frequency of the system.

It can be seen that if the rotating imbalance spins at a frequency higher than the natural frequency of the free system, the displacement of the mass does not decay to zero. This is the key difference between the mass spring oscillator and the rotating imbalance. In the mass spring oscillator, as the excitation frequency increased, the displacement of the mass decreased to the point where the inertial effects of the mass dominated the motion. On the other hand, as the rotation frequency of the rotating imbalance system increased, the displacement remained the same, while the velocity of the mass increased accordingly. This observation is also seen in the differences in the resonant plots for each system. The mass spring oscillator has a response plot that decays to zero with an increase in excitation frequency (above the natural frequency). The rotating imbalance has a response plot that decays to some value that is not zero with

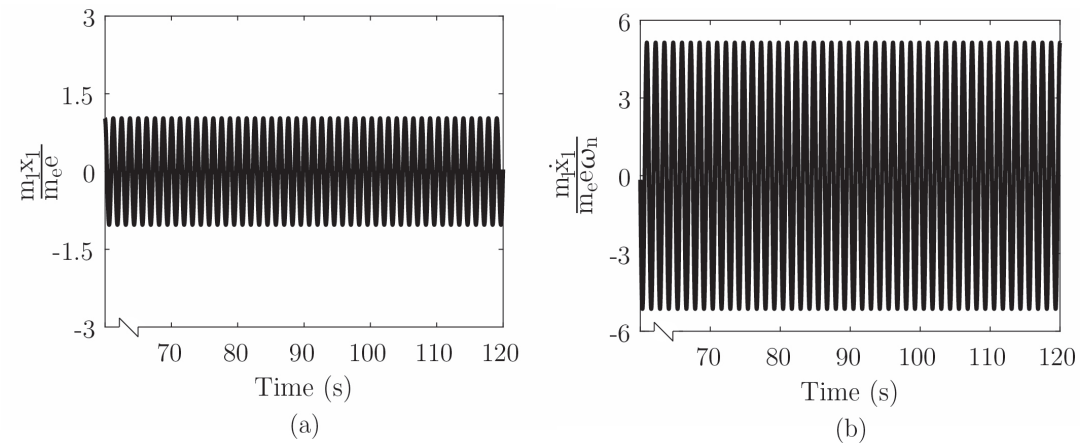

FIGURE 12 – The Displacement (a) and Velocity (b) of a Rotating Imbalance System at Five Times the Natural Frequency

an increase in excitation frequency (above the natural frequency). This difference is the reason why balancing devices are used in rotating applications. The residual displacement offset at rotational speeds above the natural frequency is undesirable, thus a balancing device aims to reduce this motion to acceptable levels.

This initial investigation is useful in reviewing simple kinematic motion and understanding the differences between a translational system versus a rotational system. The fundamentals that were presented are very simple; the one degree of freedom models can be applied to more complex systems. As can be imagined, the final ball balancer model that will be developed has many degrees of freedom and is rotational in nature; however the fundamentals for how each ball moves in the presence of damping/external forces and the rotational behavior of the system is the same as in more simple cases, like those seen in this chapter.

III. COLLISION AND SEPARATION CAPTURE TECHNIQUE

A. Introduction

Shown previously, the nature of rotational applications motivates the use of a balancing device. As stated previously, the model presented in this paper is a ball-type balancing device. To model more accurate ball behaviors as explained in Chapter I, a method to reliably and accurately compute the collisions and separations must be utilized. The following chapter details the design of the algorithm that will be used to detect a collision between two balls or a separation of a train of balls.

B. Poincaré Mapping

Traditionally, physical phenomena are always thought to advance by time. As seen in Chapter II, dynamic systems are typically written with respect to time. A problem usually is written to have time dependencies and be numerically and analytically plotted by time. More specifically, the state variables (i.e. displacement and velocity) are the dependent variables, while time is the independent variable. Normally, the dependent variables are plotted with respect to time to show how they change as the physical system progresses. However, it is also useful to plot these three variables in a three dimensional space where one can clearly see how the dependent variables change with respect to each other as well as with respect to the independent variable.

Referring to Figure 13, plotting an arbitrary function in three dimensions shows how the dependent variables, in the $\tilde{x}$ and $\tilde{y}$ directions, vary with respect to the independent variable in the $\tilde{z}$ direction. If a plane is placed at a value in the $\tilde{z}$ direction at a value of S, the intersection of the function and the plane can be called point P_S and has some value (x_S, y_S, z_S). It is clear that any section can cut through the function so that the resulting values of the function are returned. Say one is most interested when the value in the $\tilde{z}$ direction equals a different value S', then the exact value of the function can be labeled point P'_S.

To add some realism, now say that the $\tilde{x}$ direction represents the displacement of a mass, the $\tilde{y}$ direction represents the velocity of a mass and the $\tilde{z}$ represents time. Again, a section can be taken at any value of time such that the displacement and velocity of the mass can be computed. It turns out that this is exactly how traditional time stepping discretization routines work. A series of planes are placed some specified time step apart from each other, over some time period. Time integration is useful in most cases, however in some other problems (ones

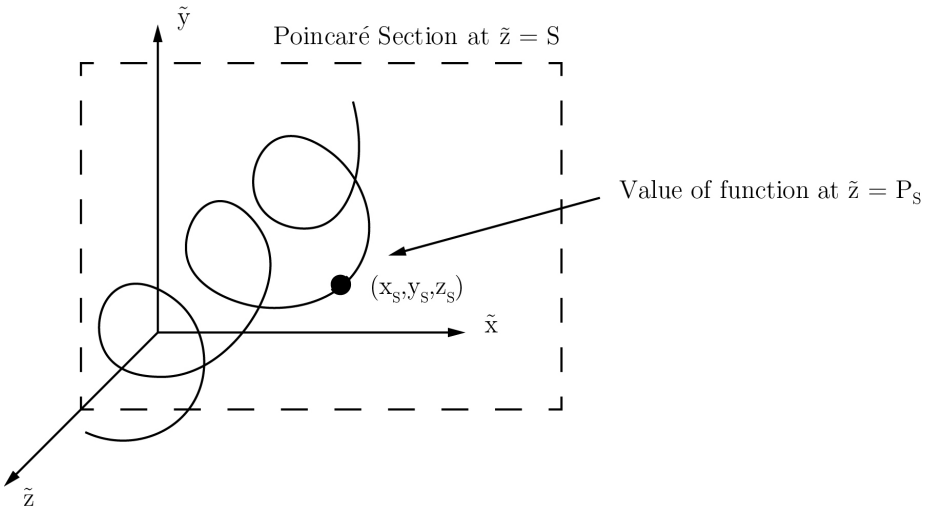

FIGURE 13 – Schematic of a Poincaré Section Taken at Some Location in the $\tilde{z}$ Direction

that contain discontinuities), it is more useful to discretize by some other variable within the problem instead of time. When discretizing by a different variable, one is simply moving the sampling section into a different plane, so that instead of sampling the function in the $\tilde{x}$-$\tilde{y}$ plane (as in the previous example), the function is sampled in some other plane ($\tilde{x}$-$\tilde{z}$ or $\tilde{y}$-$\tilde{z}$). This technique is more commonly known as Poincaré sectioning or Poincaré mapping (Tucker 2002). Poincaré sectioning is not only a great way to describe and illustrate how a discretization method works, but also serves to show how the variables of a problem can be manipulated such that a new independent variable can be chosen. Clearly, it can be seen that if one wants to know the displacement and velocity at some arbitrary time, this can be directly calculated analytically or calculated numerically by integration. One would simply substitute a time value into the analytical solution or time step using a numerical model. However, say the condition of interest was to know when the displacement or the velocity was an arbitrary value; progressing the problem through time would not allow this to be captured accurately or with great confidence for any range of problems, especially by numerical integration. It would be more useful if the problem could progress through the variable that was most interesting, such as displacement or velocity.

Poincaré sectioning can be utilized in this case since space, rather than time, can be used to determine when to plot a point or take a measurement. This can be useful since the equations of motion can be easily manipulated to progress according to whatever variable is most useful.

C. State Variable Transformation

To begin applying this method to the ball balancer model, a brief explanation will be given of a mathematical technique used to convert a collection of traditional "time-stepping" equations into a set of "any-variable-stepping" equations. As explained by Henon, by a simple alteration, a dependent variable can be converted into an independent variable by a simple manipulation of the equations of motion. The method to convert a set of equations is described below, where x_N is the variable that will become the independent variable and f_i is the ith equation within a set of arbitrary equations,

$$\frac{dx_1}{dx_N} = \frac{f_1}{f_N}$$

$$\vdots$$

$$\frac{dx_{N-1}}{dx_N} = \frac{f_{N-1}}{f_N}$$

$$\frac{dt}{dx_N} = \frac{1}{f_N}$$

D. Collision Capture Technique

To further understand the power of this transformation, first consider an unforced mass spring system. Recall that in first order form, the equations of motion (with respect to time) for this system were shown in Equations 4 and 5,

$$\dot{u}_1 = \frac{dx_1}{dt} = u_2$$

$$\dot{u}_2 = \frac{d^2x_1}{dt^2} = -2\zeta_1\omega_{n_1}u_2 - {\omega_{n_1}}^2 u_1$$

As an example, these equations can be converted to a displacement stepping scheme according to the Henon method, where x_N is the displacement x_1. The result is the following set of equations shown in Equations 24 and 25, where the superscript $'$ denotes a derivative with respect to x_1,

$$u_1' = \frac{dt}{du_1} = \frac{1}{u_2} \tag{24}$$

$$u_2' = \frac{du_2}{du_1} = -2\zeta_1\omega_{n_1} - {\omega_{n_1}}^2 \frac{u_1}{u_2} \tag{25}$$

These equations now describe the motion of an unforced mass spring system in terms of the displacement of the mass, rather than in terms of time. The use of this transformation is very valuable when determining discontinuities in dynamic events and is the foundation of

how the algorithm that will be used to solve for collisions between balls in this ball balancer model. The implementation of this manipulation will be validated for use in collisions using one dimensional systems in Chapter IV. This manipulation method will eventually be applied to the equations of motion for the ball balancer in Chapter VI such that the collisions between balls can be captured.

E. Separation Capture Technique

The method to capture a separation is slightly more complicated than simply using the method outlined by Henon as was done for a collision. To illustrate this complexity, a two mass system will be analyzed according to Figure 14,

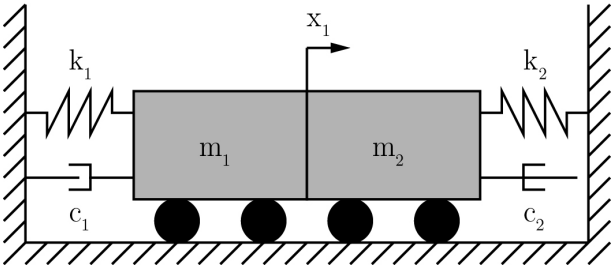

FIGURE 14 – Schematic of a Contacting Two Mass System

The equations of motion that describe the motion of each individual mass can be written in second order form as seen in Equations 26 and 27. Note that the displacement, velocity and acceleration of both masses are equal since they are moving as one body. It can be seen that an equal and opposite interaction force exists between the two masses since they are contacting each other,

$$m_1\ddot{x}_1 + c_1\dot{x}_1 + k_1x_1 = -F_I \tag{26}$$

$$m_2\ddot{x}_1 + c_2\dot{x}_1 + k_2x_1 = F_I \tag{27}$$

Equations 26 and 27 can be added to obtain the equation of motion for the two mass system moving together in second order form,

$$(m_1 + m_2)\,\ddot{x}_1 + (c_1 + c_2)\,\dot{x}_1 + (k_1 + k_2)\,x_1 = 0 \tag{28}$$

From a physical perspective, the separation of the two masses is governed by the interaction force that exists between the two masses. When the interaction force equals zero, the masses will separate from one another. In order to utilize the Henon method, the time differentiated interaction force ($\dot{F}_I$) must be present in the equations of motion. Unfortunately, Equations 26, 27 and 28 are not able to accommodate the use of the Henon method. Although

Equations 26 and 27 do contain the interaction force, neither of these equations contain the time differentiated form of the interaction force. On the other hand, Equation 28 does not contain the interaction force at all. These two issues present a problem; neither traditional form of the equations of motion for the two mass system can accommodate the use of the Henon method. Luckily, a different method can be utilized to obtain a set of equations of motion that can accommodate the use of the Henon method. The process outlined by Dedow and Murphy is able to address this issue. By implementing the Dedow-Murphy method, the time differentiated interaction force can be exposed. This allows the the implementation of the Henon method to capture a separation. The Dedow-Murphy method simply takes an additional time derivative of the equations of motion that define the motion of each individual mass, resulting in a set of equations that are of third order. The equations of motion for the two mass system that expose the time differentiated interaction force are shown in Equations 29, 30, 31 and 32. These equations are taken directly from (Dedow and Murphy 2016),

$$\dot{u}_1 = \frac{dx_1}{dt} = u_2 \tag{29}$$

$$\dot{u}_2 = \frac{d^2x_1}{dt^2} = \frac{-c_1u_2 - k_1u_1 - F_I}{m_1} \tag{30}$$

$$\dot{u}_3 = \frac{d^3x_1}{dt^3} = \frac{-c_1u_3 - k_1u_2 - \dot{F}_I}{m_1} \tag{31}$$

$$\dot{u}_4 = \frac{dF_I}{dt} = m_2\dot{u}_3 + c_3u_3 + k_2u_2 \tag{32}$$

The equations above can be recast into a set of force-stepping equations of motion by applying the Henon method such that the variable of interest is the interaction force. Although slightly more complicated, the Dedow-Murphy method (along with the Henon method) allows for an exact calculation of a separation of two bodies. The implementation of this combined method will be validated for use in separations using one dimensional systems in Chapter V. The Dedow-Murphy method will eventually be applied to the equations of motion for a train of balls in Chapter VI.

IV. COLLISION CAPTURE VALIDATION

A. Introduction

The following chapter details the validation of the collision algorithm that will be used in the ball balancer model. This algorithm is designed to detect when any two adjacent balls collide into one another during any point in the operation of the ball balancer. The technique used to model the separation of any two balls will be validated next in Chapter V. This chapter presents a numerical validation regarding the application of the Henon method to collisions with two different examples. The first example is a mass that is able to collide with a stationary wall. The second example involves two masses that are able to collide with each other. These cases will illustrate how the collision algorithm works and ensure that the model calculates the exact moment of the collision.

B. Explanation of Collision Technique

To show how the Henon transformation can be used to accurately capture collision events, first say that there is an unforced, mass spring system with no damping. Along with the mass spring system, there is a wall located at $\frac{x_1}{x_{1_0}} = 0$ such that each time the mass returns to $\frac{x_1}{x_{1_0}} = 0$, there is a collision; an introduction of a discontinuity to the system. Assume that the stiffness of the wall is much greater than the stiffness of the spring in the mass spring system such that the collision will always occur at $\frac{x_1}{x_{1_0}} = 0$. Note that a traditional time stepping solving scheme may not be able to capture the exact collision between the mass and the wall, this event is more accurately captured by displacement stepping solving method. A schematic of the system is shown below in Figure 15,

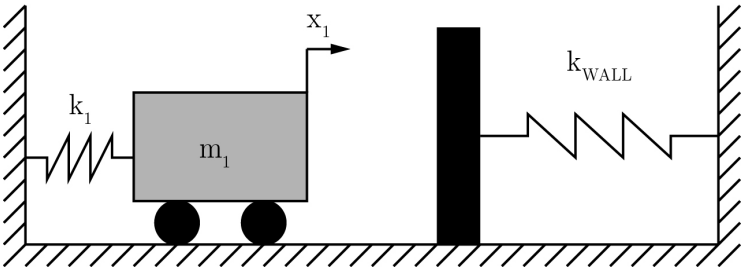

FIGURE 15 – Schematic of a Mass Colliding with a Stationary Wall

All the models presented in this paper, including the main ball balancer model, utilize a hybrid solving method that merges the computational speed of a time stepping routine, with the precision to capture discontinuities of the Henon method. Thus, the majority of the integration steps will be integrated by time, and minority of the steps will be integrated according to the Henon method. The reason for using a hybrid model is because an event necessitating a Henon step occurs somewhat infrequently, meaning that the majority of time steps do not have a collision occurring between them. So it makes sense that a "traditional" method be used unless an "untraditional" event occurs. Additionally, in the full ball balancer model, depending on the number of balls in the ball balancer, there will be many degrees of freedom. All variables are governed by time, thus it is computationally easier and more intuitive to progress the model through time and only use a Henon step when needed.

1. Collision With a Stationary Wall

The stationary wall problem will rely on a time stepping scheme when the mass resides far from the wall, and a displacement stepping scheme when the mass is about to touch the wall. To utilize this hybrid solving model, the gap between the mass and the wall is monitored at every integration step to ensure that the mass has not passed through the wall. This allows the solver to know exactly when to switch to the displacement stepping set of equations of motion. Of course, there are many ways to monitor for when the mass hits the wall. For simplicity, a collision will be detected when the gap between the mass and the wall becomes negative (the mass has passed through the wall). When this happens, the previous time integration step will be recalled, at which point the displacement stepping equations will be used to take one displacement step equal to the remaining gap so that the exact collision is captured. A schematic is shown in Figure 16 that describes this pictorially. Once the collision is captured, an isolated system assumption is made and a coefficient of restitution assumption is used to calculate the outgoing velocity of the mass. The coefficient of restitution assumes negligible deformation of the mass and wall (stiffness of mass and wall are much greater than stiffness of the spring) and that there is some proportional decrease in velocity of the mass.

The equations for the time stepping region were derived in Equations 4 and 5 in Chapter II. Likewise, the equations for the displacement stepping region were derived in Equations 24 and 25 in Chapter III. The conditions for this test case are as follows: $\zeta_1 = 0$, $\omega_{n_1} = 4.5$ rad/s, $x_1(0) = x_{1_0}$, $\dot{x}_1(0) = \dot{x}_{1_0}$ and $COR = 0.80$. The non-dimensionalization of this system is the same as was seen in the mass spring oscillator system in Chapter II.

To illustrate how the collision of the mass with the stationary wall can be captured by a numerical solving method, the following plots were generated for the stationary wall system.

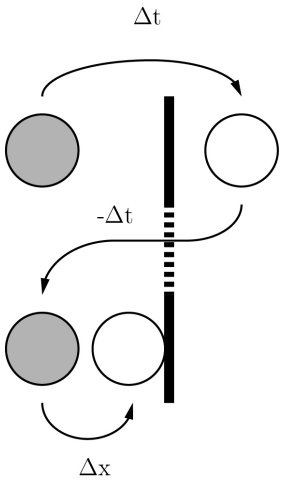

FIGURE 16 – When a Collision is Detected, the Solver Takes a Time Step Backwards, then a Displacement Step to the Point of Collision

Figure 17 shows the displacement and velocity of the mass plotted with respect to time. It can be seen that using the hybrid solving method, the collisions are accurately captured each time the mass hits the wall, where the collisions are depicted as circles. It can also be seen that the amplitude of the displacement of the mass decays after each collision. Since this system is unforced and undamped, the decay is completely due to the coefficient of restitution assumed for the system, thus there is a loss in energy every collision. Theoretically, the mass will continue to collide into the wall as time goes to infinity with smaller and smaller amplitudes. Realistically, the mass will eventually settle and stop moving, however this model does not account for other forms of damping and energy loss that would cause the eventual cease of motion,

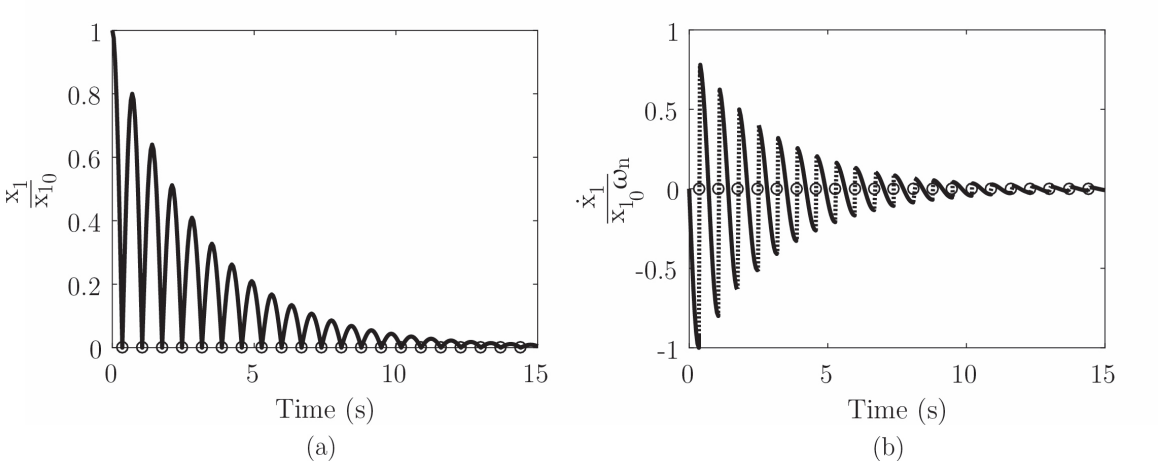

FIGURE 17 – The Displacement (a) and Velocity (b) of the Mass Colliding with a Stationary Wall

Zooming in and looking at the individual data points near the first collision, it can be seen how the integration steps clearly capture the collision. When the mass is far from the wall,

the problem progresses according to the time stepping method ($\Delta t = 0.050$ s). However, the step to the wall is captured by a Henon displacement step ($\Delta t = 0.001$ s) which is smaller than the global time step. The transition and change in integration step size are shown in Figure 18 where the circles represent the integration steps,

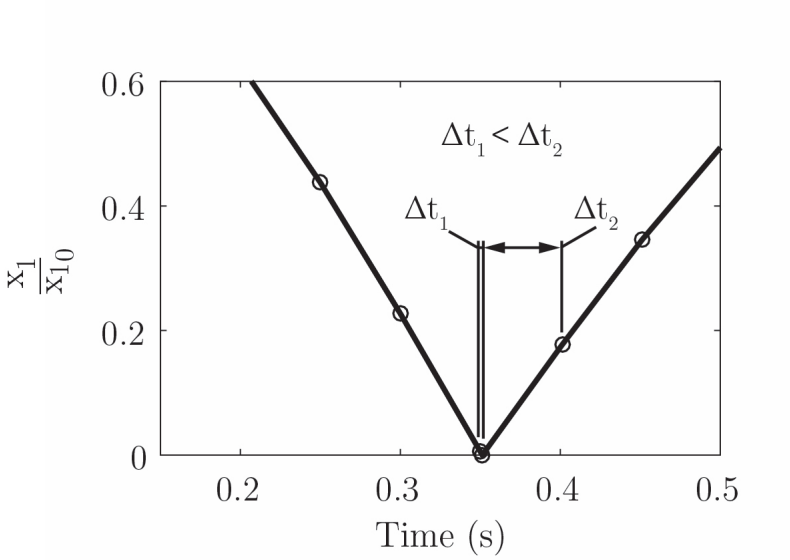

FIGURE 18 – A Zoomed In View of the Displacement of the Mass Colliding with a Stationary Wall

This simple model shows that the hybrid integration solving model can successfully capture the discontinuity of a collision and switch between the fast, time stepping solving method and the accurate, Henon displacement step. As with all techniques, this can be applied to more complicated systems. The next example covered will be a model of the motion of two masses that are able to collide with one another. Unlike the stationary wall problem where the collision always occurred at $\frac{x_1}{x_{1_0}} = 0$, the location of the collision in the two mass system can vary depending on the location of the two masses when they collide. Although a more complex model will be used to demonstrate the extension of the Henon displacement step, the general principles of the collision capture can be applied successfully.

2. Collision Between Two Masses

In the next case study, say there are two masses that are uncoupled, yet have the same resting equilibrium at $\frac{x_1}{x_{1_0}} = \frac{x_2}{x_{2_0}} = 0$. From this point forward, the mass to the left will be considered mass one, while the mass to the right will be considered mass two. Both mass one and mass two are unforced. Lastly, say that mass one is smaller than that of mass two, but the springs attached to each mass are equal. In the following simulation, mass one will be displaced to the left some set amount and will be released, while mass two will be displaced to the right

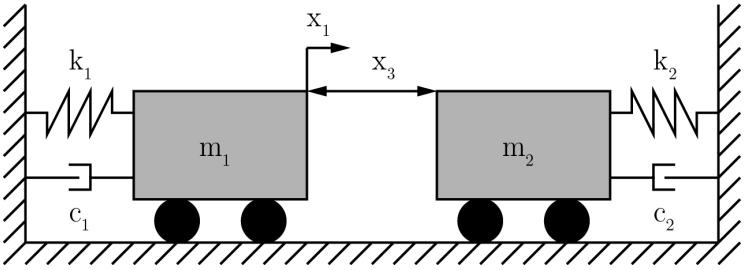

FIGURE 19 – Schematic of a Two Mass Collision

some amount and will be released. A schematic of the system is shown in Figure 19.

To use the collision technique described previously, the gap between the two masses must be monitored to check for a collision. In this case, the Henon displacement step relies on integrating with respect to the gap between the two masses. For this reason, the equations of motion must be written in terms of the relative coordinate that separates the two masses. The equations are written such that the state variables of mass one are global coordinates while the state variables of mass two are relative coordinates referenced from mass one. The equations of motion for the two mass system in relative coordinates are shown in Equations 33, 34, 35 and 36 in first order form,

$$\dot{u}_1 = u_2 \tag{33}$$

$$\dot{u}_2 = -\frac{k_1}{m_1}u_1 - \frac{c_1}{m_1}u_2 \tag{34}$$

$$\dot{u}_3 = u_4 \tag{35}$$

$$\dot{u}_2 + \dot{u}_4 = -\frac{k_2}{m_2}(u_1 + u_3) - \frac{c_2}{m_2}(u_2 + u_4) \tag{36}$$

These equations can be solved numerically as with the stationary wall case using a hybrid model where the majority of integration steps are completed with respect to time, while the integrations to the exact moment of the collisions are completed with respect to the gap between the two masses. The only difference is that the solver will monitor for the gap between the two masses, instead of the gap between the wall and a mass.

As was plotted for the stationary wall problem previously, Figure 20 is the plot of the absolute displacements and absolute velocities of the two masses with respect to time. The conditions for this test case are as follows: $\zeta_1 = 0.067$, $\zeta_2 = 0.047$, $\omega_{n_1} = 4.47$ rad/s, $\omega_{n_2} = 3.16$ rad/s, $x_1(0) = x_{1_0}$, $x_2(0) = -x_{1_0}$, $\dot{x}_1(0) = \dot{x}_{1_0}$, $\dot{x}_2(0) = -\dot{x}_{1_0}$ and $COR = 0.80$. Note that the non-dimensionalization of the displacement and velocity in this system uses the average natural frequency of the two independent systems, $\omega_{n,AVG} = \frac{\omega_{n_1}+\omega_{n_2}}{2}$. It is clearly seen that the collisions are captured accurately. It's also interesting to see how the location of the collision

changes through time as well. Any asymmetry introduced into the system due to different masses or springs will cause a shifting collision location,

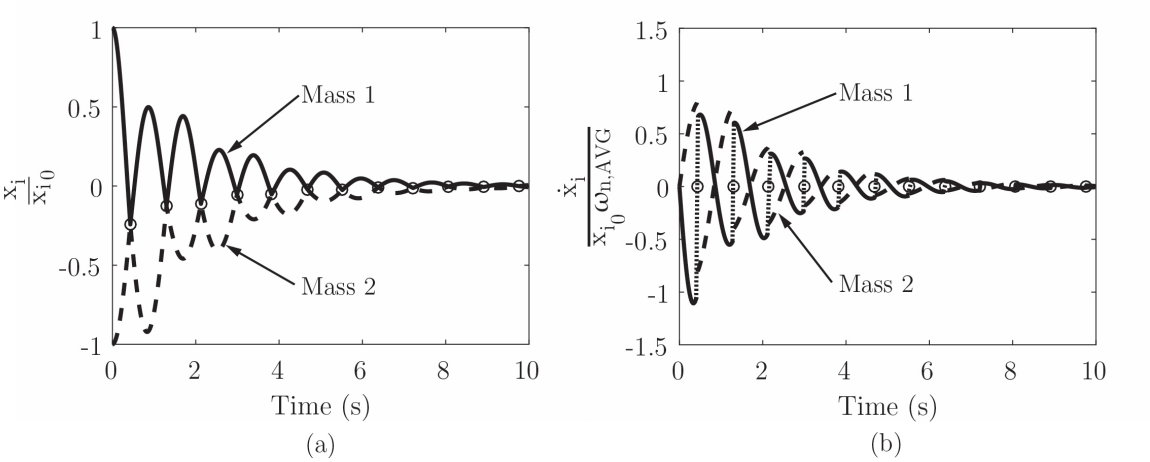

FIGURE 20 – The Displacement (a) and Velocity (b) of the Two Masses Colliding

Upon a closer look, it can be seen how the solver converts from a time stepping integration step to a Henon displacement integration step. When the masses are far from contacting, the problem progresses according to the time stepping method ($\Delta t = 0.010$ s). However, the step to the collision is captured by a Henon displacement step ($\Delta t = 0.009$ s) which is smaller than the global time step. The Henon displacement step captures the collision between the two masses exactly as seen in Figure 21 where the circles represent the integration steps,

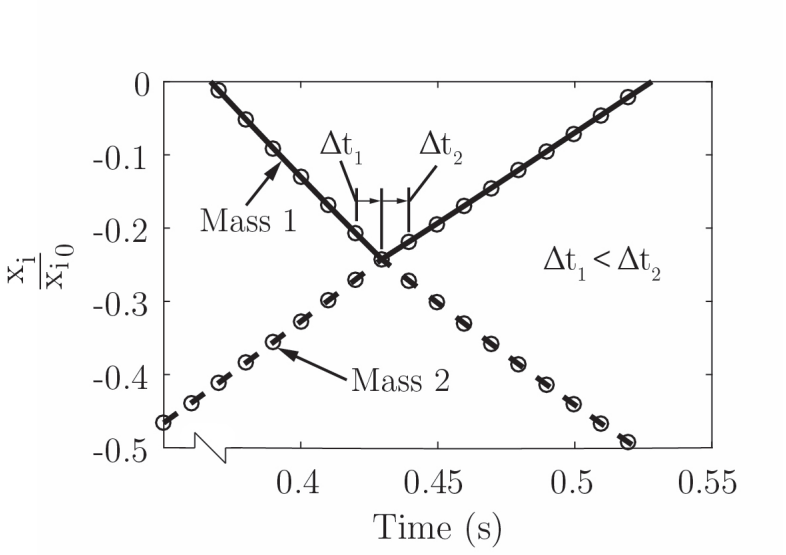

FIGURE 21 – A Zoomed In View of the Displacement of the Two Masses Colliding

It can be seen that the hybrid solving method can be used to capture a collision moving through space and time; all that needs to be done is monitor for the relative displacement

between two bodies. The more complicated ball balancer model is simply an extension of this example. Instead of two masses, there will be n number of balls in the ball balancer that can all collide with their neighboring balls. Instead of the collisions occurring on a linear scale as seen with the simple mass spring examples above, the location of the collision can be anywhere from 0 to 2π rad within the ball balancer. Next, it will be shown that the same method used to capture collisions can be used to capture train separations. Simply an adjustment to the equations of motion needs to be implemented.

V. SEPARATION CAPTURE VALIDATION

A. Introduction

The following chapter details the validation of the separation algorithm that will eventually be used in the presented ball balancer model. This algorithm is designed to detect when a single train separates into two trains during any point in the operation of the model. This paper will refer to a "train" as a collection of masses or balls that exhibit prolonged physical contact with a neighboring mass or ball. The bodies within a train all have the same velocity and acceleration at any instant in time. A numerical validation of the separation method is presented by enlisting two examples. The first example is a two mass system where the two masses begin with the same initial conditions. The second example is two mass system where the two mass begin with unique initial conditions such that a grazing condition results.

B. Explanation of Separation Technique

To show how the Henon method can be used to accurately capture a separation event, the previous two mass spring system discussed in Chapter IV will be revisited. For the first example, the initial conditions of the two masses are the same, however the spring stiffnesses acting on each mass are different, such that $k_1 > k_2$. Due to the selection of the initial conditions and the spring stiffnesses, the two masses move together up to the moment when the interaction force between the masses becomes zero, at which point the masses will separate and move as separate bodies. The model will time step according to Equations 29, 30, 31 and 32 using a traditional integration method until the separation event is detected. The separation event will be detected when the interaction force between the two masses goes from positive to negative. When a separation is detected, the model will back up a time step, recall the previous condition of the system and take a force step to the exact moment of separation. Again, note that a traditional time stepping solving scheme will not be able to capture the exact separation accurately between the two masses, this event is more accurately captured by force stepping solving method. The force stepping set of equations of motion for a two mass spring system were derived by Dedow and Murphy. A schematic of the two mass system is again shown in Figure 22. The following parameters are selected for use in both of the test cases presented in this chapter: $\omega_{n_1} = 0.63$ rad/s, $\omega_{n_2} = 0.45$ rad/s, $\zeta_{n_1} = 0.16$, $\zeta_{n_2} = 0.22$ and $COR = 0.80$.

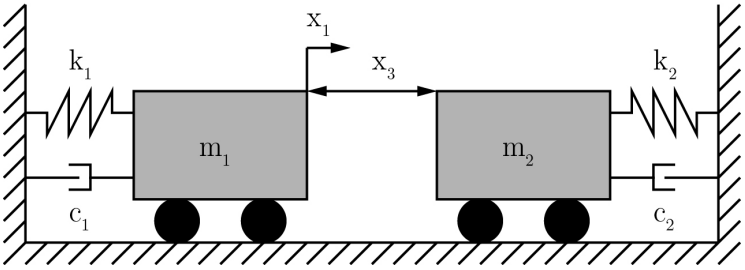

FIGURE 22 – Schematic of Two Masses Separating

1. Two Masses with the Same Initial Conditions

As was mentioned previously, the two mass problem will rely on a time stepping scheme for when the two masses are contacting, and a force stepping scheme when the two masses are about to separate. To utilize this hybrid solving model, the interaction force between the two masses is monitored at every integration step to ensure that the two masses have not separated. This allows the model to know exactly when to switch to a force stepping scheme. When this occurs, the previous time step will be recalled, at which point the force stepping equations will be used to take one force step equal to the remaining normal force between the two masses such that the exact separation is captured. This is same method that was used with the collision capture, the only difference is the integration variable.

In the first validation case, the two masses are released together and are allowed to separate naturally whenever separation occurs. The initial conditions for the two masses are $x_1(0) = x_2(0) = x_{1_0}$ and $\dot{x}_1(0) = \dot{x}_2(0) = \dot{x}_{1_0}$. The equations of motion for the region where the masses are contacting were derived in Equations 29, 30, 31 and 32. The equations of motion for the region where the masses are not contacting were derived in Equations 33, 34, 35 and 36. Lastly, the equations of motion for the force stepping integration were derived by Dedow and Murphy. To illustrate how the separation of the two masses can be captured by a numerical solving method, the following plots were generated for the system. Figure 23 shows the displacement and velocity of the masses with respect to time, as well as the normal force acting between the masses with respect to time. Note that the non-dimensionalization of the displacement and velocity is according to the average natural frequency of each mass system and the non-dimensionalization of the interaction force is according to the average initial spring force, $F_I^* = \frac{2F_{I_1}}{(k_1+k_2)x_{1_0}}$.

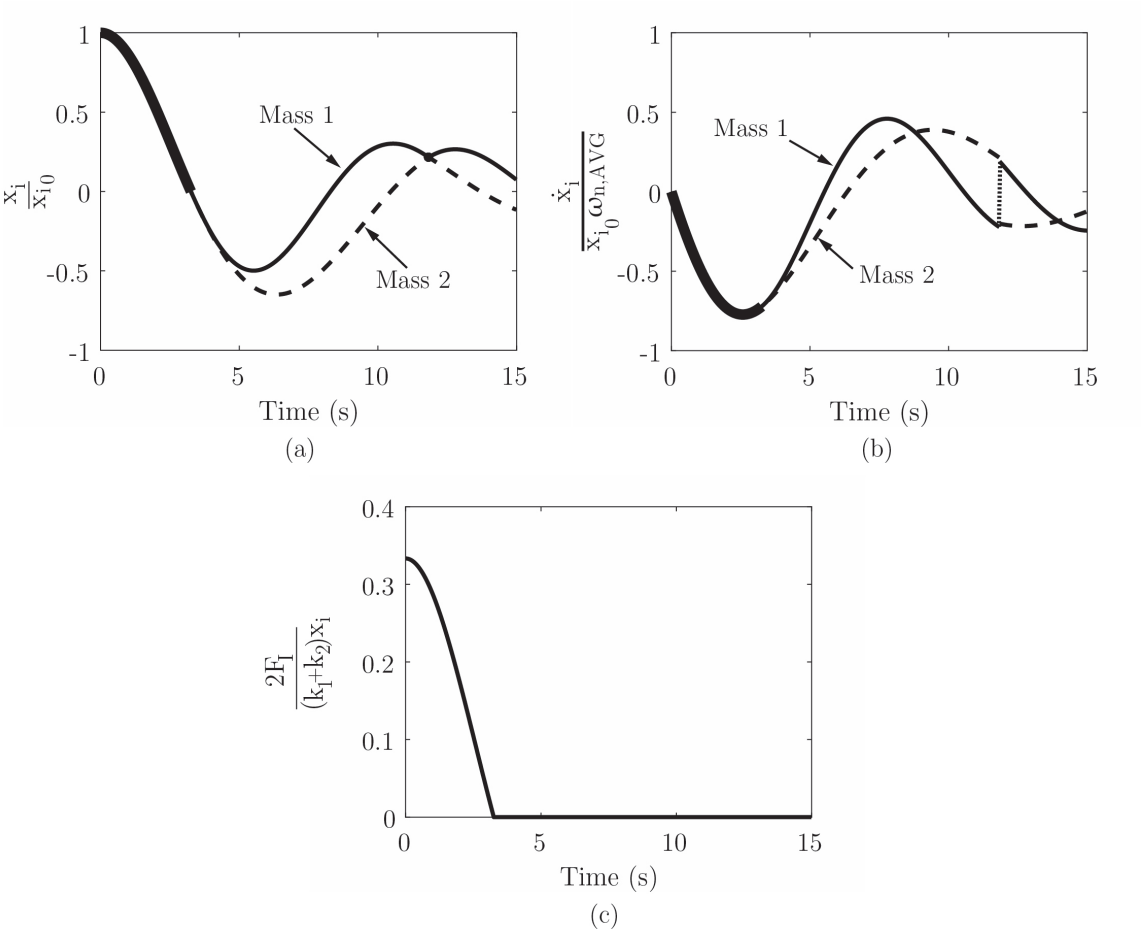

FIGURE 23 – The Displacement (a), Velocity (b) and Interaction Force (c) for the Two Masses in the Same Initial Conditions Case. The Solid Line Denotes Mass One and the Dotted Line Denotes Mass Two. The Thick Line in (a) and (b) Denotes the Region where the Masses are Touching

It can be seen that the two masses are indeed moving together during the first phase of the motion. At some point the interaction force goes to zero and the masses begin to separate. Once separated, the masses now behave as two independent bodies moving free of the other mass. It can be seen that at some time later, a collision is identified ($t = 12$ s). Once the collision is identified, the coefficient restitution assumption is applied ($COR = 0.80$) such that the outgoing velocities of the masses are reduced, but no sticking occurs.

Zooming in and looking at the individual data points near the separation, it can be seen in Figure 24 how the integration steps clearly captures the separation event. When the masses are far from the separation, the problem progresses according to the global time step ($\Delta t = 0.010$ s). However, the step to the separation is captured by a Henon force step ($\Delta t = 0.008$ s) which is smaller than the global time step. The transition and change in integration step size is shown below,

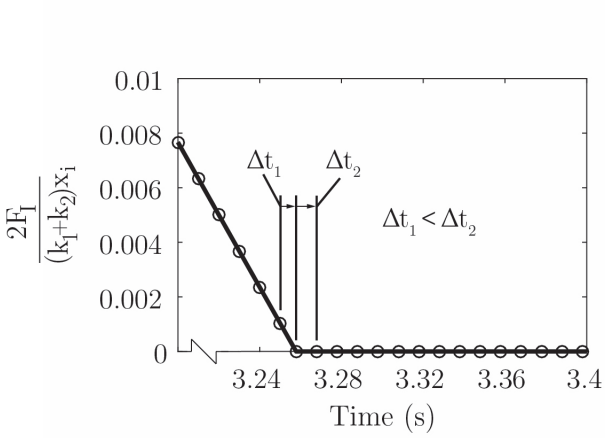

FIGURE 24 – A Zoomed In View of the Interaction Force Between the Two Masses when the Separation Occurs

This simple model shows that the hybrid integration solving model can successfully capture the discontinuity of a separation and can switch between the fast, time stepping solving method and the accurate, Henon force step. Similar to the collision technique, the separation technique can be applied to more complicated systems. The next example covered will be the same model of the motion of two masses, however a grazing condition develops. Unlike the "same initial conditions" problem, the two masses start out as singular bodies, but form a train during the simulation, then separate again. Although a more complex case will be used to demonstrate the extension of the Henon force step, the general principles of the separation capture can be applied successfully.

2. Two Masses Develop a Grazing Condition

In the second case, the two masses start out with different initial conditions. However, the initial conditions are chosen such that the masses graze one another allowing a collision with equal outgoing velocities. The initial conditions for the two masses are $x_{1_0} = 0.879773$ ft, $x_{2_0} = 3.768875$ ft, $\dot{x}_{1_0} = 1.611922$ ft/s and $\dot{x}_{2_0} = 0.325024$ ft/s. To illustrate how the separation of the two masses can be captured by a numerical solving method, the following plots were generated for the system. Figure 25 shows the plots of the displacement and velocity of the masses with respect to time, as well as the normal force acting between the balls with respect to time.

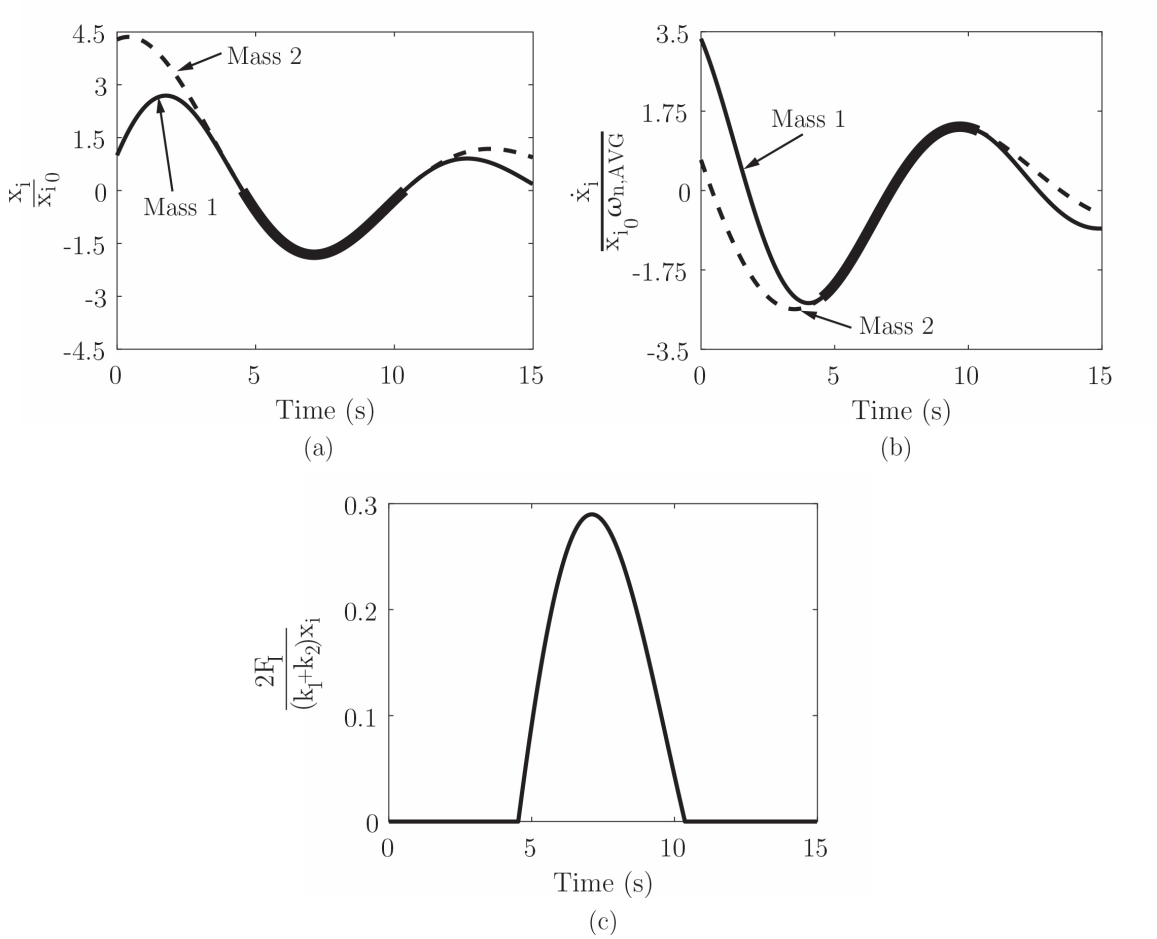

FIGURE 25 – The Displacement (a), Velocity (b) and Interaction Force (c) for the Two Masses in the Grazing Condition Case. The Solid Line Denotes Mass One and the Dotted Line Denotes Mass Two. The Thick Line in (a) and (b) Denotes the Region where the Masses are Touching

It can be seen from Figure 25 that the two masses start out separated during the first phase of the motion and behave as two independent bodies. At some point the masses graze one another and begin moving together, thus the interaction force becomes non-zero indicating that a force is being exerted from one mass to the other. The masses continue to move together until the interaction force becomes zero again. Once separated, the masses now behave as two independent bodies moving free of the other mass.

Zooming in and looking at the individual data points near the separation, it can be seen in Figure 26 how the integration steps clearly captures the separation event. When the masses are far from the separation, the problem progresses according to the global time step ($\Delta t = 0.010$ s). However, the step to the separation is captured by a Henon force step ($\Delta t = 0.006$ s) which is smaller than the global time step. The transition and change in integration step size is seen in Figure 26.

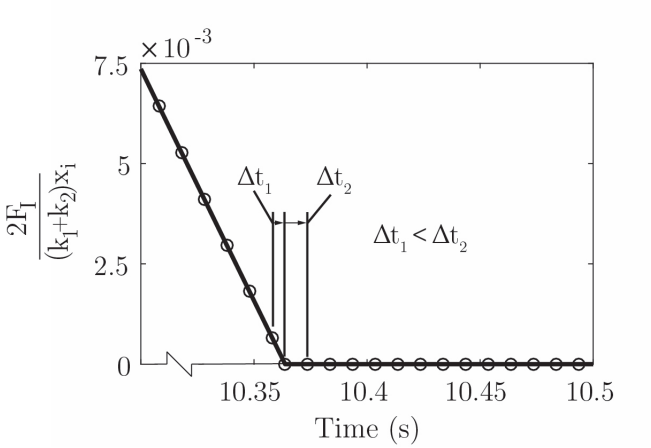

FIGURE 26 – A Zoomed In View of the Interaction Force Between the Two Masses when the Separation Occurs

As with the "same initial conditions" case, it can be seen that the hybrid solving method can be used to capture a separation moving through space and time; all that need be done is to monitor the interaction force between two bodies. The more complicated ball balancer model is simply an extension of this example. Instead of two masses, there will be n number of balls in the ball balancer that can all form trains and separate with their neighboring ball. Instead of the separations occurring on a linear scale as seen with the simple mass-spring examples above, the location of the separation can be anywhere from 0 to 2π rad within the ball balancer. The next step is to extend this discontinuity-capturing method explained for collisions and separations to the ball balancer equations of motion. To do this, the ball balancer equations must be derived.

VI. EQUATIONS OF MOTION OF THE BALL BALANCER MODEL

A. Introduction

The following chapter details the derivation of the equations of motion for the vertically-oriented ball balancer model presented in this paper. The derivation uses a Lagrangian energy approach. The ball balancer presented is a single rotor system that can move horizontally, vertically and rotationally about its center. n number of balls can be present, which are fixed at some specified radius R from the center of rotation of the ball balancer and are assumed to move purely angularly. The rotational inertia of the balls is taken into account as well as the rolling friction between the balls and the ball balancer. Translational damping acts on the ball balancer and viscous drag acts on the balls. Additionally, the equations of motion used for train separation are derived by applying the Dedow-Murphy method such that a set of force stepping equations can be obtained.

B. Simplified Reference Frames

The ball balancer system can be described by six simplified reference frames which will be discussed below. These six reference frames allow for the proper derivation of the equations of motion that will fully describe the motion of the ball balancer and the balls during operation. The first reference frame is centered at point F and is orientated according to $\mathbf{I}_k$. This is the global frame that governs the ball balancer model,

$$\psi_0 = \{F; \mathbf{I}_k\}$$

Point F describes the location of the geometric center of the ball balancer in an undeformed state. Additionally, this reference frame governs the angular motion of the ball balancer as it spins about Point F. A schematic of reference frame ψ_0 can be seen in Figure 27a.

The second reference frame is centered at point O and is orientated according to $\mathbf{i}_k$. This is the first child frame for the ball balancer model,

$$\psi_1 = \{O; \mathbf{i}_k\}$$

Point O describes the center of gravity of the ball balancer when there is an eccentric

mass present in the ball balancer. The shift in center of gravity is caused by eccentricities due to inherent manufacturing defects or rotational imbalances in the ball balancer. This reference frame describes the motion of the shifted center of gravity in an undeformed state. A schematic of reference frame ψ_1 can be seen in Figure 27a.

The third reference frame is centered at point F' and is orientated according to $\mathbf{j}'_k$. This is the second child frame for the ball balancer model,

$$\psi_2 = \{F'; \mathbf{j}'_k\}$$

Point F' describes the motion of the geometric center of the ball balancer in a deformed state, that is when it has moved some amount in the horizontal and/or vertical directions. A schematic of reference frame ψ_2 can be seen in Figure 27b.

The fourth reference frame is centered at point O' and is orientated according to $\mathbf{i'}_k$. This is the third child frame for the ball balancer model,

$$\psi_3 = \{O'; \mathbf{i'}_k\}$$

Point O' is the center of gravity of the ball balancer when there is an eccentric mass present and when the ball balancer is in a deformed state. Again, the eccentricity is caused by inherent manufacturing defects or rotational imbalances in the system. A schematic of reference frame ψ_3 can be seen in Figure 27a.

The fifth reference frame is centered at point P_1 and is orientated according to $\mathbf{e}_k$. This is the fourth child frame for the ball balancer model, where it is understood that the local polar reference frame $\mathbf{e}_k$ refers to the local reference frame for each respective ball,

$$\psi_4 = \{P_1; \mathbf{e}_k\}$$

Point P_1 describes the motion of the first (global) ball as it travels around the ball balancer. Note that in the ball balancer model presented in this paper, the state variables used to describe the motion of the global ball are global coordinates, while the state variables that describe any additional ball are relative coordinates with respect to the previous, neighboring ball. A schematic of reference frame ψ_4 can be seen in Figure 27b.

The sixth reference frame is centered at point P_j and is orientated according to $\mathbf{e}_k$. This is the fifth child frame for the ball balancer model, where it is understood that the local polar

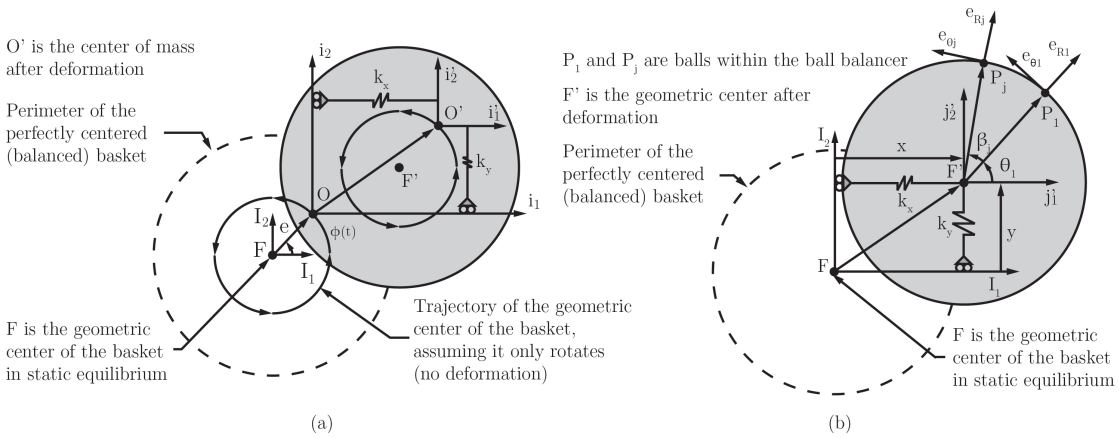

FIGURE 27 – Schematic (a) and Schematic (b) Show the Reference Frames Used to Simplify the Ball Balancer Model

reference frame $\mathbf{e}_k$ refers to the local reference frame for each respective ball,

$$\psi_5 = \{P_j; \mathbf{e}_k\}$$

Point P_j describes the motion of the jth ball as it travels around the ball balancer. The state variables that describe any additional ball are relative coordinates with respect to the previous, neighboring ball. A schematic of reference frame ψ_5 can be seen in Figure 27b.

C. Velocity of Points O', P_1 and P_j

The velocities of points O', P_1 and P_j are derived below which will be used in the development of the kinetic energy expressions needed for the Lagrangian formulation. Again, point O' describes the motion of the deformed center of gravity of the ball balancer. The velocity of point O' can be written as seen in Equation 37, where $\mathbf{e}$ is the displacement vector defining point O' relative to point O, $\mathbf{v}_O$ is the absolute velocity of point O and $\dot{\boldsymbol{\phi}}$ is the rotation of point O' relative to the ψ_1 reference frame,

$$\mathbf{v}_{O'} = \frac{\delta \mathbf{e}}{\delta t} + \mathbf{v}_O + \dot{\boldsymbol{\phi}} \times \mathbf{e} \tag{37}$$

This expression can be simplified to Equation 38 since $\mathbf{e}$ is fixed with respect to point O. The velocity of point O' is simply the global motion of point O, plus the relative motion of point O' relative to point O. The simplification of the velocity expression for point O' is shown below,

$$\mathbf{v}_{O'} = \frac{\delta \overset{0}{\mathbf{e}}}{\delta t} + \mathbf{v}_O + \dot{\boldsymbol{\phi}} \times \mathbf{e}$$

$$\mathbf{v}_{O'} = [\dot{x}\mathbf{i}_1 + \dot{y}\mathbf{i}_2] + [-e\dot{\phi}\sin(\phi)\mathbf{i}_1 + e\dot{\phi}\cos(\phi)\mathbf{i}_2]$$

$$\mathbf{v}_{O'} = (\dot{x} - e\dot{\phi}\sin(\phi))\mathbf{i}_1 + (\dot{y} + e\dot{\phi}\cos(\phi))\mathbf{i}_2 \tag{38}$$

Point P_1 describes the motion of the global ball, which defines the global coordinate for the location of additional balls. The velocity of point P_1 can be written as seen in Equation 39, where $\mathbf{R}_1$ is the displacement vector defining the location of P_1 relative to point F', $\mathbf{v}_{F'}$ is the absolute velocity of point F', $\mathbf{\Omega}_1$ is the rotation of point F' relative to the ψ_0 reference frame, and $\dot{x}$ and $\dot{y}$ define the velocity of F' relative to the ψ_0 reference frame,

$$\mathbf{v}_{P_1} = \frac{\delta \mathbf{R}_1}{\delta t} + \mathbf{v}_{F'} + \mathbf{\Omega}_1 \times [\dot{x}\mathbf{I}_1 + \dot{y}\mathbf{I}_2] \tag{39}$$

This expression can be reduced to Equation 40 since ψ_2 does not rotate with respect to ψ_0 and P_1 is held at a fixed distance from point F'. The velocity of point P_1 is simply the global motion of point F', plus the relative motion of point P_1 relative to point F'. The simplification of the velocity expression for point P_1 is shown below,

$$\mathbf{v}_{P_1} = \frac{\delta \mathbf{R}_1}{\delta t} + \mathbf{v}_{F'} + \cancelto{0}{\mathbf{\Omega}_1 \times [\dot{x}\mathbf{I}_1 + \dot{y}\mathbf{I}_2]}$$

$$\mathbf{v}_{P_1} = [\cancelto{0}{\dot{R}\mathbf{e}_{R_1}} + R\dot{\theta}_1\mathbf{e}_{\theta_1}] + [\dot{x}\mathbf{i}_1 + \dot{y}\mathbf{i}_2]$$

$$\mathbf{v}_{P_1} = R\dot{\theta}_1[-\sin(\theta_1)\mathbf{i}_1 + \cos(\theta_1)\mathbf{i}_2] + [\dot{x}\mathbf{i}_1 + \dot{y}\mathbf{i}_2]$$

$$\mathbf{v}_{P_1} = (\dot{x} - R\dot{\theta}_1\sin(\theta_1))\mathbf{i}_1 + (\dot{y} + R\dot{\theta}_1\cos(\theta_1))\mathbf{i}_2 \tag{40}$$

The balls are assumed to roll as well as translate, thus the pure rotation of the balls must be added to the kinetic energy of the system. Assuming that the balls never slip, there is a fixed relationship between the angular velocity of the ball and the pure rotational velocity of the ball. Equation 41 shows the pure rotation of the ball in terms of the angular velocity of the ball, where ω_{P_1} is the pure rotation of the global ball about its center of mass,

$$\mathbf{q}_{P_1} = \omega_{P_1}\mathbf{i}_3$$

$$\mathbf{q}_{P_1} = \frac{R}{r}\left[\dot{\phi} - \dot{\theta}_1\right]\mathbf{i}_3 \tag{41}$$

Point P_j describes the motion of the jth ball relative to the position of the $(j-1)th$ ball. The velocity of point P_j can be written as seen in Equation 42, which is simply the global motion of point F', plus the relative angular motion of point P_j relative to point F'. θ_j describes

the global coordinate of the jth ball such that $\theta_j = \theta_1 + \sum_{j=2}^{n} \beta_j$, where β_j is the relative angular displacement of the jth ball to its neighboring ball,

$$\mathbf{v}_{P_j} = (\dot{x} - R\dot{\theta}_j \sin(\theta_j))\mathbf{i}_1 + (\dot{y} + R\dot{\theta}_j \cos(\theta_j))\mathbf{i}_2 \tag{42}$$

Similar to the pure rotation of the global ball, Equation 43 shows the pure rotation for any additional ball,

$$\mathbf{q}_{P_j} = \frac{R}{r}\left[\dot{\phi} - \dot{\theta}_j\right]\mathbf{i}_3 \tag{43}$$

D. Kinetic Energy Terms

Now that the velocities of the different bodies within the system have been derived, the kinetic energy terms can be written which will eventually be used in the Lagrangian expression. The total kinetic energy in the system is simply the sum of the kinetic energy of the ball balancer and of the balls,

$$T_{TOT} = T_{BB} + \sum_{i=1}^{n} T_{P_i}$$

First, the kinetic energy of the ball balancer is shown in Equation 44 using the expression for the velocity of point O',

$$T_{BB} = \frac{1}{2} m_{BB}(\mathbf{v}_{O'} \cdot \mathbf{v}_{O'})$$

$$T_{BB} = \frac{1}{2} m_{BB}[\dot{x}^2 + \dot{y}^2 + e^2\dot{\phi}^2 + 2e\dot{\phi}(\dot{y}\cos(\phi) - \dot{x}\sin(\phi))] \tag{44}$$

The kinetic energy of the balls are shown in Equation 45 using the expression for the velocity of point P_1 for the first ball and point P_j for any additional ball. Note that the kinetic energy of a ball is the sum of the translational kinetic energy and the pure rotational kinetic energy,

$$T_{P_i} = \frac{1}{2} m_{P_i}(\mathbf{v}_{P_i} \cdot \mathbf{v}_{P_i}) + \frac{1}{2} I_{P_i}(\mathbf{q}_{P_i} \cdot \mathbf{q}_{P_i})$$

$$\begin{aligned} T_P = {} & \frac{1}{2} m_{P_1}[\dot{x}^2 + \dot{y}^2 + R^2\dot{\theta}_1^2 + 2R\dot{\theta}_1(\dot{y}\cos(\theta_1) - \dot{x}\sin(\theta_1))] + \frac{1}{2} I_{P_1}\left[\frac{R}{r}\left(\dot{\phi} - \dot{\theta}_1\right)\right]^2 + \\ & \sum_{j=2}^{n}\left\{\frac{1}{2} m_{P_j}\left[\dot{x}^2 + \dot{y}^2 + R^2\dot{\theta}_j^2 + 2R\dot{\theta}_j(\dot{y}\cos(\theta_j) - \dot{x}\sin(\theta_j))\right] + \frac{1}{2} I_{P_j}\left[\frac{R}{r}\left(\dot{\phi} - \dot{\theta}_j\right)\right]^2\right\} \end{aligned} \tag{45}$$

Combining the kinetic energies of the ball balancer and the balls, the total kinetic energy

of the system can be written. The expression for the total kinetic energy is shown in Equation 46,

$$T_{TOT} = \frac{1}{2}m_{BB}[\dot{x}^2 + \dot{y}^2 + e^2\dot{\phi}^2 + 2e\dot{\phi}(\dot{y}\cos(\phi) - \dot{x}\sin(\phi))] + \frac{1}{2}m_{P_1}[\dot{x}^2 + \dot{y}^2 + R^2\dot{\theta}_1^2 + 2R\dot{\theta}_1(\dot{y}\cos(\theta_1) - \dot{x}\sin(\theta_1))] + \frac{1}{2}I_{P_1}\left[\frac{R}{r}\left(\dot{\phi} - \dot{\theta}_1\right)\right]^2 + \sum_{j=2}^{n}\left\{\frac{1}{2}m_{P_j}\left[\dot{x}^2 + \dot{y}^2 + R^2\dot{\theta_j}^2 + 2R\dot{\theta}_j(\dot{y}\cos(\theta_j) - \dot{x}\sin(\theta_j))\right] + \frac{1}{2}I_{P_j}\left[\frac{R}{r}\left(\dot{\phi} - \dot{\theta}_j\right)\right]^2\right\} \quad (46)$$

E. Potential Energy Terms

To complete the Lagrangian expression, the potential energy terms must now be written. As seen in the expression below, the total potential energy in the system is simply the sum of the potential energy of the springs in the system, and the gravitational potential of the ball balancer and balls,

$$V_{TOT} = V_{k_x} + V_{k_y} + V_{BB} + \sum_{i=1}^{n} V_{P_i}$$

First, the potential energies of the springs in the system are shown in Equations 47 and 48 using Hook's Law for linear springs. The potential energy is stored in the springs, where x refers to the horizontal motion of the ball balancer and y refers to the vertical motion of the ball balancer,

$$V_{k_x} = \frac{1}{2}k_x x^2 \quad (47)$$

$$V_{k_y} = \frac{1}{2}k_y y^2 \quad (48)$$

Next, the gravitational potential of the bodies within the system must be added to the potential energy total. The gravitational potential of the ball balancer and the balls are written in Equation 49, where the position of the center of gravity of the ball balancer is given by the expression $y + e\sin(\phi)$ and the position of the ith ball is given by the expression $y + R\sin(\theta_i)$,

$$V_G = m_{BB}g\left(y + e\sin(\phi)\right) + m_{P_1}g\left(y + R\sin(\theta_1)\right) + \sum_{j=2}^{n} m_{P_j}g\left(y + R\sin(\theta_j)\right) \quad (49)$$

Combining the potential energies of the springs and the gravitational potential of the ball balancer and balls, the total potential energy of the system can be written. The expression for the total potential energy is shown in Equation 50,

$$V_{TOT} = \frac{1}{2}k_x x^2 + \frac{1}{2}k_y y^2 + m_{BB}g(y + e\sin(\phi)) + m_{P_1}g(y + R\sin(\theta_1)) + \sum_{j=2}^{n}\left[m_{P_j}g(y + R\sin(\theta_j))\right] \quad (50)$$

F. Non-Conservative Forces

Lastly, the non-conservative forces need to be derived to complete the full Lagrangian derivation. The contribution of non-conservative forces are assumed to originate from elements of the system that remove energy. The elements that contribute to the non-conservative forces are the dampers that resist the translational motion of the ball balancer, the viscous fluid drag that resists the angular motion of the balls and the rolling friction that resists the pure rotation of the balls. The expressions for these non-conservative forces are shown below in Equation 51 where F_{N_i} is the normal force between the ith ball and the ball balancer,

$$Q_{NC} = \left[-c_x\dot{x}\right]\mathbf{I}_1 + \left[-c_y\dot{y}\right]\mathbf{I}_2 + \left[-d\left(\dot{\theta}_1 - \dot{\phi}\right) - \mu_R F_{N_1}\right]\mathbf{e}_{\theta_1} + \left[-\sum_{j=2}^{n} d\left(\dot{\theta}_j - \dot{\phi}\right) - \mu_R F_{N_j}\right]\mathbf{e}_{\theta_j} \tag{51}$$

The normal force acting on the ith ball is simply the mass of the ith ball multiplied by the radial acceleration of the ith ball, $F_{N_i} = m_{P_i} a_{P_i}^R$. The radial acceleration of the ith ball can be derived by differentiating the expression of the velocity of the ith ball in the radial direction. The expression for the velocity of the ith ball will simply be rewritten in the $\psi_{4,5}$ reference frame by using the identities $\mathbf{i}_1 = \cos(\theta_i)\mathbf{e}_{R_i} - \sin(\theta_i)\mathbf{e}_{\theta_i}$ and $\mathbf{i}_2 = \sin(\theta_i)\mathbf{e}_{R_i} + \cos(\theta_i)\mathbf{e}_{\theta_i}$. There is an additional cross product $\left(\dot{\mathbf{\Omega}}_i \times \mathbf{R}_i\right)$ which accounts for the rotation of the $\psi_{4,5}$ reference frame with respect to the ψ_2 reference frame. The acceleration due to gravity is also included. Gravity will dominate at low rotational speeds. The final expression for the normal force acting on the ith ball is seen in Equation 52. Once the fluid in the ball balancer is able to pick up the ball such that the ball begins to rotate with the ball balancer, the rotational acceleration will then begin to dominate,

$$F_{N_i} = m_{P_i}\left(\frac{dv_{P_i}^R}{dt} + g\sin(\theta_i)\right)$$

$$\mathbf{v}_{P_i} = \left[\dot{x}\cos(\theta_i) + \dot{y}\sin(\theta_i)\right]\mathbf{e}_{R_i} + \left[-\dot{x}\sin(\theta_i) + \dot{y}\cos(\theta_i)\right]\mathbf{e}_{\theta_i} + \left(\dot{\mathbf{\Omega}}_i \times \mathbf{R}_i\right)$$

$$\frac{dv_{P_i}^R}{dt} = \left[\left(\ddot{x} + \dot{y}\dot{\theta}_i\right)\cos(\theta_i) + \left(\ddot{y} - \dot{x}\dot{\theta}_i\right)\sin(\theta_i) - R\dot{\theta}_i^2\right]\mathbf{e}_{R_i}$$

$$F_{N_i} = m_{P_i}\left[\left(\ddot{x} + \dot{y}\dot{\theta}_i\right)\cos(\theta_i) + \left(\ddot{y} - \dot{x}\dot{\theta}_i\right)\sin(\theta_i) - R\dot{\theta}_i^2 + g\sin\left(\theta_i\right)\right] \tag{52}$$

G. Lagrangian Energy Approach

Now that the kinetic energies, potential energies and non-conservative forces have been derived, the full Lagrangian expression can be written. The Lagrangian energy method is shown below, where the Lagrangian L is equal to $T_{TOT} - V_{TOT}$ and x_N denotes a respective state

variable,

$$\frac{\partial}{\partial t}\left(\frac{\partial L}{\partial \dot{x}_N}\right) - \left(\frac{\partial L}{\partial x_N}\right) = Q_{NC}$$

The full Lagrangian for the ball balancer model is shown below in Equation 53,

$$\begin{aligned} L = T_{TOT} - V_{TOT} = \frac{1}{2}m_{BB}[\dot{x}^2 + \dot{y}^2 + e^2\dot{\phi}^2 + 2e\dot{\phi}(\dot{y}\cos(\phi) - \dot{x}\sin(\phi))] + \\ \frac{1}{2}m_{P_1}[\dot{x}^2 + \dot{y}^2 + R^2\dot{\theta}_1^2 + 2R\dot{\theta}_1(\dot{y}\cos(\theta_1) - \dot{x}\sin(\theta_1))] + \frac{1}{2}I_{P_1}\left[\frac{R}{r}\left(\dot{\phi} - \dot{\theta}_1\right)\right]^2 + \\ \sum_{j=2}^{n}\left\{\frac{1}{2}m_{P_j}\left[\dot{x}^2 + \dot{y}^2 + R^2\dot{\theta}_j^2 + 2R\dot{\theta}_j(\dot{y}\cos(\theta_j) - \dot{x}\sin(\theta_j))\right] + \frac{1}{2}I_{P_j}\left[\frac{R}{r}\left(\dot{\phi} - \dot{\theta}_j\right)\right]^2\right\} - \\ \frac{1}{2}k_x x^2 - \frac{1}{2}k_y y^2 - m_{BB}g(y + e\sin(\phi)) - m_{P_1}g(y + R\sin(\theta_1)) - \sum_{j=2}^{n}\left[m_{P_j}g(y + R\sin(\theta_j))\right] \end{aligned} \quad (53)$$

Applying the Lagrangian energy approach, the equations of motion for the state variables that describe the ball balancer model can be derived. These equations are shown in the next sections. This model uses the state variables defined by the horizontal location of the center of gravity of the ball balancer, the vertical location of the center of gravity of the ball balancer and the angular location of each ball within the ball balancer.

H. Final Equations of Motion - Second Order

The next section lists the expressions for each state variable which are used in the ball balancer model.

1. Ball Balancer Motion in the Horizontal Direction

The derivation will begin with the state variable defining the horizontal motion of the center of gravity of the ball balancer. Equation 54 shows the horizontal motion of the ball balancer in second order form. Note that the contribution of the balls to the horizontal motion is broken up between the global ball (which is the global coordinate) and any subsequent ball (which are relative coordinates),

$$\begin{aligned} \left(m_{BB} + m_{P_1} + \sum_{j=2}^{n} m_{P_j}\right)\ddot{x} - m_{P_1}R[\ddot{\theta}_1\sin(\theta_1) + \dot{\theta}_1^2\cos(\theta_1)] + \\ \sum_{j=2}^{n}\left\{-m_{P_j}R\left[\ddot{\theta}_j\sin(\theta_j) + \dot{\theta}_j^2\cos(\theta_j)\right]\right\} + c_x\dot{x} + k_x x = \\ m_{BB}e(\ddot{\phi}\sin(\phi) + \dot{\phi}^2\cos(\phi)), \end{aligned} \quad (54)$$

where $\theta_j = \theta_1 + \sum_{k=2}^{j} \beta_k$, showing that each additional ball utilizes relative coordinates with respect to its neighboring ball.

2. Ball Balancer Motion in the Vertical Direction

Similar to the procedure for the horizontal motion of the ball balancer, the vertical motion of the center of gravity of the ball balancer can be derived. The equation for the vertical motion of the ball balancer in second order form is shown in Equation 55. Again, note that the contribution of the balls to the vertical motion is broken up between the global ball (global coordinate) and any subsequent ball (relative coordinates),

$$\left(m_{BB} + m_{P_1} + \sum_{j=2}^{n} m_{P_j}\right) \ddot{y} + m_{P_1} R[\ddot{\theta}_1 \cos\theta_1 - \dot{\theta}_1^2 \sin(\theta_1)] + \sum_{j=2}^{n} \left\{ m_{P_j} R \left[\ddot{\theta}_j \cos(\theta_j) - \dot{\theta}_j^2 \sin(\theta_j) \right] \right\} + c_y \dot{y} + k_y y = m_{BB} e(\dot{\phi}^2 \sin(\phi) - \ddot{\phi} \cos(\phi)) - \left(m_{BB} + m_{P_1} + \sum_{j=2}^{n} m_{P_j}\right) g, \quad (55)$$

where $\theta_j = \theta_1 + \sum_{k=2}^{j} \beta_k$, showing that each additional ball utilizes relative coordinates with respect to its neighboring ball.

3. Angular Motion of Ball 1 and jth Ball

Lastly, the angular motion of the balls in the ball balancer can be derived. The equation for the angular motion of the balls in second order form are shown below. The equations of motion for the global ball and the jth ball are shown in Equations 56 and 57, respectively. Note that the absolute value of the radial acceleration is taken when computing the rolling friction force. This is done to ensure that the rolling friction force will always oppose the pure rotation of the ball. The normal force for the ith ball was defined in Equation 52,

$$\left[m_{P_1} R^2 + I_{P_1} \left(\frac{R}{r}\right)^2 \right] \ddot{\theta}_1 + m_{P_1} R[\ddot{y} \cos(\theta_1) - \ddot{x} \sin(\theta_1)] = - m_{P_1} g R \cos(\theta_1) - d\left(\dot{\theta}_1 - \dot{\phi}\right) + \ddot{\phi} I_{P_1} \left(\frac{R}{r}\right)^2 + sign\left(\dot{\phi} - \dot{\theta}_1\right) |F_{R_1}| \quad (56)$$

$$\left[m_{P_j}R^2 + I_{P_j}\left(\frac{R}{r}\right)^2\right]\ddot{\theta}_j + m_{P_j}R[\ddot{y}\cos(\theta_j) - \ddot{x}\sin(\theta_j)] =$$
$$- m_{P_j}gR\cos(\theta_j) - d\left(\dot{\theta}_j - \dot{\phi}\right) + \ddot{\phi}I_{P_j}\left(\frac{R}{r}\right)^2 + sign\left(\dot{\phi} - \dot{\theta}_j\right)\left|F_{R_j}\right|, \quad (57)$$

where $\theta_j = \theta_1 + \sum_{k=2}^{j}\beta_k$, showing that each additional ball utilizes relative coordinates with respect to its neighboring ball. Additionally, the rolling friction force for the ith ball is given by $|F_{R_i}| = \mu_R\,|F_{N_i}|$.

I. Train Equation Derivation

The previous section showed the steps to derive the horizontal and vertical motion of the ball balancer, as well as the angular motion of a single ball. However, through experimental observations, it is known that the balls do not always behave as separate bodies. Depending on the characteristics of the system, the balls are able to collide with one another and in some instances, form trains. The balls within a train all have the same velocity and acceleration at any instant in time. Additionally, there is an external force acting on a ball within a train due to contact with its neighboring balls. Care must be taken to account for the possibility of the separation of a train, since at any point in time, a train of n balls can break apart into a maximum of n smaller trains.

As explained in Chapter III, this ball balancer model utilizes the technique outlined by Henon to directly solve for discontinuous events. This technique is used to accurately capture the exact moment of a collision as well as capture the exact moment of a train separation. According to Dedow and Murphy, a simple manipulation can be applied to the equations of motion to account for the train separation phenomena such that the Henon integration method can be used on separating bodies as well.

To begin, first consider a train of three balls as seen in Figure 28. Each ball has some applied external force in the radial direction as well as in the angular direction. When in a train, there is an additional applied force due to contact with an adjacent ball. When the balls are in a train, this interaction force is present, when the balls are not in a train, this interaction force is absent. To begin the derivation, the equations of motion can be written by summing the forces acting on each ball; these were shown in Equations 56 and 57. Once this is complete, the Dedow-Murphy method can be applied to create a force stepping set of equations of motion. Figure 28 is a free body diagram of three ball system that shows the forces acting on each ball.

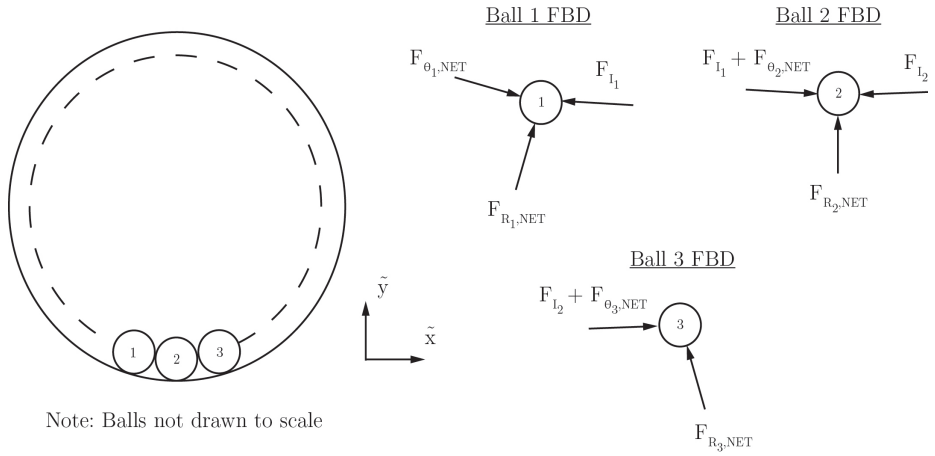

FIGURE 28 – A Free Body Diagram of a Train of Three Balls

Before deriving the equations for a train of balls, the collision angle, α, must be defined. The collision angle is defined as the angle that separates two contacting balls. Using the Law of Cosines, an expression for the collision angle can be developed which is seen in Equation 58, where α is a function of the ball radius and the ball balancer radius,

$$\alpha = \cos^{-1}\left[\frac{R^2 - 2r^2}{R^2}\right] \tag{58}$$

Figure 29 shows a schematic of how this expression was derived. The model will use the collision angle to determine when to switch to a displacement stepping solving method to solve for a collision, and when the solver determines if a train has developed,

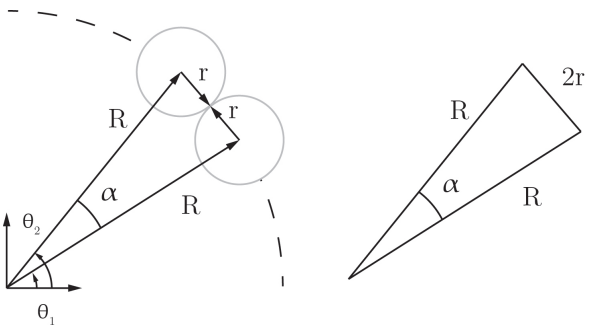

FIGURE 29 – The Collision Angle is a Function of the Ball Radius and the Ball Balancer Radius

The equations of motion describing the motion of a train can be written, where the equation for the first ball, an interior ball and the last ball are shown in Equations 59, 60 and 61, respectively. Note that the rolling friction force now includes the addition of the radial force due to the component of the ball interaction forces acting in the radial direction. This is only added when a train is present in the system.

Equation of motion for the first ball in the train,

$$\left[m_{P_1}R^2 + I_{P_1}\left(\frac{R}{r}\right)^2\right]\ddot{\theta}_1 + m_{P_1}R\left[\ddot{y}\cos(\theta_1) - \ddot{x}\sin(\theta_1)\right] = -m_{P_1}gR\cos(\theta_1) - d\left(\dot{\theta}_1 - \dot{\phi}\right) + \ddot{\phi}I_{P_1}\left(\frac{R}{r}\right)^2 + sign\left(\dot{\phi} - \dot{\theta}_1\right)|F_{R_1}| - F_{I_1}\cos\left(\frac{\alpha}{2}\right) \quad (59)$$

$$\text{where } |F_{R_1}| = \mu_R\left[|F_{N_1}| + |F_{I_1}|\sin\left(\tfrac{\alpha}{2}\right) + |F_{I_n}|\sin\left(\tfrac{\alpha}{2}\right)\right]$$

Equation of motion for any interior ball in the train k, where $2 \leq k \leq (n-1)$,

$$\left[m_{P_k}R^2 + I_{P_k}\left(\frac{R}{r}\right)^2\right]\ddot{\theta}_k + m_{P_k}R\left[\ddot{y}\cos(\theta_k) - \ddot{x}\sin(\theta_k)\right] = -m_{P_k}gR\cos(\theta_k) - d\left(\dot{\theta}_k - \dot{\phi}\right) + \ddot{\phi}I_{P_k}\left(\frac{R}{r}\right)^2 + sign\left(\dot{\phi} - \dot{\theta}_k\right)|F_{R_k}| + F_{I_{(k-1)}}\cos\left(\frac{\alpha}{2}\right) - F_{I_k}\cos\left(\frac{\alpha}{2}\right) \quad (60)$$

$$\text{where } |F_{R_k}| = \mu_R\left[|F_{N_k}| + \left|F_{I_{(k-1)}}\right|\sin\left(\tfrac{\alpha}{2}\right) + |F_{I_k}|\sin\left(\tfrac{\alpha}{2}\right)\right]$$

Equation of motion for the last ball in the train,

$$\left[m_{P_n}R^2 + I_{P_n}\left(\frac{R}{r}\right)^2\right]\ddot{\theta}_n + m_{P_n}R\left[\ddot{y}\cos(\theta_n) - \ddot{x}\sin(\theta_n)\right] = -m_{P_n}gR\cos(\theta_n) - d\left(\dot{\theta}_n - \dot{\phi}\right) + \ddot{\phi}I_{P_n}\left(\frac{R}{r}\right)^2 + sign\left(\dot{\phi} - \dot{\theta}_n\right)|F_{R_n}| + F_{I_{(n-1)}}\cos\left(\frac{\alpha}{2}\right) \quad (61)$$

$$\text{where } |F_{R_n}| = \mu_R\left[|F_{N_n}| + \left|F_{I_{(n-1)}}\right|\sin\left(\tfrac{\alpha}{2}\right) + |F_{I_n}|\sin\left(\tfrac{\alpha}{2}\right)\right]$$

Note that these equations are generalized to a train with any number of balls greater than two. However, these equations can be applied to any size train by adding on additional equations for interior balls. Again, note that the rolling friction force not only includes the absolute radial acceleration of the ball, but also the radial contribution from the interaction forces between each ball.

Following the Dedow-Murphy method, the technique will simply be applied to the ball equations above to form a force stepping set of equations. First, it should be noted that since the balls have a physical nature about them, when touching, they do not have the same angular displacement. In the following equations, θ_1 will refer to the absolute position of the first ball in the train and θ_2 will refer to the absolute position of the second ball in the train, etc. Although the angular displacements are different for each ball within a train, the velocity, acceleration and jerk are equivalent for all balls within the same train. To begin, the velocity of the first ball will be defined as v_2 as seen in Equation 62. An additional time derivative can be taken to arrive at the acceleration of the first ball as seen in Equation 63. This equation was derived previously in Equation 59 and will be defined as v_3. Another time derivative can be taken to arrive at the jerk

of the first ball shown in Equation 64 which is defined as $\dot{v_3}$. Equations 65 and Equation 66 refer to the time derivative of the acceleration for any interior ball k and the last ball in the train n, respectively. Additionally, $\dot{v}_{i+2}$ defines the internal normal force $\dot{F}_i$, and $\left|\dot{F}_{R_i}\right|$ is defined later in this chapter in Equation 70,

$$\dot{v}_1 = \dot{\theta}_1 = v_2 \tag{62}$$

$$\dot{v}_2 = \ddot{\theta}_1 = v_3 \tag{63}$$

$$\left[m_{P_1}R^2 + I_{P_1}\left(\frac{R}{r}\right)^2\right]\dot{v}_3 - m_{P_1}R\left[\dddot{x}\sin(\theta_1) - \dddot{y}\cos(\theta_1)\right] + \dot{v}_4\cos\left(\frac{\alpha}{2}\right) =$$
$$m_{P_1}R\left[\ddot{x}v_2\cos(\theta_1) + \ddot{y}v_2\sin(\theta_1)\right] + m_1gRv_2\sin(\theta_1) - d\left(v_3 - \ddot{\phi}\right) +$$
$$\dddot{\phi}I_{P_1}\left(\frac{R}{r}\right)^2 + sign\left(\ddot{\phi} - \ddot{\theta}_1\right)\left|\dot{F}_{R_1}\right| \tag{64}$$

$$\left[m_{P_k}R^2 + I_{P_k}\left(\frac{R}{r}\right)^2\right]\dot{v}_3 - m_{P_k}R\left[\dddot{x}\sin(\theta_k) - \dddot{y}\cos(\theta_k)\right] - \dot{v}_{k+2}\cos\left(\frac{\alpha}{2}\right) + \dot{v}_{k+3}\cos\left(\frac{\alpha}{2}\right) =$$
$$m_{P_k}R\left[\ddot{x}v_2\cos(\theta_k) + \ddot{y}v_2\sin(\theta_k)\right] + m_kgRv_2\sin(\theta_k) - d\left(v_3 - \ddot{\phi}\right) +$$
$$\dddot{\phi}I_{P_k}\left(\frac{R}{r}\right)^2 + sign\left(\ddot{\phi} - \ddot{\theta}_k\right)\left|\dot{F}_{R_k}\right| \tag{65}$$

$$\left[m_{P_n}R^2 + I_{P_n}\left(\frac{R}{r}\right)^2\right]\dot{v}_3 - m_{P_n}R\left[\dddot{x}\sin(\theta_n) - \dddot{y}\cos(\theta_n)\right] - \dot{v}_{n+2}\cos\left(\frac{\alpha}{2}\right) =$$
$$m_{P_n}R\left[\ddot{x}v_2\cos(\theta_n) + \ddot{y}v_2\sin(\theta_n)\right] + m_ngRv_2\sin(\theta_n) - d\left(v_3 - \ddot{\phi}\right) +$$
$$\dddot{\phi}I_{P_n}\left(\frac{R}{r}\right)^2 + sign\left(\ddot{\phi} - \ddot{\theta}_n\right)\left|\dot{F}_{R_n}\right| \tag{66}$$

Equations 62, 63 and 64 describe the velocity, acceleration and jerk of the first ball in the train, respectively. The timing of the separation of the two balls is governed by the equal and opposite interaction force acting between the balls. Note that this set of equations allows a force stepping integration method that can be used in a similar manner as the collision algorithm, since the time derivatives of the internal forces are present in the equations. All that need be done is apply the Henon method to this set of equations with a different transformation variable.

J. Final Equations of Motion - Third Order

Note that third derivatives are present in the equations that define the motion of a train of balls. To successfully implement the equations describing the train motion, the third

derivatives should also be taken for Equations 54, 55, 56 and 57 that were derived previously. Note that in the final ball balancer model presented in this paper, all integration steps use the third order form of the equations of motion. This is done out of simplicity so there is no difference in the construction of the equations of motion whether a train is present or absent.

1. Ball Balancer Motion in the Horizontal Direction

The third derivative for the horizontal motion of the center of gravity of the ball balancer is derived in Equation 67,

$$\left(m_{BB} + m_{P_1} + \sum_{j=2}^{n} m_{P_j}\right) \dddot{x} - m_{P_1} R \left[\dddot{\theta}_1 \sin(\theta_1) + 3\dot{\theta}_1 \ddot{\theta}_1 \cos(\theta_1) - \dot{\theta}_1^3 \sin(\theta_1)\right] + \sum_{j=2}^{n} \left\{-m_{P_j} R \left[\dddot{\theta}_j \sin(\theta_j) + 3\dot{\theta}_j \ddot{\theta}_j \cos(\theta_j) - \dot{\theta_j}^3 \sin(\theta_j)\right]\right\} + c_x \ddot{x} + k_x \dot{x} = m_{BB} e \left[\dddot{\phi} \sin(\phi) + 3\dot{\phi}\ddot{\phi} \cos(\phi) - \dot{\phi}^3 \sin(\phi)\right], \quad (67)$$

where $\theta_j = \theta_1 + \sum_{k=2}^{j} \beta_k$, showing that each additional ball utilizes relative coordinates with respect to its neighboring ball.

2. Ball Balancer Motion in the Vertical Direction

The third order form of the vertical motion of the center of gravity of the ball balancer is derived in Equation 68,

$$\left(m_{BB} + m_{P_1} + \sum_{j=2}^{n} m_{P_j}\right) \dddot{y} + m_{P_1} R \left[\dddot{\theta}_1 \cos(\theta_1) - 3\dot{\theta}_1 \ddot{\theta}_1 \sin(\theta_1) - \dot{\theta}_1^3 \cos(\theta_1)\right] + \sum_{j=2}^{n} \left\{m_{P_j} R \left[\dddot{\theta}_j \cos(\theta_j) - \dot{\theta}_j \ddot{\theta}_j \sin(\theta_j) - 2\dot{\theta}_j \ddot{\theta}_j \sin(\theta_j) - \dot{\theta}_j^3 \cos(\theta_j)\right]\right\} + c_y \ddot{y} + k_y \dot{y} = m_{BB} e \left[3\dot{\phi}\ddot{\phi} \sin(\phi) + \dot{\phi}^3 \cos(\phi) - \dddot{\phi} \cos(\phi)\right] \quad (68)$$

where $\theta_j = \theta_1 + \sum_{k=2}^{j} \beta_k$, showing that each additional ball utilizes relative coordinates with respect to its neighboring ball.

3. Angular Motion of Ball 1 and jth Ball

The third order form of the angular motion of the ith ball is derived in Equation 69,

$$\left[m_{P_i}R^2 + I_{P_i}\left(\frac{R}{r}\right)^2\right]\dddot{\theta}_i - m_{P_i}R\left[\dddot{x}\sin(\theta_i) - \dddot{y}\cos(\theta_i)\right] = m_{P_i}R\left[\ddot{x}\dot{\theta}_i\cos(\theta_i) + \ddot{y}\dot{\theta}_i\sin(\theta_i)\right] + m_{P_i}gR\dot{\theta}_i\sin(\theta_i) - d\left(\ddot{\theta}_i - \ddot{\phi}\right) + \dddot{\phi}I_{P_i}\left(\frac{R}{r}\right)^2 + sign\left(\ddot{\phi} - \ddot{\theta}_i\right)\left|\dot{F}_{R_i}\right| \quad (69)$$

where $\theta_j = \theta_1 + \sum_{k=2}^{j}\beta_k$, showing that each additional ball utilizes relative coordinates with respect to its neighboring ball. Additionally, the time derivative of the rolling friction force acting on the ith ball is given in Equation 70, where CCW and CW refer to the ball that is either counterclockwise or clockwise from the ith ball,

$$\left|\dot{F}_{R_i}\right| = \mu_R\left[m_{P_i}\left|\left(\dddot{x} + 2\ddot{y}\dot{\theta}_i + \dot{y}\ddot{\theta}_i - \dot{x}\dot{\theta}_i^2\right)\cos(\theta_i) + \left(\dddot{y} - 2\ddot{x}\dot{\theta}_i - \dot{x}\ddot{\theta}_i - \dot{y}\dot{\theta}_i^2\right)\sin(\theta_i) - 2R\dot{\theta}_i\ddot{\theta}_i + g\dot{\theta}_i\cos(\theta_i)\right| + \left|\dot{F}_{I_{CCW}}\right|\sin\left(\frac{\alpha}{2}\right) + \left|\dot{F}_{I_{CW}}\right|\sin\left(\frac{\alpha}{2}\right)\right] \quad (70)$$

The equations of motion have been derived for the ball balancer motion, single ball motion and train motion. Additionally, it has been shown in Chapter IV and V that the Henon method can be applied to both collisions and separations. However, in the event of a collision, there is a momentum transfer between the bodies of the system such that the post-collision velocities are different than before the collision. Due to the geometry of the problem, this is more complicated than a simple proportional velocity change. The next chapter details the impulse-momentum calculations such that a full momentum analysis is conducted after a collision.

VII. VELOCITY TRANSFORMATION AFTER A COLLISION

A. Introduction

The following chapter details the derivation of the equations that describe the transfer in momentum when a collision occurs between two balls within the ball balancer. This chapter covers the explanation of the impulse equations that are used to solve for the post-collision velocities of the system.

B. Velocity Transformation

The models presented in Chapter IV, the "one mass-stationary wall" and the "two mass" model, contained collisions that were one dimensional. The calculations of the outgoing velocities of the masses after a collision were simple and straightforward; simply a proportional reduction in velocity. In reality, collisions may not always be one dimensional and may be more complex than just a simple computation.

Say there are two adjacent balls that are contacting each other at some arbitrary angular location on the ball balancer. The angle between the two balls is equal to the collision angle α and the balls are assumed to only have an angular component of motion; the velocity vector is oriented orthogonal to the radial vector defining the position of each ball. Figure 30a below shows the two balls at the instant before the collision,

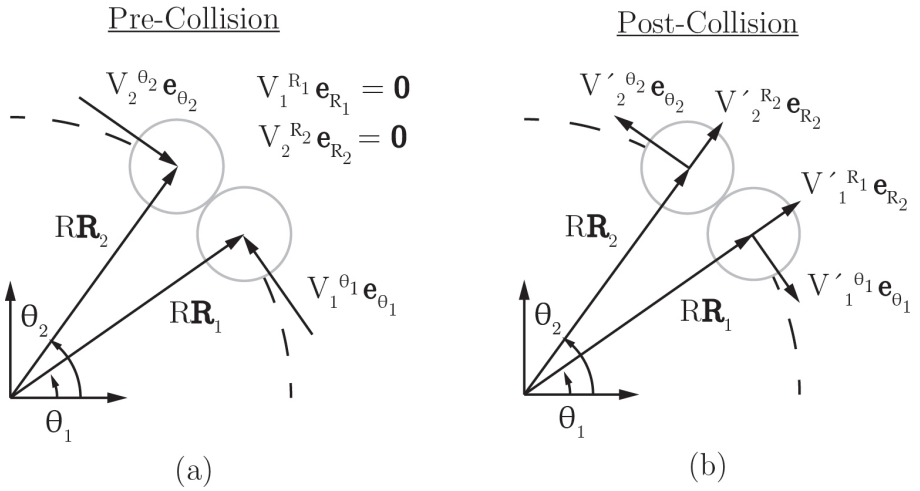

FIGURE 30 – The Velocities of the Balls Before the Collision are Purely Angular (a). The Velocities of the Balls After the Collision are both Angular and Radial (b)

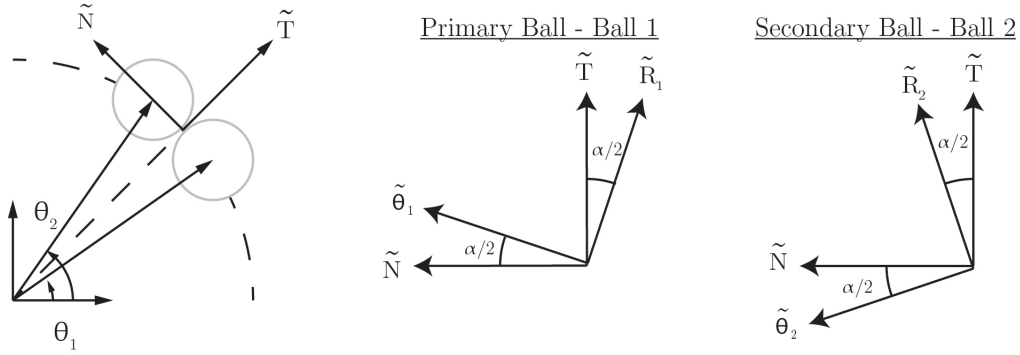

FIGURE 31 – The Velocities for Each Ball Must be Rewritten in the N-T Reference Frame

Once the balls contact each other, there is an exchange in momentum which results in a change in velocity of each ball; magnitude and/or direction. Figure 30b shows the balls after the collision. It can be seen that there is not only an angular component to the ball velocity, but also a radial component to the ball velocity. This radial component results from the fact that there is a physical radius associated with each ball and that the pre-collision velocity vectors are not aligned when the two balls collide. The collision takes on the characteristics of an oblique impact, meaning that the collision occurs in two dimensions. In this case, energy is not only transferred normally between balls, but also radially into the ball balancer. To account for the two dimensional element of a collision, the impulses must be summed in two dimensions.

1. Impulses Acting on the Balls

Before the collision, each ball has a purely angular velocity within the R-θ reference frame for that specific ball. Since the center of gravity of the two balls do not lie at the same absolute angle when contacting, the respective R-θ reference frames for each ball are oriented at a slightly different angle from each other. To properly apply the conservation of momentum principles, a third reference frame can be developed that is in the normal-tangential direction (N-T) between the two balls. The N-T reference frame is oriented according to the R-θ direction at an angle halfway between the two impacting balls as seen in Figure 31. This reference frame was selected out of simplicity; the impulses due to the collision are assumed to only act in the normal direction, while there are no impulses due to the collision in the tangential direction. The selection of this third reference frame simplifies the conservation of momentum equations and is a typical step of impact problems.

The velocities of both contacting balls must be re-written in the N-T reference frame by a simple rotation by half of the collision angle, as well as written in terms of absolute velocities. The absolute velocity of the balls include the velocity of the ball balancer plus the relative velocity of the ball with respect to the ball balancer. From this point forward, the ball with

the lesser absolute angular location will be referred to as the "primary ball" or ball one, while the ball with the greater absolute angular location will be referred to as the "secondary ball" or ball two. Shown below are the expressions for the absolute velocities of the primary and secondary balls written in the N-T reference frame, where the superscript denotes the direction of the velocity,

$$V_1^N = V_{BB}^N + V_1^{\theta_1} \sin\left(\frac{\alpha}{2}\right) \qquad V_1^T = V_{BB}^T + V_1^{\theta_1} \cos\left(\frac{\alpha}{2}\right)$$

$$V_2^N = V_{BB}^N + V_2^{\theta_2} \sin\left(-\frac{\alpha}{2}\right) \qquad V_2^T = V_{BB}^T + V_2^{\theta_2} \cos\left(-\frac{\alpha}{2}\right)$$

where

$$V_{BB}^N = V_{BB}^x \cos\left(\theta_2 - \frac{\alpha}{2}\right) + V_{BB}^y \sin\left(\theta_2 - \frac{\alpha}{2}\right)$$

and

$$V_{BB}^T = -V_{BB}^x \sin\left(\theta_2 - \frac{\alpha}{2}\right) + V_{BB}^y \cos\left(\theta_2 - \frac{\alpha}{2}\right)$$

Once the absolute pre-collision velocities for each ball have been written in the N-T reference frame, the impulses in both the normal and tangential directions can be summed for each ball. The impulse is defined as the time integral of an applied force, which is equal to the change in momentum of a body, $\mathbf{J} = \int \mathbf{F} dt = \Delta\mathbf{p}$, where $\mathbf{J}$ is the linear impulse, $\mathbf{F}$ is the applied force and $\Delta\mathbf{p}$ is the change in linear momentum of the body. The impulse equations in the normal and tangential direction are shown in Equations 71 and 72, respectively for the primary ball. In these equations, F_C is the collision force acting normally between the balls, R_i is the radial force on the ball due to the ball balancer, F_{R_i} is the angular force due to the rolling friction force acting on the ball and F_{I_i} is the angular force due to the interaction force acting on the ball from a neighboring ball within the train (if applicable). Note that there is no collision force acting between the two balls in the tangential direction and that all rolling friction forces are assumed to act at the center of gravity of each respective ball,

$$-\int F_C dt + \sin\left(\frac{\alpha}{2}\right)\int R_1 dt - \cos\left(\frac{\alpha}{2}\right)\int F_{R_1} dt + \sum \int F_{I_1}^N dt = m_{P_1}\left[V_{BB}^{'N} + \left|V_1^{'\theta_1}\right| \cos\left(\frac{\alpha}{2}\right)\right] - m_{P_1}\left[V_{BB}^N + \left|V_1^{\theta_1}\right| \cos\left(\frac{\alpha}{2}\right)\right] \quad (71)$$

$$-\cos\left(\frac{\alpha}{2}\right)\int R_1 dt - \sin\left(\frac{\alpha}{2}\right)\int F_{R_1} dt + \sum \int F_{I_1}^T dt = m_{P_1}\left[V_{BB}^{'T} + \left|V_1^{'\theta_1}\right| \sin\left(\frac{\alpha}{2}\right)\right] - m_{P_1}\left[V_{BB}^T + \left|V_1^{\theta_1}\right| \sin\left(\frac{\alpha}{2}\right)\right] \quad (72)$$

Likewise, the impulse equations in the normal and tangential directions are shown in Equations 73 and 74, respectively, for the secondary ball. Again, note that there is no collision force acting between the two balls in the tangential direction,

$$\int F_C dt + \sin\left(-\frac{\alpha}{2}\right)\int R_2 dt - \cos\left(-\frac{\alpha}{2}\right)\int F_{R_2} dt + \sum \int F_{I_2}^N dt = m_{P_2}\left[V_{BB}^{'N} + \left|V_2^{'\theta_2}\right|\cos\left(-\frac{\alpha}{2}\right)\right] - m_{P_2}\left[V_{BB}^N + \left|V_2^{\theta_2}\right|\cos\left(-\frac{\alpha}{2}\right)\right] \quad (73)$$

$$-\cos\left(-\frac{\alpha}{2}\right)\int R_2 dt - \sin\left(-\frac{\alpha}{2}\right)\int F_{R_2} dt + \sum \int F_{I_2}^T dt = m_{P_2}\left[V_{BB}^{'T} + \left|V_2^{'\theta_2}\right|\sin\left(-\frac{\alpha}{2}\right)\right] - m_{P_2}\left[V_{BB}^T + \left|V_2^{\theta_2}\right|\sin\left(-\frac{\alpha}{2}\right)\right] \quad (74)$$

As seen from the equations above, there are more unknown quantities than equations, thus additional equations must be written to solve for these unknowns. Next, the ball balancer impulse equations will be written.

2. Impulses Acting on the Ball Balancer

Similar to the procedure for the balls, the impulse equations can be written out for the ball balancer. Note that the radial impulse terms that were present in the ball impulse equations are simply equal and opposite in the ball balancer equations. Equations 75 and 76 are the impulse equations for the ball balancer in the normal and tangential directions, respectively. If there are any additional balls in the ball balancer that are not involved in the collision, these must also be added to make sure all the momentum is being accounted. The following equations reflect this addition if needed,

$$-\sin\left(\theta_2 - \frac{\alpha}{2}\right)\int F_{EXT}^x + \cos\left(\theta_2 - \frac{\alpha}{2}\right)\int F_{EXT}^y - \sin\left(\frac{\alpha}{2}\right)\int R_1 dt - \sin\left(-\frac{\alpha}{2}\right)\int R_2 dt + \sum_{j=3}^{n} -\sin\left(\theta_2 - \theta_j - \frac{\alpha}{2}\right)\int R_j dt + \cos\left(\frac{\alpha}{2}\right)\int F_{R_1} dt + \cos\left(-\frac{\alpha}{2}\right)\int F_{R_2} dt + \sum_{j=3}^{n}\cos\left(\theta_2 - \theta_j - \frac{\alpha}{2}\right)\int F_{R_j} dt = m_{BB}\left[V_{BB}^{N'} - V_{BB}^N\right] \quad (75)$$

$$\cos\left(\theta_2-\frac{\alpha}{2}\right)\int F_{EXT}^{x}+\sin\left(\theta_2-\frac{\alpha}{2}\right)\int F_{EXT}^{y}+\cos\left(\frac{\alpha}{2}\right)\int R_1dt+\cos\left(-\frac{\alpha}{2}\right)\int R_2dt+$$
$$\sum_{j=3}^{n}\cos\left(\theta_2-\theta_j-\frac{\alpha}{2}\right)\int R_jdt+\sin\left(\frac{\alpha}{2}\right)\int F_{R_1}dt+\sin\left(-\frac{\alpha}{2}\right)\int F_{R_2}dt+$$
$$\sum_{j=3}^{n}\sin\left(\theta_2-\theta_j-\frac{\alpha}{2}\right)\int F_{R_j}dt=m_{BB}\left[V_{BB}^{T'}-V_{BB}^{T}\right] \quad (76)$$

3. Coefficient of Restitution

This ball balancer model applies a coefficient of restitution assumption for the collisions that occur during the operation of the ball balancer. The coefficient of restitution assumption assumes that collisions occur over an instantaneous increment in time and that there is a proportional loss in velocity (due to heat generation, noise or other inefficiencies) when a collision occurs. The definition of the coefficient of restitution is simply the ratio between the restoring impulse and the deforming impulse,

$$COR=\frac{\int F_{RESTORE}dt}{\int F_{DEFORM}dt}$$

The coefficient of restitution equation can be written for the primary and secondary balls involved in the collision, for the normal direction only, where the velocity at the maximum point of deformation, V^{N0}, is equal for both balls,

$$COR=\frac{m_{P_1}V_1^{'N}-m_{P_1}V_1^{N0}-\int R_1^Ndt-\int F_{R_1}^Ndt-\sum\int F_{I_1}^Ndt}{m_{P_1}V_1^{N0}-m_{P_1}V_1^{N}-\int R_1^Ndt-\int F_{R_1}^Ndt-\sum\int F_{I_1}^Ndt} \quad (77)$$

$$COR=\frac{m_{P_2}V_2^{'N}-m_{P_2}V_2^{N0}-\int R_2^Ndt-\int F_{R_2}^Ndt-\sum\int F_{I_2}^Ndt}{m_{P_2}V_2^{N0}-m_{P_2}V_2^{N}-\int R_2^Ndt-\int F_{R_2}^Ndt-\sum\int F_{I_2}^Ndt} \quad (78)$$

Solving for V^{N0} and equating, Equations 77 and 78 can be simplified to obtain the final coefficient of restitution expression shown in Equation 79,

$$\left|V_1^{'\theta_1}\right|\cos\left(\frac{\alpha}{2}\right)-\left|V_2^{'\theta_2}\right|\cos\left(-\frac{\alpha}{2}\right)+\frac{1}{m_{P_1}}\sin\left(\frac{\alpha}{2}\right)(COR-1)\int R_1dt+$$
$$\frac{1}{m_{P_2}}\sin\left(-\frac{\alpha}{2}\right)(1-COR)\int R_2dt+\frac{1}{m_{P_1}}\cos\left(\frac{\alpha}{2}\right)(COR-1)\int F_{R_1}dt+$$
$$\frac{1}{m_{P_2}}\cos\left(-\frac{\alpha}{2}\right)(1-COR)\int F_{R_2}dt+\frac{1}{m_{P_1}}(COR-1)\sum\int F_{I,1}^Ndt+$$
$$\frac{1}{m_{P_2}}(1-COR)\sum\int F_{I,2}^Ndt=COR\left[\left|V_2^{\theta_2}\right|\cos\left(-\frac{\alpha}{2}\right)-\left|V_1^{\theta_1}\right|\cos\left(\frac{\alpha}{2}\right)\right] \quad (79)$$

4. Impulses Due to Additional Balls in Colliding Train

The equations derived above were for the case where only one ball was present in the primary train and one ball was present in the secondary train. However, there is a possibility that multiple balls can be in either the primary or secondary trains. The equations for additional balls in the colliding trains are very similar to those for the colliding balls, but just a change in the rotation angle from the respective R-θ frame to the N-T frame. Equations 80 and 81 show the normal and tangential direction impulse equations, respectively, for an additional ball in the primary train, where $a = 3, 5, 7, ...$ for each additional ball clockwise from the colliding ball in the primary train,

$$\sin\left(a\frac{\alpha}{2}\right)\int R_j dt - \cos\left(a\frac{\alpha}{2}\right)\int F_{R_j} dt + \sum\int F_{I_j}^N dt = m_{P_j}\left[V_{BB}^{'N} + \left|V_j^{'\theta_j}\right|\cos\left(a\frac{\alpha}{2}\right)\right] - m_{P_j}\left[V_{BB}^N + \left|V_j^{\theta_j}\right|\cos\left(a\frac{\alpha}{2}\right)\right] \quad (80)$$

$$-\cos\left(a\frac{\alpha}{2}\right)\int R_j dt - \sin\left(a\frac{\alpha}{2}\right)\int F_{R_j} dt + \sum\int F_{I_j}^T dt = m_{P_j}\left[V_{BB}^{'T} + \left|V_j^{'\theta_j}\right|\sin\left(a\frac{\alpha}{2}\right)\right] - m_{P_j}\left[V_{BB}^T + \left|V_j^{\theta_j}\right|\sin\left(a\frac{\alpha}{2}\right)\right] \quad (81)$$

Likewise, Equations 82 and 83 below are the normal and tangential direction impulse equations, respectively, for an additional ball in the secondary train where $b = 3, 5, 7, ...$ for each additional ball counterclockwise from the colliding ball in the secondary train,

$$\sin\left(-b\frac{\alpha}{2}\right)\int R_j dt - \cos\left(-b\frac{\alpha}{2}\right)\int F_{R_j} dt + \sum\int F_{I_j}^N dt = m_{P_j}\left[V_{BB}^{'N} + \left|V_j^{'\theta_j}\right|\cos\left(-b\frac{\alpha}{2}\right)\right] - m_{P_j}\left[V_{BB}^N + \left|V_j^{\theta_j}\right|\cos\left(-b\frac{\alpha}{2}\right)\right] \quad (82)$$

$$-\cos\left(-b\frac{\alpha}{2}\right)\int R_j dt - \sin\left(-b\frac{\alpha}{2}\right)\int F_{R_j} dt + \sum\int F_{I_j}^T dt = m_{P_j}\left[V_{BB}^{'T} + \left|V_j^{'\theta_j}\right|\sin\left(-b\frac{\alpha}{2}\right)\right] - m_{P_j}\left[V_{BB}^T + \left|V_j^{\theta_j}\right|\sin\left(-b\frac{\alpha}{2}\right)\right] \quad (83)$$

Note with more than one ball in the colliding train, a multiple-ball train is present. The internal normal forces are included in the above equations for completeness, however the impulses due to these interaction forces are assumed to be negligible. An explanation for this assumption is presented at the end of this chapter.

5. Impulses Due to Additional Balls Not in Colliding Train

More than likely, there will be more than two balls present in the ball balancer during operation. In the event that a collision occurs while any number of additional balls are present in the ball balancer, the additional balls must also be included in the system level conservation of momentum equations. The impulse equations are very similar to those seen for balls located within the primary and secondary trains. The main difference is the angular offset due to the absolute angular location of the particular ball, and the absence of the collision force impulse. The normal and tangential impulse equations, respectively, for any additional ball are seen in Equations 84 and 85,

$$\sum_{j=3}^{n} \sin\left(\theta_2 - \theta_j - \frac{\alpha}{2}\right) \int R_j dt - \sum_{j=3}^{n} \cos\left(\theta_2 - \theta_j - \frac{\alpha}{2}\right) \int F_{R_j} dt + \sum \int F_{I_j}^{N} dt = m_{P_j} \left[V_{BB}^{'N} + \left|V_j^{'\theta_j}\right| \cos\left(\theta_2 - \theta_j - \frac{\alpha}{2}\right)\right] - m_{P_j} \left[V_{BB}^{N} + \left|V_j^{\theta_j}\right| \cos\left(\theta_2 - \theta_j - \frac{\alpha}{2}\right)\right] \quad (84)$$

$$\sum_{j=3}^{n} -\cos\left(\theta_2 - \theta_j - \frac{\alpha}{2}\right) \int R_j dt - \sum_{j=3}^{n} \sin\left(\theta_2 - \theta_j - \frac{\alpha}{2}\right) \int F_{R_j} dt + \sum \int F_{I_j}^{T} dt = m_{P_j} \left[V_{BB}^{'T} + \left|V_j^{'\theta_j}\right| \sin\left(\theta_2 - \theta_j - \frac{\alpha}{2}\right)\right] - m_{P_j} \left[V_{BB}^{T} + \left|V_j^{\theta_j}\right| \sin\left(\theta_2 - \theta_j - \frac{\alpha}{2}\right)\right] \quad (85)$$

Note that with each additional ball, there is a possibility that they will form a combination of trains with one another. Similar to the balls in the primary and secondary trains, the internal normal forces are included in the equations above for completeness, however the impulses due to the interaction forces are assumed to be negligible.

6. Impulses Due to External Forces On the Ball Balancer

The external impulses acting on the ball balancer are still unknown. These external impulses are due to the spring and damper acting in the horizontal and vertical directions on the ball balancer. To obtain two additional equations, two more impulse equations can be written which are applied to the surroundings in the normal and tangential directions. Equations 86 and 87 are shown below, assuming that these external forces are the only forces acting upon the surroundings,

$$-\sin\left(\theta_2 - \frac{\alpha}{2}\right) \int F_{EXT}^{x} + \cos\left(\theta_2 - \frac{\alpha}{2}\right) \int F_{EXT}^{y} = m_{SURR}(V_{SURR}^{'N} - V_{SURR}^{N}) \quad (86)$$

$$\cos\left(\theta_2 - \frac{\alpha}{2}\right) \int F_{EXT}^{x} + \sin\left(\theta_2 - \frac{\alpha}{2}\right) \int F_{EXT}^{y} = m_{SURR}(V_{SURR}^{'T} - V_{SURR}^{T}) \quad (87)$$

In reality, there may be any number of forces acting on the surroundings at any given time. If the surroundings are assumed to be the Earth, the forces that are applied to the Earth at any point in time are very difficult to determine. However in this analysis, the ball balancer is assumed to be isolated from the surroundings such that there is no impulse imparted on the ball balancer due to the surroundings. If the ball balancer system is assumed to be isolated, due to the very definition of the impulse, no momentum is transferred to the surroundings, and vice versa. Although the ball balancer is indeed mounted to the Earth in some mechanical fashion, the momentum that is transferred between the Earth and the ball balancer is assumed to be negligible such that $\int F_{EXT}^{N} dt = \int F_{EXT}^{T} dt = \mathbf{0}$.

7. Angular Impulses due to Rolling Friction Acting on Balls

Specific to this ball balancer model, the rolling inertia of the balls is included, thus the rotational contribution to the system momentum must also be included in the system level conservation of momentum equations. These impulses are rotational in nature and act about the center of gravity of each ball. Assuming a no-slip condition, it is no issue incorporating these angular impulses with the previous linear impulses; the torques acting on the balls can be resolved into a force by simply dividing by the ball radius.

The angular impulse is defined as $\mathbf{L} = l \int \mathbf{F} dt = I \boldsymbol{\Delta q}$, where $\mathbf{L}$ is the angular impulse, l is the moment arm, I is the mass moment of inertia of the body and $\boldsymbol{\Delta q}$ is the change in pure rotational velocity of the body. Assuming that all torques act in the positive $\mathbf{e}_k$ direction, it is very easy to write the angular impulse equations. Note that the following equations assume that there is no interaction between the rolling balls within a train; the rolling friction force acting between two rolling balls is negligible compared to the rolling friction force acting between the ball and the ball balancer. Equation 88 is relevant to all balls, regardless of their inclusion to the colliding trains,

$$-r \int F_{R_i} dt = I_{P_i} \left(\omega'_{P_i} - \omega_{P_i} \right) = \frac{I_{P_i}}{r} \left(\left| V_i^{\theta_i} \right| - \left| V_i^{'\theta_i} \right| \right) \tag{88}$$

8. Angular Impulses due to Rolling Friction Acting on the Ball Balancer

Similar to the linear impulses that acted between the balls and the ball balancer, the angular impulses that act on the balls are equal and opposite to those acting on the ball balancer. The last angular impulse equation that is added to the system of equations is due to the external torque applied to the ball balancer. Since the ball balancer has some prescribed spin profile, the rotational velocity of the ball balancer before the collision and after the collision is assumed to

be the same. This simplification is seen in Equation 89,

$$\sum_{i=1}^{n} (R+r) \int F_{R_i} dt - \int T_{R_{BB}} dt = I_{BB} \left(\omega'_{BB} - \omega_{BB}\right) = 0 \tag{89}$$

9. Impulses Due to Interaction Forces Between Balls in a Train

The final element for the velocity transformation analysis outlined in this chapter involves the interaction forces that are present when a train of balls has formed, regardless if the train is involved in a collision or not. Any train present in the ball balancer has normal interaction forces acting between all adjacent balls. This normal force is seen in Chapter VI from the equations of motion of a train. During a collision, the impulses due to the normal interaction forces are assumed to be zero, $\int \mathbf{F}_{I_i} dt = \mathbf{0}$. The interaction impulses are assumed to be negligible compared to the other angular impulses present in the system. Thus, the model views each ball as a separate, individual body when the velocity transformation equations are being solved.

C. Final Conservation of Momentum Analysis

Once the impulse equations have been applied to the current state of the ball balancer, a series of equations develop which turn out to be a system of linear equations. The output of this system of equations details all the unknowns in the post-collision state of the system. After all the unknowns have been calculated, the new initial conditions for the next integration step have been solved, thus the model can continue solving the equations describing the ball balancer motion.

D. Discussion on Collisions Between Trains

Up to this point, a collision has only involved two singular balls impacting one another. However, in experimental observation, the balls do not always move as singular, independent bodies. The balls can also form trains as discussed in Chapter VI. As a thought experiment, assume that the radii of the balls are negligible compared to the ball balancer radius and that all balls have the same mass. The balls within a ball balancer can be thought of as several pendulums that move at some fixed radius R. Say there are five total balls in the ball balancer, and one ball is pulled back to $\theta_1 = \pi$ rad, while the other four balls remain at rest at $\theta_{2-5} \approx -\frac{\pi}{2}$ rad. Ball one is released and allowed to contact the stationary train sitting at the bottom of the ball balancer. Assume that all energy is conserved in the collision and there is negligible ball balancer motion. Upon contact, ball five swings off the other end of the train and rises until $\theta_5 = 0$ rad. The velocity of ball five decreases to zero at its maximum height, then begins

to swing back down and collide with the stationary train of balls sitting at the bottom of the ball balancer. Ball five comes to a stop while ball one swings off the end of the train and rises to $\theta_1 = \pi$ rad. Since energy is conserved and no damping is present, this behavior continues forever. This progression is seen pictorially in Figure 32.

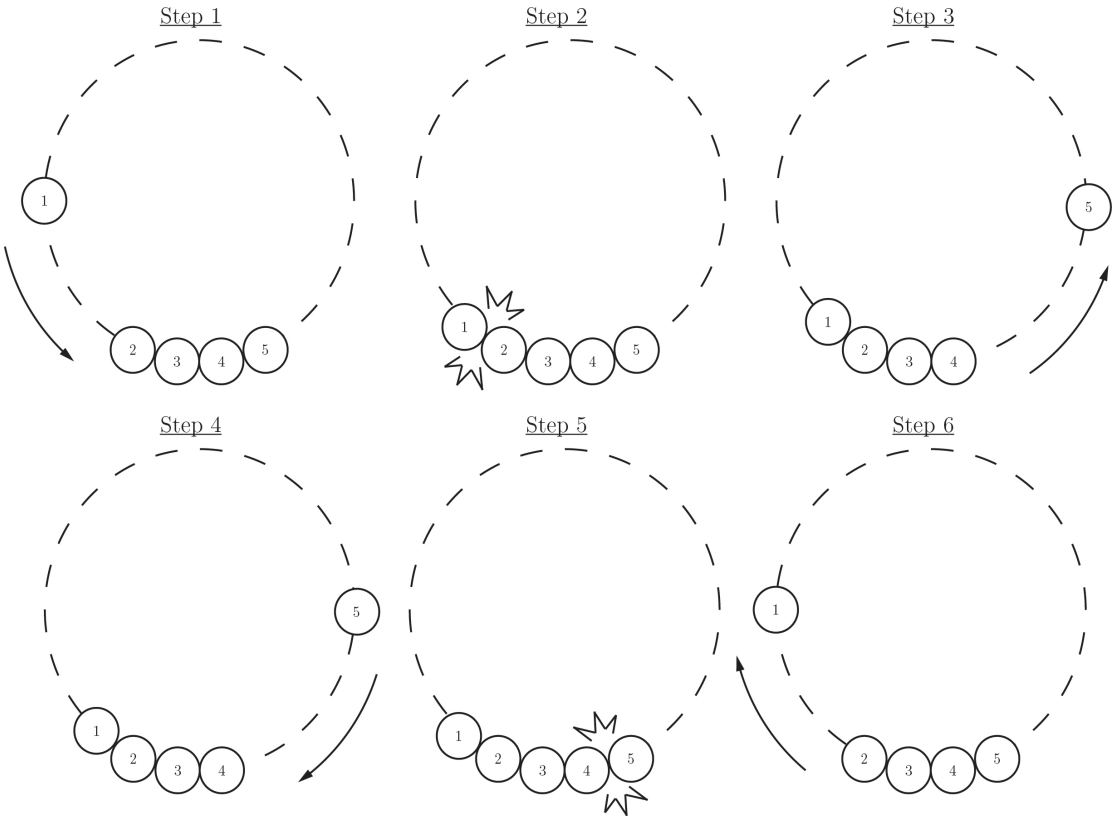

FIGURE 32 – The Experimental Result of One Ball Colliding with a Train

Now say that balls one and two are pulled back initially, such that $\theta_1 \approx \theta_2 \approx \pi$ rad and the other three balls are left stationary at the bottom of the ball balancer $\theta_{3-5} \approx -\frac{\pi}{2}$ rad. Experiments show that in this scenario, balls four and five will swing off the other end of the train; not one ball with a larger velocity or more balls with lesser velocity. This is the physics of the collision of trains which needs to be accurately captured in the ball balancer model. This progression is seen pictorially in Figure 33.

Simply put, the collisions involving a train can be thought of as separate, simultaneous events. The collision of one train to the next happens near instantaneously, but can be explained by thinking about each individual impact on its own as if there were some time gap between each. Again, say balls one and two are pulled back to some initial height, while the remaining three balls are stationary at the bottom of the ball balancer. As balls one and two swing down and contact the stationary train, the collision for ball two can be thought to occur first since this ball contacts the stationary train directly. When ball two collides with ball three, the momentum

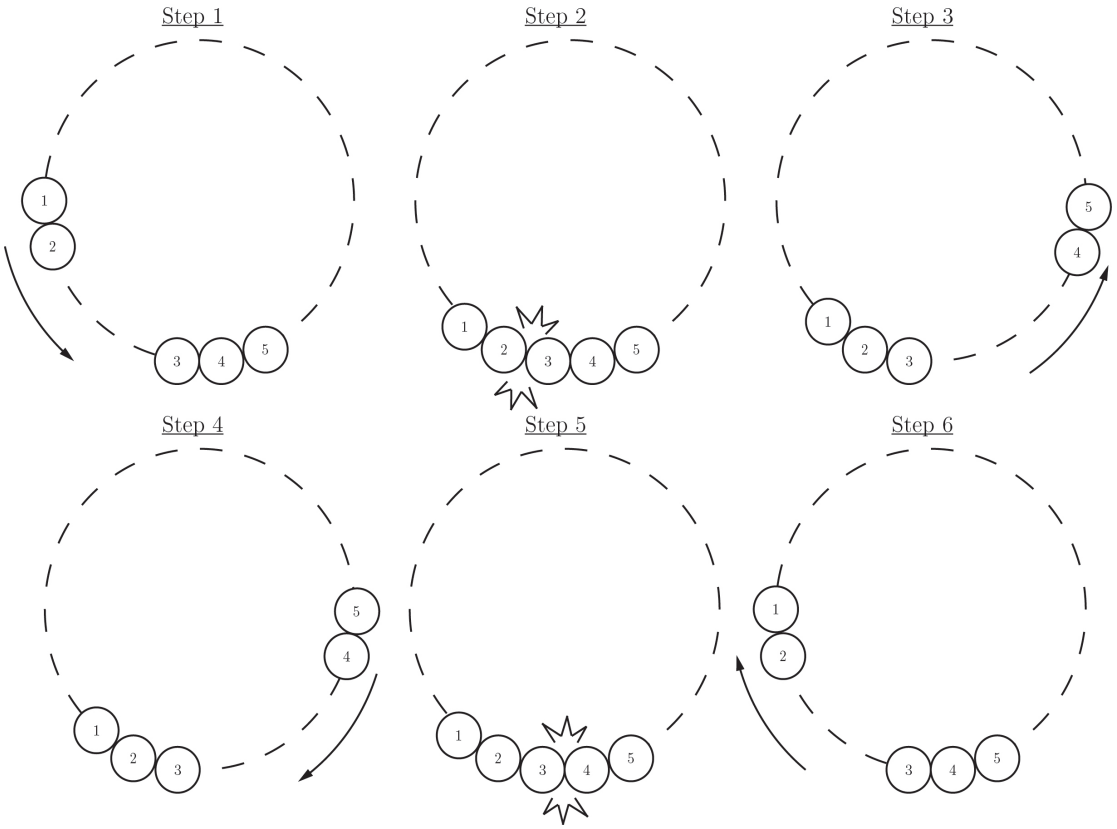

FIGURE 33 – The Experimental Result of Two Balls Colliding with a Train

begins to propagate through the train; ball three hits ball four, ball four hits ball five, then ball five (being the last ball in the train) swings away from the train. At some infinitesimal time after ball two hit ball three, ball one contacts the now stationary ball two. When ball one collides with ball two, the momentum begins to propagate through the train; ball two hits ball three, ball three hits ball four, then ball four (now being the last ball in the train) swings away from the train. At this point, balls four and five swing away and reach a maximum height where the velocity of the two balls equals zero and then swing back towards the stationary train. The previous succession of events proceeds in reverse, which causes balls one and two to swing away from the train. The momentum from the balls in the incoming train (train with larger absolute value of velocity) must each propagate through the entire receiving train of balls (train with smaller absolute value of velocity). This progression is seen pictorially in Figure 34.

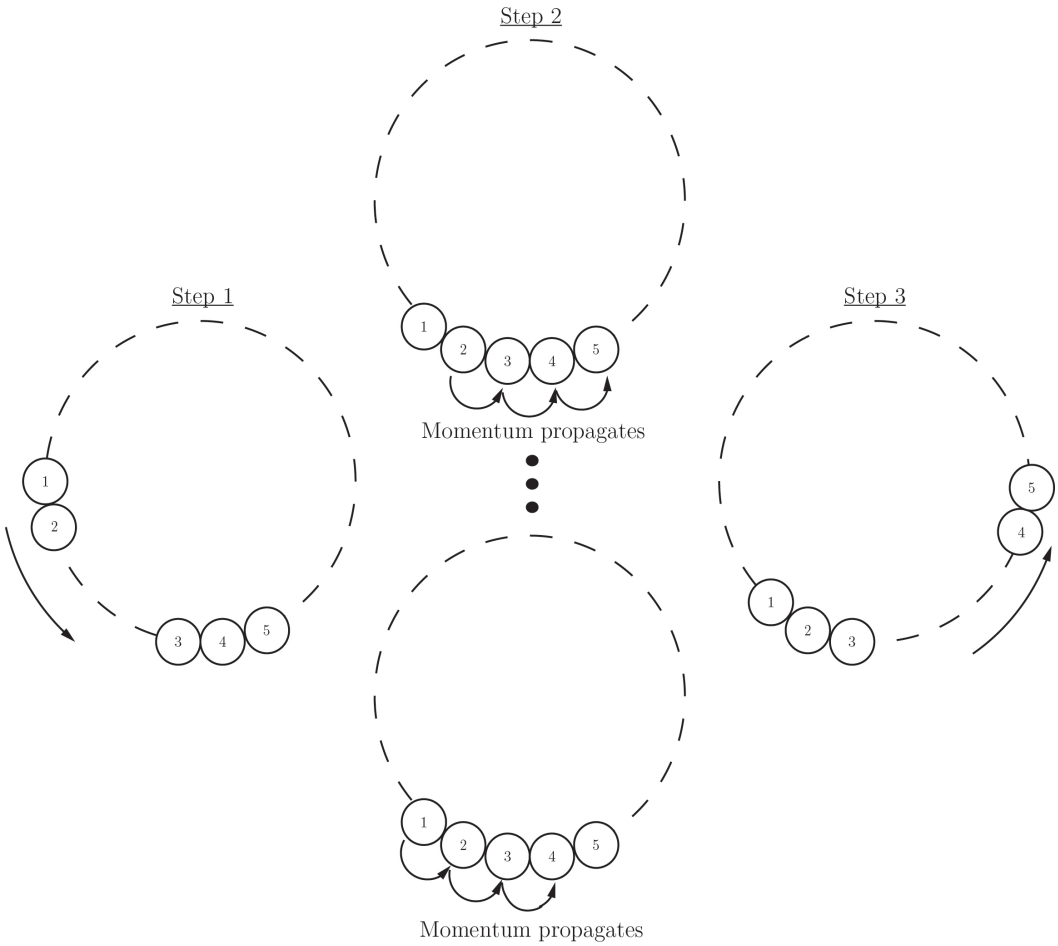

FIGURE 34 – The Momentum of Each Colliding Ball Propagates Through the Train of Balls

Although, the impulse-momentum equations discussed previously in this chapter only involve one ball contacting one other ball, the equations can be applied to two trains with any number of balls. The equations need only be applied to the total number of collision that will occur during the entire collision event. This method assumes that the momentum must be propagated through the entirety of the colliding trains by assuming that the collisions are separate events. By enabling this conservation of momentum method, the energy propagation and energy loss throughout the entire collision event is captured. By performing a full momentum analysis, the full effect of ball interactions can be captured.

Now that the equations of equations that totally describe the ball balancer motion have been derived, the model must be validated. The validation of the numerical model follows in the next chapter.

VIII. BALL BALANCER MODEL VALIDATION

A. Introduction

The following chapter details the test cases that validate the full ball balancer model. These validation cases include a comparison between the ball balancer model and three simple one degree of freedom systems: an unforced mass spring oscillator, an unforced swinging pendulum and a rotating imbalance. Additionally, an energy conservation analysis is conducted for more complicated test cases that pertain to the novelty of this ball balancer model.

B. One Degree of Freedom Systems

To ensure that the ball balancer model has physical meaning when more complicated test cases are conducted, it is very important to validate the model against more simple, and well known test cases. Three one degree of freedom models will be analyzed to determine if the ball balancer model can return the same output. The first test case is a comparison between the motion of the ball balancer and a traditional mass spring oscillator with damping. The second test case is a comparison between the motion of a ball in the ball balancer and a traditional swinging pendulum with damping. The third test case is the comparison of a rotating ball balancer with an eccentricity (with no balls) and a rotating imbalance with damping.

1. Ball Balancer Motion

To determine if the equations of motion pertaining to the translational motion of the ball balancer are correct, a comparison can be made to a simple, unforced mass spring oscillator with damping. The equations of motion for the mass spring oscillator are widely known and accepted. The equations describing motion in the horizontal direction (no gravitational forces) were shown in Chapter II, but are shown again in Equations 90 and 91 in first order form,

$$\dot{u}_1 = u_2 \tag{90}$$

$$\dot{u}_2 = -\frac{c_x}{m_{BB}}u_2 - \frac{k_x}{m_{BB}}u_1 \tag{91}$$

The equations of motion describing motion in the vertical direction (gravitational forces

included) are shown in Equations 92 and 93 in first order form,

$$\dot{y}_1 = y_2 \tag{92}$$

$$\dot{y}_2 = -\frac{c_y}{m_{BB}} y_2 - \frac{k_y}{m_{BB}} y_1 - g \tag{93}$$

The physical parameters for the horizontal case study are as follows: $c_x = 0.153$ lbs-s/ft, $k_x = 15$ lbs/ft and $m_{BB} = 0.155$ slugs. The initial displacement and velocity in the horizontal test case are $x_1(0) = x_0$ and $\dot{x}_1(0) = \dot{x}_0$. Figure 35 shows the comparison of the displacement, velocity and acceleration between the ball balancer and mass spring oscillator in the horizontal direction,

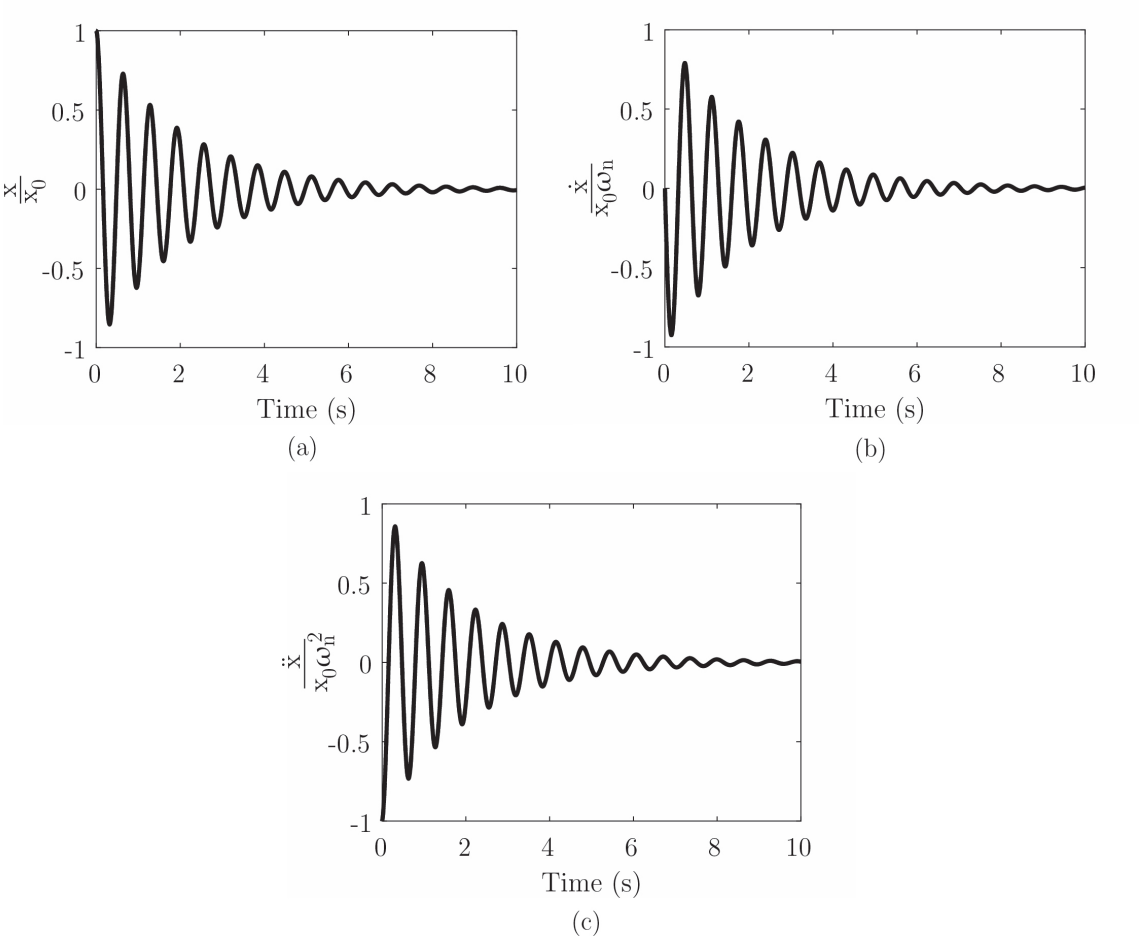

FIGURE 35 – The Displacement (a), Velocity (b) and Acceleration (c) of the Ball Balancer Model and the Traditional Horizontal Mass Spring System Produce the Same Results

It can be seen that the motion of the accepted one degree of freedom model and the ball balancer model are indistinguishable. This shows that the ball balancer model equations of motion accurately capture the motion of the ball balancer when moving in the horizontal direction.

Similarly, the physical parameters for the vertical case study are as follows: $g = 32.2$ ft/sec^2, $c_y = 0.153$ lbs-s/ft, $k_y = 15$ lbs/ft and $m_{BB} = 0.155$ slugs. The initial displacement and velocity in the vertical test case are $y_1(0) = y_0$ and $\dot{y}_1(0) = \dot{y}_0$. Figure 36 shows the comparison of the displacement, velocity and acceleration between the ball balancer and mass spring oscillator in the vertical direction,

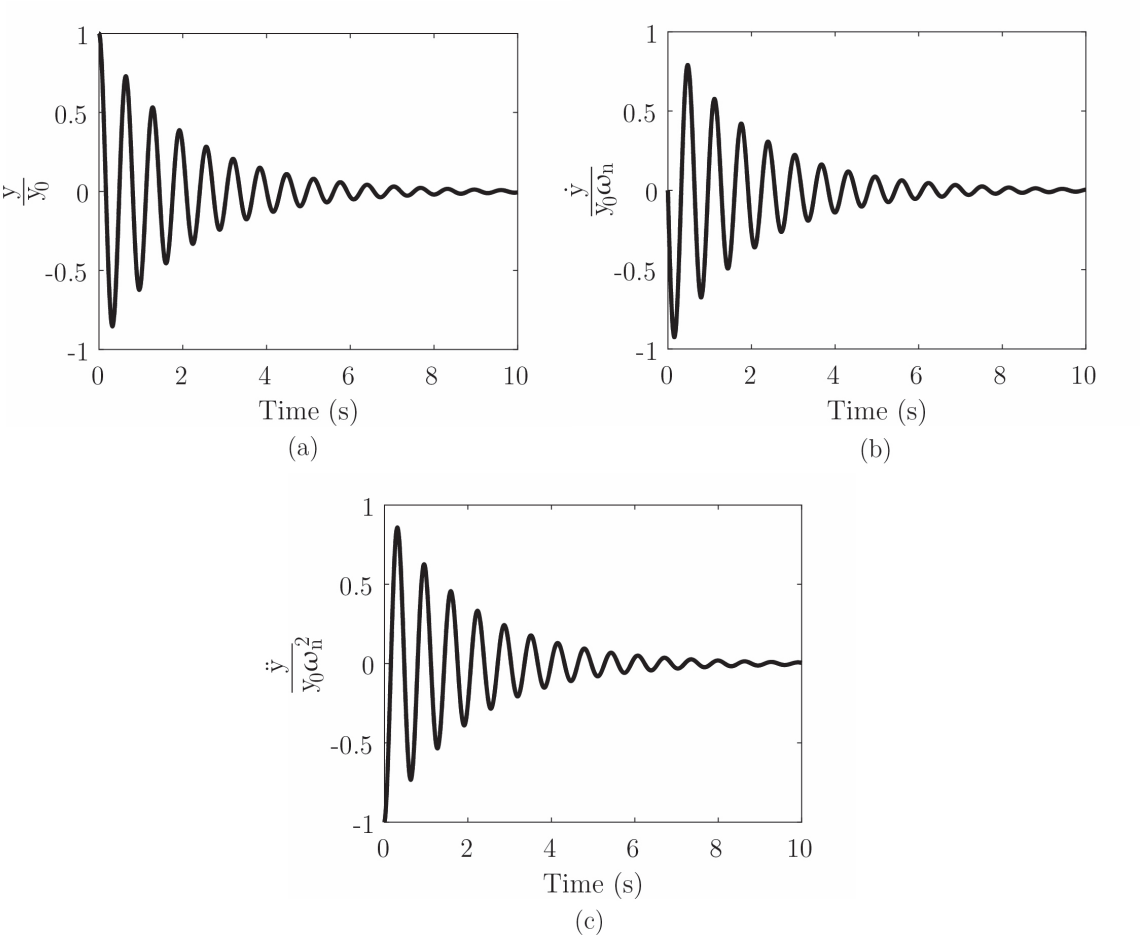

FIGURE 36 – The Displacement (a), Velocity (b) and Acceleration (c) of the Ball Balancer Model and the Traditional Vertical Mass Spring System Produce the Same Results

It can be seen that the motion of the accepted one degree of freedom model and of the ball balancer model are indistinguishable. This shows that the ball balancer model equations of motion accurately capture the motion of the ball balancer when moving in the vertical direction.

2. Ball Motion

To determine if the equations of motion describing the angular motion of a ball are correct, a comparison can be made to a simple, unforced pendulum with damping. The equations

of motion for the pendulum are shown below in Equations 94 and 95 in first order form,

$$\dot{\nu}_1 = \nu_2 \tag{94}$$

$$\dot{\nu}_2 = -\frac{g}{R}\sin(\nu_1) - \frac{d}{m_{P_1}}\nu_2 \tag{95}$$

The physical parameters for the case study are as follows: $g = 32.2$ ft/sec^2, $R = 1$ ft, $d = 0.005$ lbs-s/rad and $m_{P_1} = 0.0016$ slugs. The initial displacement and velocity for this test case are $\nu(0) = \nu_0$ and $\dot{\nu}(0) = \dot{\nu}_0$. The ball balancer model can again be compared to this simple model to ensure simple motion is accurately captured. Figure 37 shows the comparison of the displacement, velocity and acceleration between the pendulum motion and the ball motion with damping,

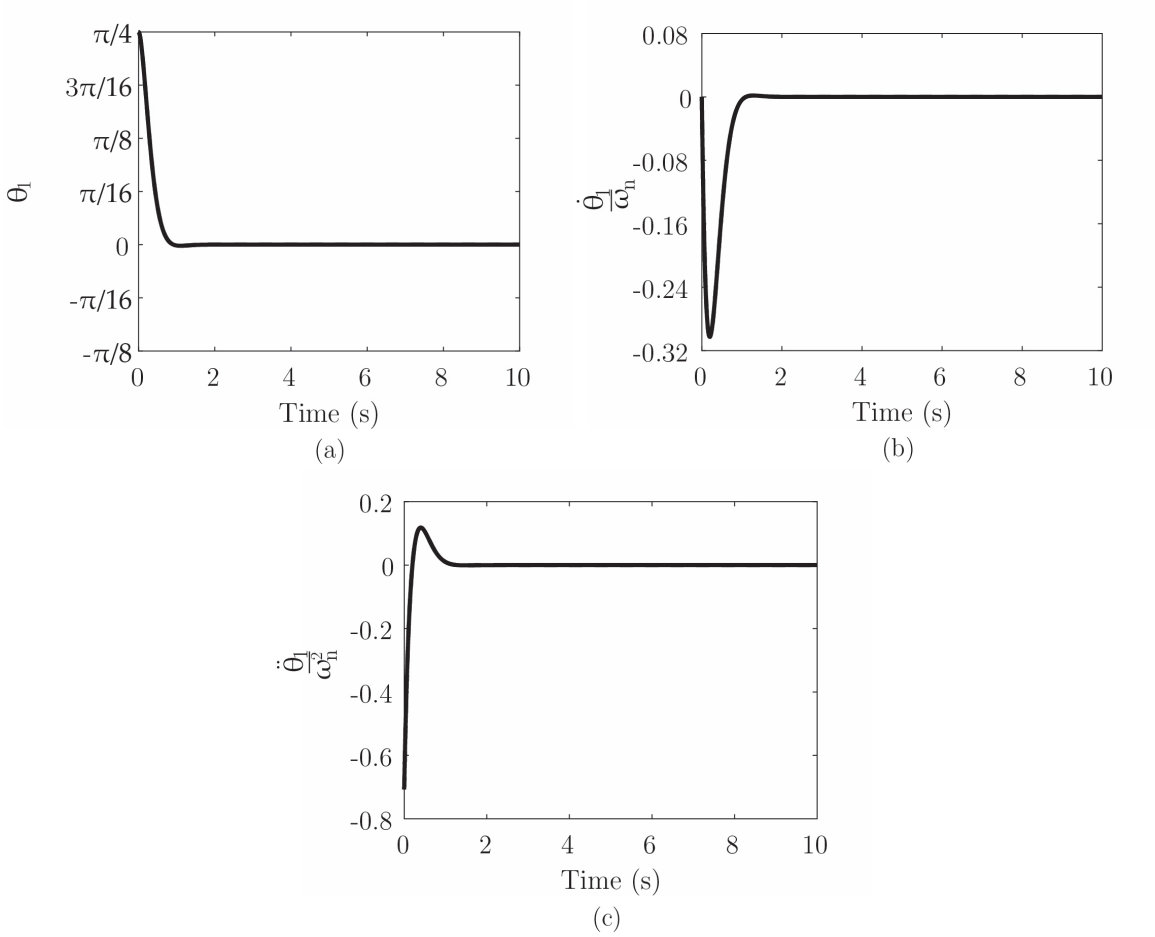

FIGURE 37 – The Displacement (a), Velocity (b) and Acceleration (c) of the Ball Balancer Model and the Traditional Pendulum Produce the Same Results

It can be seen that the motion of the accepted one degree of freedom model and of the ball balancer model are indistinguishable. This shows that the ball equations of motion accurately capture the motion of a single ball when moving in an unforced manner.

3. Ball Balancer Center of Gravity Rotational Motion

Lastly, to determine if the mathematical terms describing the rotational motion of the eccentricity are correct, a comparison can be made to a one degree of freedom rotating imbalance. The equations describing the rotating imbalance in the horizontal direction (no gravitational forces) where shown in Chapter II, but are shown again in Equations 96 and 97 in first order form,

$$\dot{u}_1 = u_2 \tag{96}$$

$$\dot{u}_2 = -\frac{k_x}{m_{BB}}u_1 - \frac{c_x}{m_{BB}}u_2 + \frac{m_e}{m_{BB}}e\omega_f^2 \sin(\omega_f t) \tag{97}$$

The equations of motion describing motion in the vertical direction (gravitational forces included) are shown below in Equations 98 and 99 in first order form,

$$\dot{y}_1 = y_2 \tag{98}$$

$$\dot{y}_2 = -\frac{k_y}{m_{BB}}y_1 - \frac{c_y}{m_{BB}}y_2 + \frac{m_e}{m_{BB}}e\omega_f^2 \sin(\omega_f t) - g \tag{99}$$

The physical parameters for the horizontal case study are as follows: $g = 32.2$ ft/sec^2, $R = 1$ ft, $c_x = 0.153$ lbs-s/ft, $k_x = 15$ lbs/ft, $m_e = 0.0016$ slugs, $m_{BB} = 0.155$ slugs and $\omega_f = 100$ RPM. The initial displacement and velocity in the horizontal test case are $x_1(0) = x_0$ and $\dot{x}_1(0) = \dot{x}_0$. Figure 38 shows the comparison of the displacement, velocity and acceleration between the ball balancer and rotating imbalance with damping in the horizontal direction.

It can be seen that the motion of the accepted one degree of freedom model and of the ball balancer model are indistinguishable. This shows that the ball balancer model equations of motion accurately capture the horizontal motion of the ball balancer when forced by the rotational motion of the eccentricity.

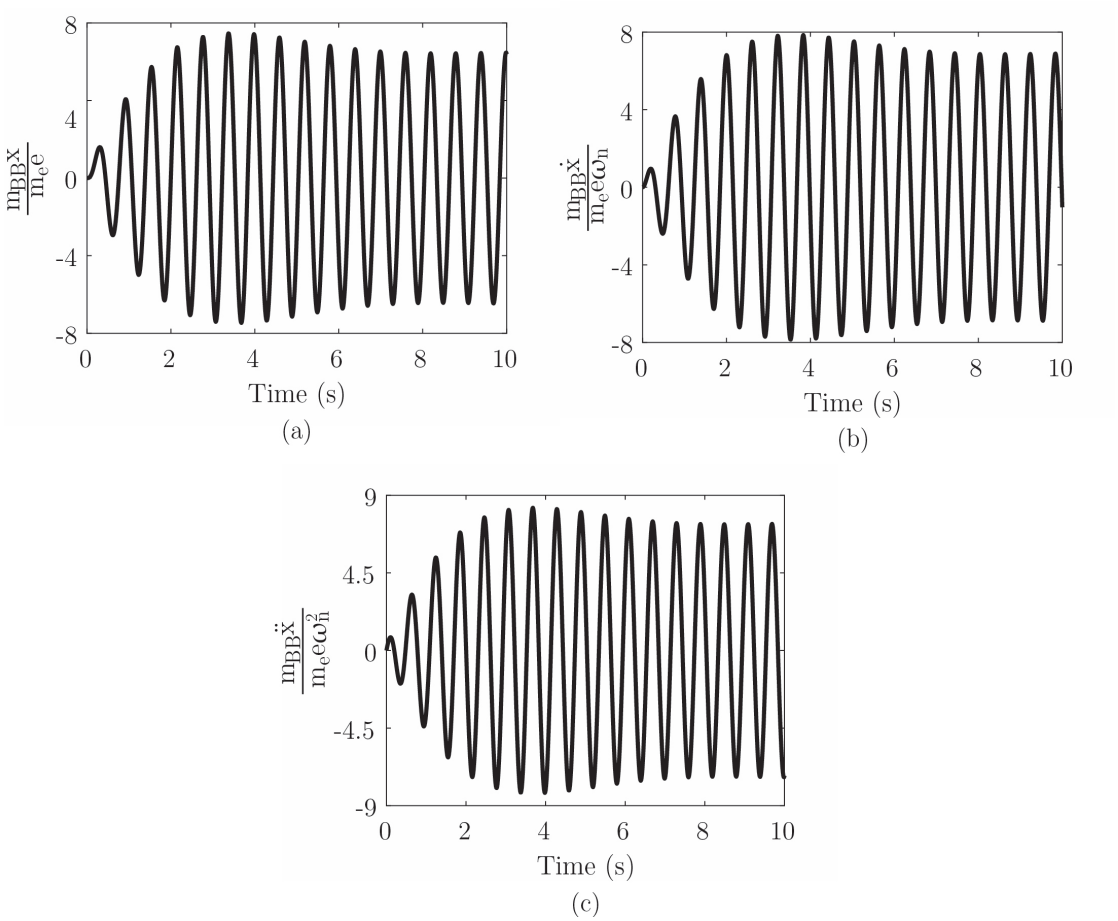

FIGURE 38 – The Displacement (a), Velocity (b) and Acceleration (c) of the Ball Balancer Model and the Traditional Horizontal Rotating Imbalance Produce the Same Results

Similarly, the physical parameters for the vertical case study are as follows: $g = 32.2$ ft/sec^2, $R = 1$ ft, $c_y = 0.153$ lbs-s/ft, $k_y = 15$ lbs/ft, $m_e = 0.0016$ slugs, $m_{BB} = 0.155$ slugs and $\omega_f = 100$ RPM. The initial displacement and velocity in the vertical test case are $y_1(0) = y_0$ and $\dot{y}_1(0) = \dot{y}_0$. Figure 39 shows the comparison of the displacement, velocity and acceleration between the ball balancer and mass spring oscillator with damping in the vertical direction.

It can be seen that the motion of the accepted one degree of freedom model and of the ball balancer model are indistinguishable. This shows that the ball balancer model equations of motion accurately capture the vertical motion of the ball balancer when forced by the rotational motion of the eccentricity.

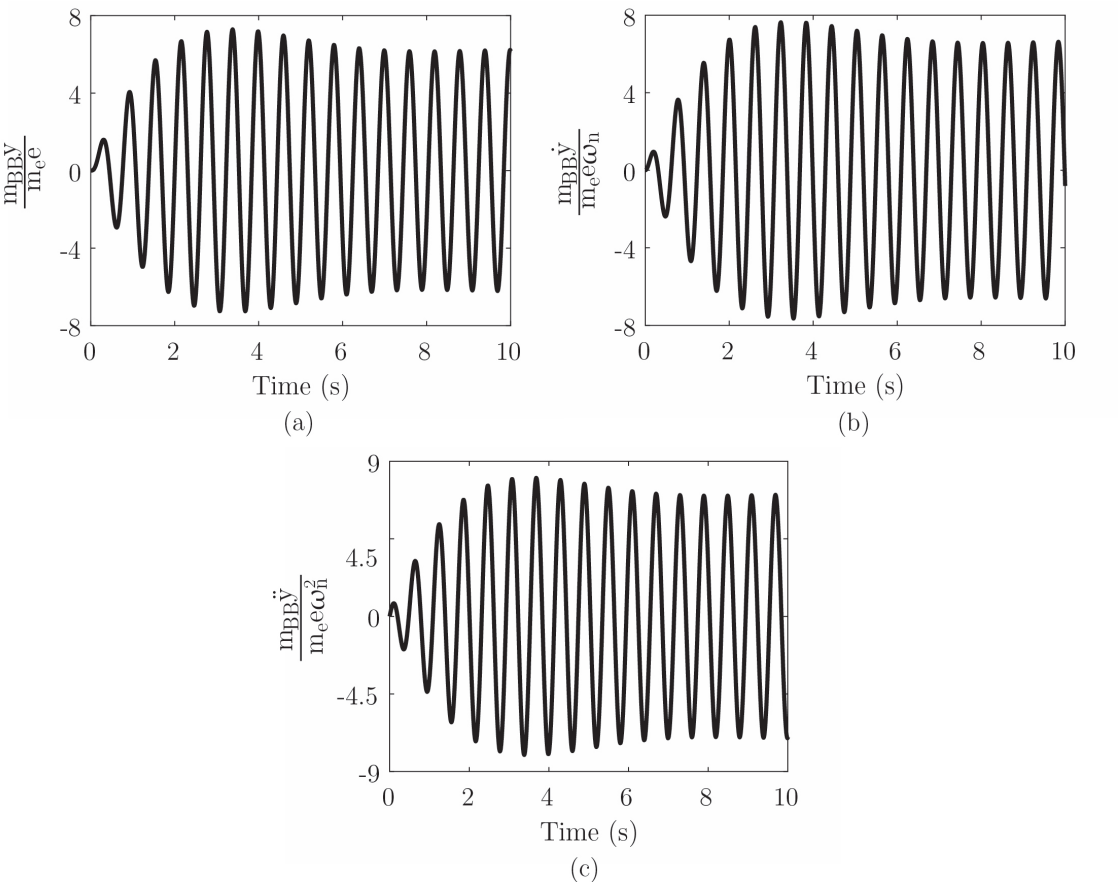

FIGURE 39 – The Displacement (a), Velocity (b) and Acceleration (c) of the Ball Balancer Model and the Traditional Vertical Rotating Imbalance Produce the Same Results

The previous validation analyses prove that the terms in the ball balancer equations of motion describing the sole motion of the ball balancer in the horizontal and vertical direction, the terms describing the sole angular motion of a ball, and the terms describing the rotation of the eccentricity are in fact correct. The following section will prove that the remaining terms in the equations of motion are also correct, as well as validating the integration method for collision and separation capture.

C. Collisions and Separations

When in service, a ball balancer has very complicated motion which couples the horizontal and vertical ball balancer motion to the angular ball motion. In addition to this, complexity is also added due to discontinuities that are introduced from ball interactions. Although easy to compare, one degree of freedom systems do not accurately depict these complicated motions. Short of running experiments to gain confidence in the accuracy of the ball balancer model, a more in-depth analysis must be performed to show that the ball balancer model is accurate and produces physically significant results. Since there are no simple models that can be used to

illustrate the accuracy of the coupled motion of the ball balancer, and collisions and separations, an energy analysis will be used. Several test cases are set up such that energy will always be conserved. If energy is lost or gained in these simulations, this is an indication that there is an error with the model; either the equations of motion are incorrect or there is some book-keeping mistake. The energy analysis will aid in making sure that the physics are correct and that the model is producing meaningful results.

To begin the energy analysis, all the different sources of energy must be identified to ensure total accountability. These sources of energy are as follows: the potential energy of the springs within the system, the gravitational potential energy of the bodies within the system, and the kinetic energy of the bodies within the system. The system begins the simulation with some amount of energy, which is based on initial conditions and the physical attributes of the system. Summing the energies at each integration step throughout the simulation should produce the same energy level. If there is some significant change, there is an error in the fidelity of the model.

The energy analysis will focus on the discontinuities that occur due to collisions and separations, but also on more complicated interactions between the balls and ball balancer. Test cases include the following: two balls allowed to collide with one another, two balls allowed to separate from one another and ten balls allowed to collide with one another. These three cases should give confidence in the ball balancer model when running more complicated simulations.

1. Two Balls Colliding

The first test case will detail the coupled motion between the ball balancer and the balls as well as further the confidence in the collision algorithm explained in Chapter III. In the following test case, no sources of energy dissipation are present, such that the energy analysis will simply be the addition of all the potential and kinetic energies present in the system.

The physical parameters for the case study are as follows: $g = 32.2$ ft/sec^2, $R = 1$ ft, $r_{1,2} = 0.5$ in, $c_x = c_y = 0$ lbs-s/ft, $k_x = k_y = 15$ lbs-s/ft, $m_{BB} = 0.155$ slugs, $m_{P_{1,2}} = 0.0016$ slugs, $I_{P_{1,2}} = 1.11 \times 10^{-6}$ slugs-ft^2 and $COR = 1.0$. The initial ball balancer displacement and velocity in the horizontal and vertical directions are $x(0) = x_0$, $y(0) = y_0$, $\dot{x}(0) = \dot{x}_0$, $\dot{y}(0) = \dot{y}_0$, respectively. The initial ball displacements are $\theta_1(0) = \theta_{1_0}$, $\beta_2(0) = \beta_{2_0}$ for the first and second ball, respectively. The initial ball velocities are $\dot{\theta}_1(0) = \dot{\theta}_{1_0}$, $\dot{\beta}_2(0) = \dot{\beta}_{2_0}$ for the first and second ball, respectively. Figure 40 shows the orientation of the two balls within the ball balancer at the beginning of the simulation.

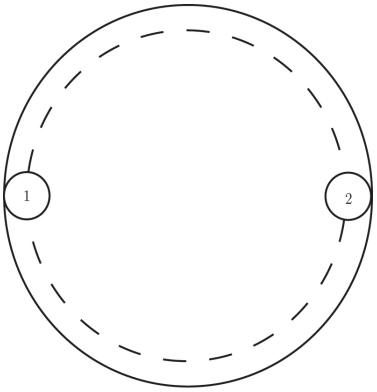

Note: Balls not drawn to scale

FIGURE 40 – The Initial Starting Positions of the Two Balls Inside the Ball Balancer

Figure 41 shows the total energy of the system over the course of the simulation time of this particular test case. The potential and kinetic energy sources that are summed for the system are the potential energy stored in the springs, the gravitational potential energy of the ball balancer and balls, the rotational energy of the rolling balls and the translational kinetic energy of the ball balancer and balls,

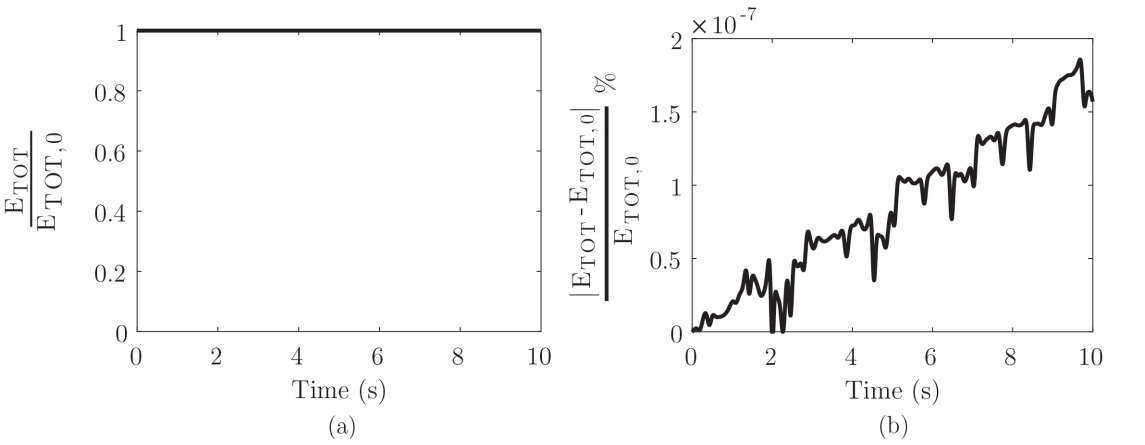

FIGURE 41 – The Total Energy in the System During the Simulation (a) and the Absolute Value of the Error in Energy During the Simulation (b)

It can be seen that there is little difference between the total energy of the system and the total amount of initial energy, with the loss in energy being on the order of $10^{-7}\%$, which is an acceptable error percentage. This shows that the ball balancer model equations of motion conserves energy, which gives confidence to the ball balancer model. It should be noted that over time, the error does increase slowly, which is directly due to the size of the time step chosen to integrate the equations of motion. The slope of the error versus time plot can be used to ensure that the error remains acceptable even after long simulation times using a particular step size. The displacement of the ball balancer and the ball displacements from this simulation are shown

in Figure 42 as well. For simplicity, only the first two ball collisions are shown,

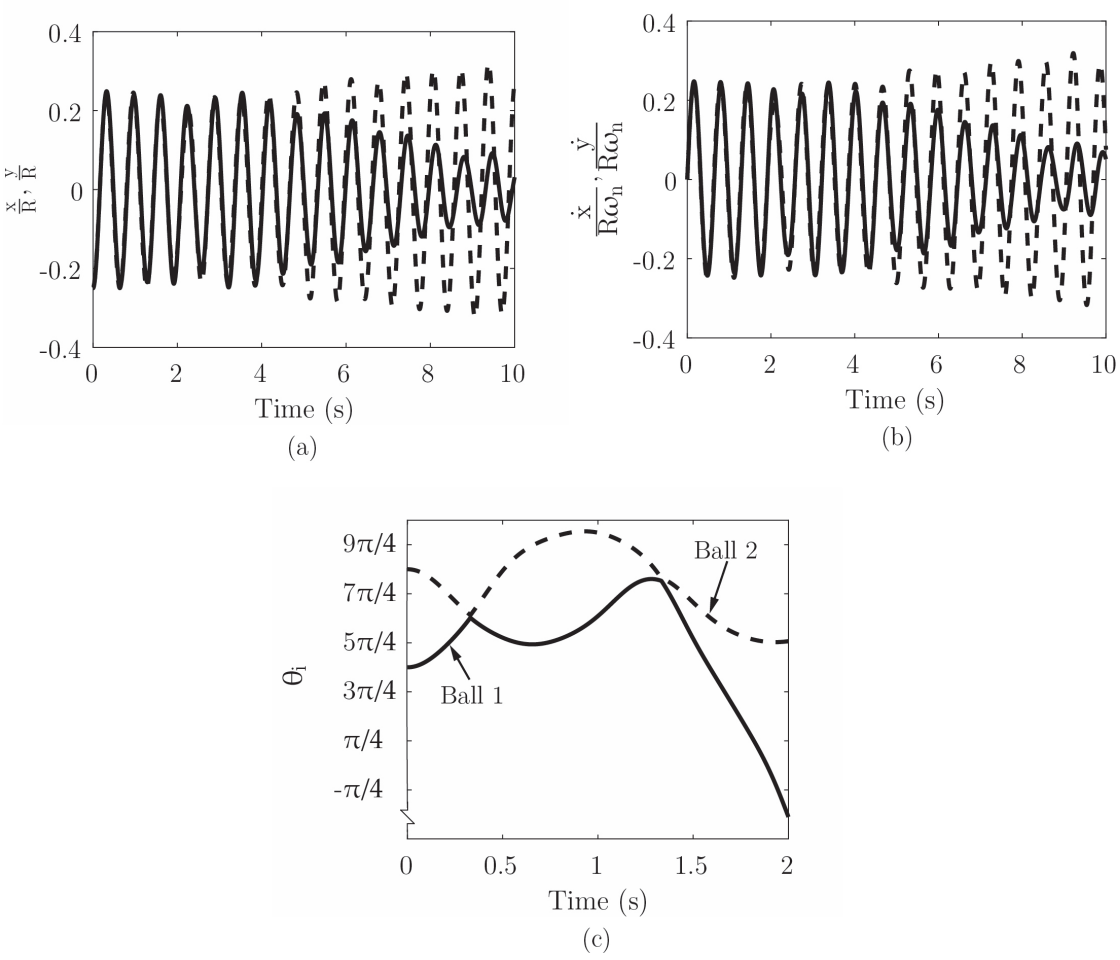

FIGURE 42 – The Displacement (a), Velocity (b) and Ball Locations (c) of the Ball Balancer Model. The Solid Line in (a) and (b) Represents the Horizontal Ball Balancer Motion, the Dashed Line Represents the Vertical Ball Balancer Motion

2. Two Balls Separating

The second test case will detail the coupled motion between the ball balancer and the balls as well as further the confidence in the separation algorithm explained in Chapter III. From this test case, two balls are in a train formation to begin, and then allowed to separate from one another as the simulation progresses. In the following model, no sources of energy dissipation are present, so the energy analysis will simply be the addition of all the potential and kinetic energies present in the system.

The physical parameters for the case study are exactly the same as the collision test case. The initial ball balancer displacement and velocity in the horizontal and vertical directions are $x(0) = x_0$, $y(0) = y_0$, $\dot{x}(0) = \dot{x}_0$, $\dot{y}(0) = \dot{y}_0$, respectively. The initial ball displacements are $\theta_1(0) = \theta_{1_0}$, $\beta_1(0) = \alpha$ for the first and second ball, respectively. The initial ball velocities are $\dot{\theta}_1(0) = \dot{\theta}_{1_0}$, $\dot{\beta}_2(0) = \dot{\beta}_{2_0}$ for the first and second ball, respectively. Figure 43 shows the

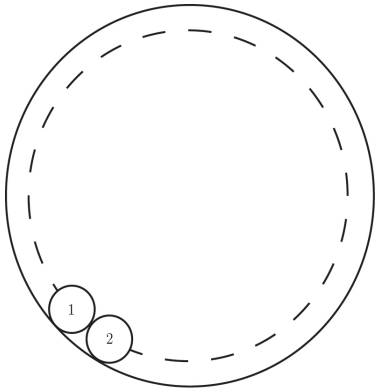

Note: Balls not drawn to scale

FIGURE 43 – The Initial Starting Positions of the Two Balls Inside the Ball Balancer

orientation of the two balls at the beginning of the simulation.

Figure 44 shows the total energy of the system over the course of the simulation time of this particular test case. The potential and kinetic energy sources that are summed for the system are the potential energy stored in the springs, the gravitational potential energy of the ball balancer and balls, the rotational energy of the rolling balls and the translational kinetic energy of the ball balancer and balls,

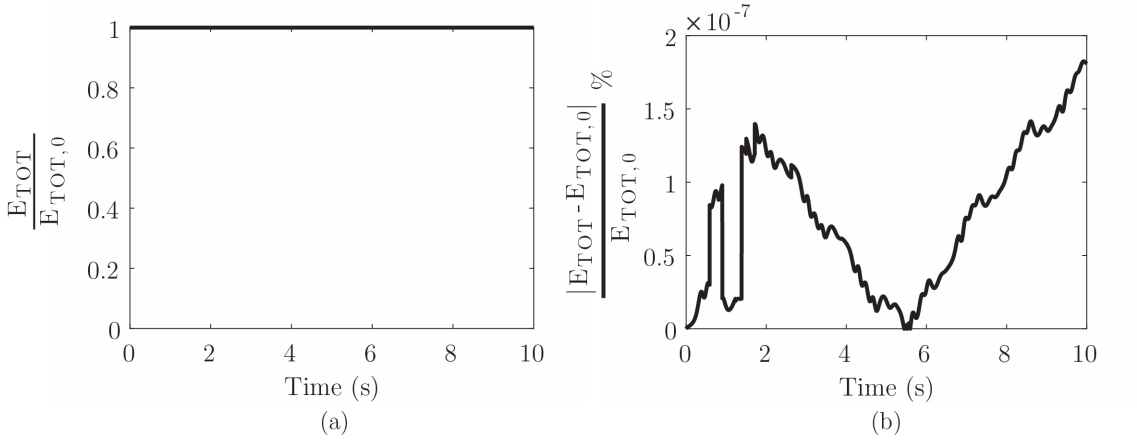

FIGURE 44 – The Total Energy in the System During the Simulation (a) and the Absolute Value of the Error in Energy During the Simulation (b)

It can be seen that there is little difference between the total energy of the system and the total amount of initial energy, with the loss in energy being on the order of 10^{-7}%. This again is an acceptable error percentage. This shows that the ball balancer model equations of motion conserve energy, which again gives confidence in the ball balancer model. The displacement of the ball balancer and the ball displacements from this simulation are shown in Figure 45 as well.

Note that there is a significant shift in the absolute value of the percent error near $t = 0.75$ s and $t = 1.50$ s. This shift is due to the Henon force step for a separation and a

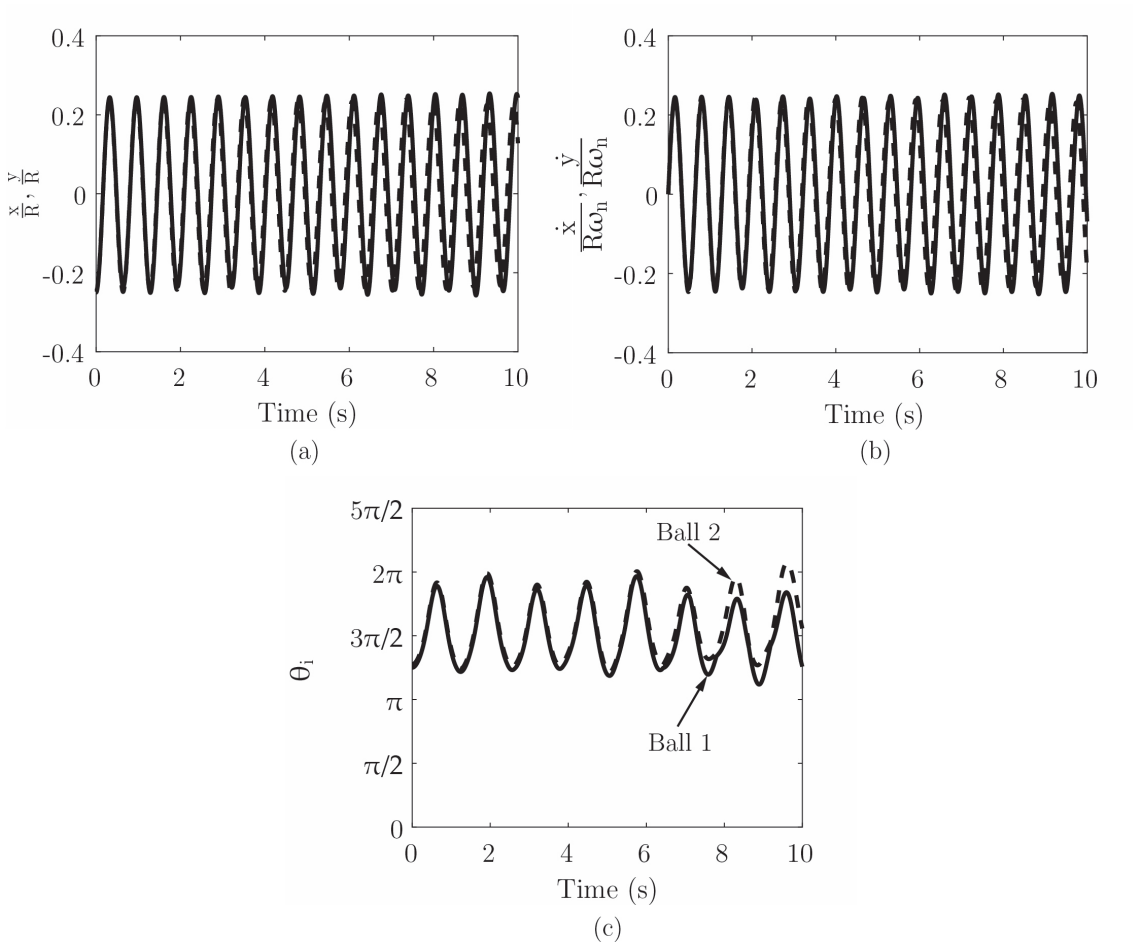

FIGURE 45 – The Displacement (a), Velocity (b) and Ball Location (c) of the Ball Balancer Model. The Solid Line in (a) and (b) Represents the Horizontal Ball Balancer Motion, the Dashed Line Represents the Vertical Ball Balancer Motion

Henon displacement step for a collision, respectively. This offset is simply an indication of the degree on non-linearity of these equations of motion. The transformation of the equations of motion sometimes leads to an abrupt change in energy like seen here. Although the change looks very drastic, energy is still being conserved within reasonable limits ($\approx 1 \times 10^{-7}\%$). Even though this behavior is undesirable, it is the reality of using the Henon method to solve for the discontinuities that occur within the model. This is also another reason why the Henon method is used sparingly and used only when needed.

3. Ten Balls Colliding

To conclude the validation section of this paper, the last test case will detail the coupled motion between the ball balancer and ten balls to gain full confidence in the equations of motion presented in Chapter VI and the book-keeping of the model. From this test case, there are ten balls evenly spaced throughout the ball balancer. As in the previous models, no sources of energy dissipation are present, so the energy analysis will simply be the addition of all the potential

and kinetic energies present in the system.

The physical parameters for this case study are very similar to the previous studies with the differences being: $r_{1-10} = 0.5$ in, $m_{P_{1-10}} = 0.0016$ slugs and $I_{P_{1-10}} = 1.11 \times 10^{-6}$ slugs-ft^2. The initial ball balancer displacement and velocity in the horizontal and vertical directions are $x(0) = x_0$, $y(0) = y_0$, $\dot{x}(0) = \dot{x}_0$, $\dot{y}(0) = \dot{y}_0$, respectively. The initial ball displacements are $\theta_1(0) = \theta_{1_0}$, $\beta_{2-10}(0) = \beta_{2-10_0}$. The initial ball velocities are $\dot{\theta}_1(0) = \dot{\theta}_{1_0}$, $\dot{\beta}_{2-10}(0) = \dot{\beta}_{2-10_0}$. Figure 46 shows the orientation of the ten balls in the ball balancer at the beginning of the simulation,

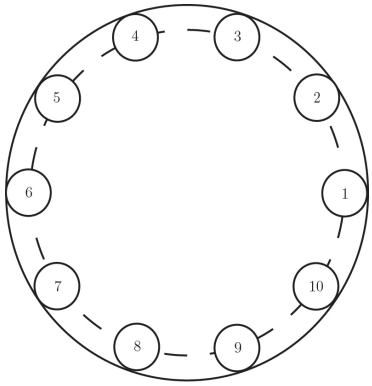

Note: Balls not drawn to scale

FIGURE 46 – The Initial Starting Positions of the Ten Balls Inside the Ball Balancer

Figure 47 shows the total energy of the system over the course of the simulation time of the ten ball test case. The same sources of kinetic and potential energies are summed as the previous examples,

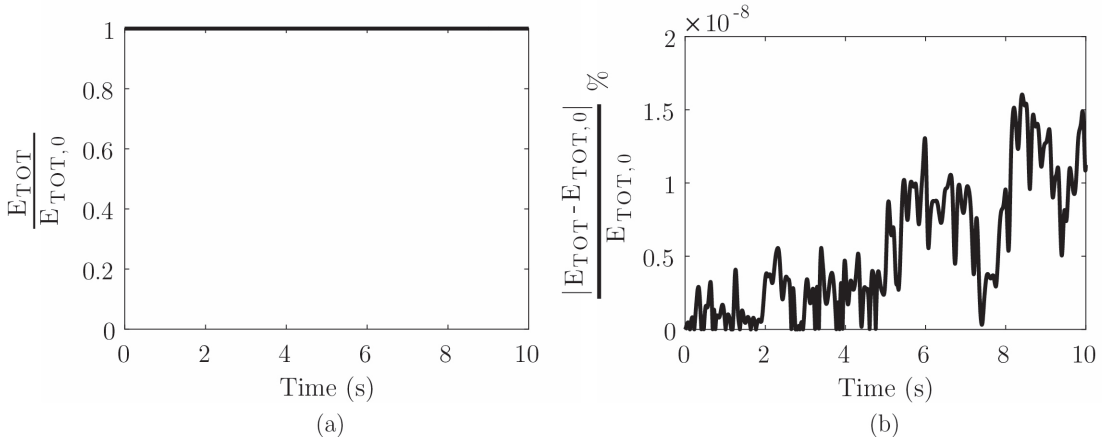

FIGURE 47 – The Total Energy in the System During the Simulation (a) and the Absolute Value of the Error in Energy During the Simulation (b)

It can be seen that there is little difference between the total energy of the system and the total amount of initial energy, with the loss in energy being on the order of 10^{-8}%, which

is an acceptable error percentage. This shows that the ball balancer model equations of motion conserve energy, which shows confidence in the ball balancer model. The displacement, velocity and acceleration of the ball balancer from this simulation are shown in Figure 48 as well,

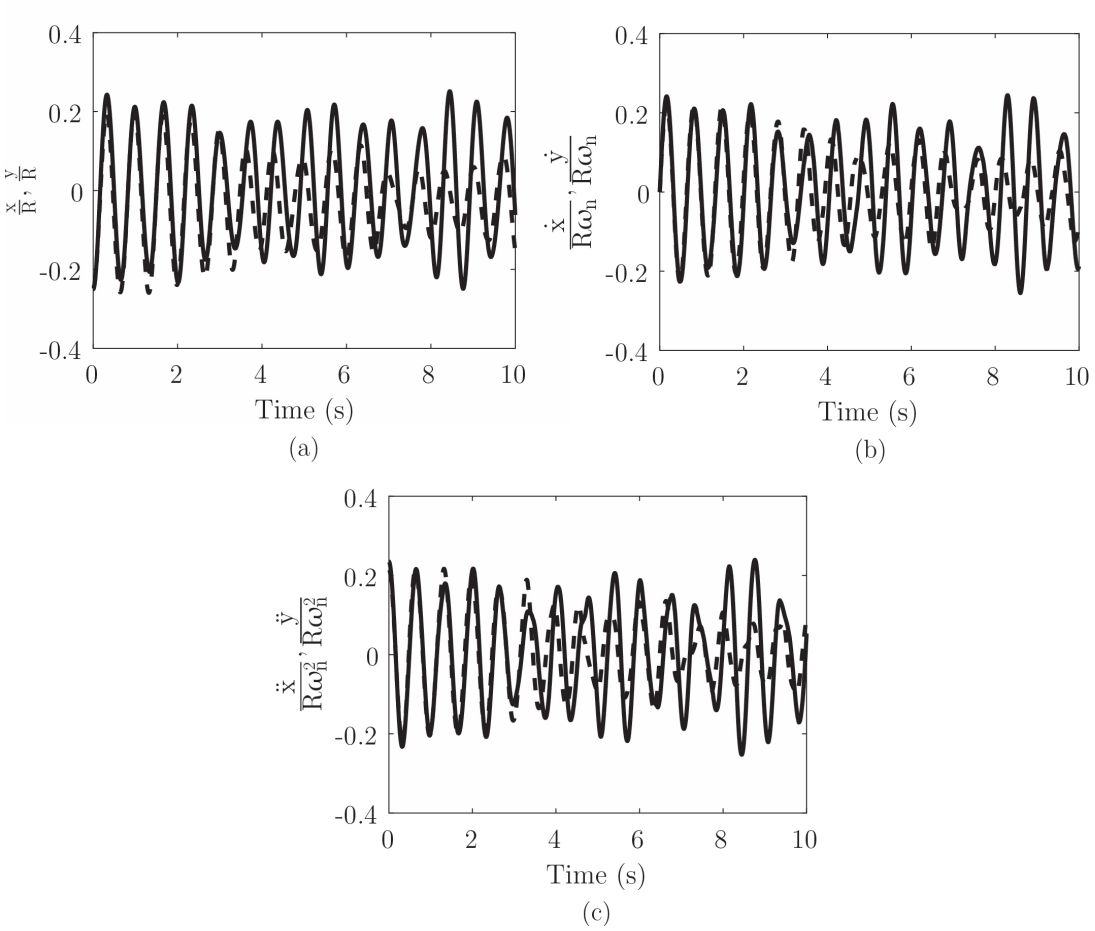

FIGURE 48 – The Displacement (a), Velocity (b) and Acceleration (c) of the Ball Balancer Model. The Solid Line Represents the Horizontal Ball Balancer Motion, the Dashed Line Represents the Vertical Ball Balancer Motion

The validation studies shown above, as well as the previous validation studies for the collision and separation algorithms presented in Chapters IV and V, give full confidence in the ball balancer model. Since the model was able to correctly output simple one degree of freedom motion, as well as illustrate energy conservation in complex ball balancer motion, there is reasonable confidence in the model to accept the conclusions from the analysis in the upcoming chapter.

Lastly, it should be noted that in the event of multiple collisions and/or separations during a single time step, the model is capable of discerning which collision or separation event comes first. This is done by simply solving for a specific collision or separation, and checking to make sure no other collisions or separations occurred within that integration step. If no other collisions or separations occurred, then the integration step is accepted and the model

resumes normal operation. If any number of other collisions or separations occur when solving for a different collision or separation, the model then recalls the data from the last successful integration step and solves for a different collision or separation event. The model will continue trying different collision or separation events until the correct collision or separation has been solved.

IX. STEADY STATE ANALYSIS

A. Introduction

The following chapter details the steady state analysis of the ball balancer that is described by the equations of motion presented in the previous chapters. An in-depth analysis will be presented that investigates the balancing effect that occurs above the system translational resonant frequency. The following analysis draws behavior comparisons when different amounts of eccentric mass are used, as well as when zero, one and two balls are present in the ball balancer. Additionally, comparisons are made between the consideration and negligence of collisions and train formation between balls.

B. Steady State Bifurcation

The beginning of this analysis makes use of steady state bifurcation plots to show the steady state behavior of the ball balancer with respect to rotational velocity. The main parameter of interest is the motion of the ball balancer from equilibrium; the horizontal and vertical motion. Ball balancer motion is very important for rotational and spin performance; it determines the motion envelope of the rotating body and the effectiveness of a ball balancer at offsetting an eccentricity. For this reason, ball balancer motion at steady state will be studied further.

The bifurcation plots that are presented were generated by sweeping through ball balancer rotation frequencies from 0 to $2\omega_n$. The amplitude response data was sampled at a frequency equal to the ball balancer rotation frequency, such that one Poincaré sample was collected for each period of ball balancer rotation. Care was also taken to ensure that the system was in fact at steady state, such that all transient motion had dissipated. This included adequate settling time and several revolutions of sampling to ensure that sufficient Poincaré samples of the ball balancer motion were captured. The bifurcation plots of the horizontal and vertical motion are presented when appropriate, but the total horizontal motion of the ball balancer from equilibrium will be observed more closely for simplicity.

Note that the following physical parameters were used in all analyses that follow: $c_x = c_y = 0.153$ lbs-s/ft, $k_x = k_y = 15$ lbs/ft, $m_{P_{1,2}} = 0.0016$ slugs, $m_{BB} = 0.155$ slugs, $COR = 0.85$, $\mu_R = 0.024$, $d = 0.015$ lbs-s/rad, $g = 32.2$ ft/s^2, $R = 1$ ft, $r_{1,2} = 0.5$ in and $I_{1,2} = \frac{2}{5} m_{P_i} r^2 = 1.08 \times 10^{-6}$ slugs-ft^2. The specific parameters regarding the amount of eccentric mass used in each simulation, number of balls, and consideration/negligence of collisions and separations will

be referenced specifically for each test case.

As mentioned previously, bifurcation plot generation involves recording Poincaré samples taken at a frequency equal to the ball balancer rotation frequency. For the sake of explanation, the study will begin with a ball balancer with the physical parameters listed above, and an eccentric mass equal to 0.05 lbs and one ball. Figure 49 shows the bifurcation plots for the horizontal displacement from equilibrium and vertical displacement from equilibrium for this particular test case,

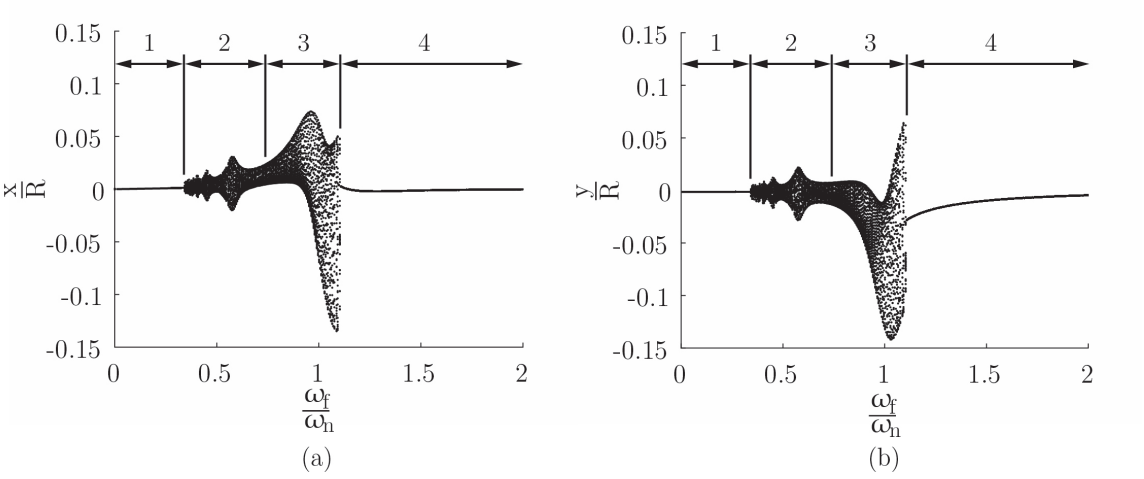

FIGURE 49 – Steady State Bifurcation Plots for the Horizontal (a) and Vertical (b) Ball Balancer Motion with 0.05 lbs of Eccentric Mass and One Ball

The plots shown in Figure 49 show that very interesting behavior develops as the rotational velocity of the ball balancer is varied. The characteristics of the bifurcation plot indicate that the ball balancer model is somewhat complicated; the additional degree of freedom coming from the ball adds in new and interesting behaviors. To investigate these different behaviors further, the bifurcation plot can be split up into zones to classify the steady state response within different ranges of rotational velocities. This paper will split the bifurcation plot into four zones and will give a high level explanation of what is happening within each zone. These four zones help to break down the different behaviors of the ball balancer and to show where the focus of this chapter will lie.

1. Zone One - $\dot{\phi} < 0.34\omega_n$

The first zone represents the region where the ball balancer is spinning at very low speeds ($\dot{\phi} < 0.34\omega_n$). In this zone, the ball has not started rolling around the ball balancer because the drag forces on the ball that initiate rotation are not yet high enough to overcome the gravitational force acting on the ball. The amplitude of the bifurcation plot is near zero for this zone since the motion of the ball balancer is very small. The horizontal motion of the

ball balancer and the ball displacement are shown in Figures 50a and b, respectively, for a ball balancer velocity of $0.2\omega_n$. The Poincaré samples used to develop the bifurcation plot at this velocity are shown by circles in Figure 50a. Additionally, a rotating reference frame is placed at point F', which is oriented according to $\mathbf{j}_1'$-$\mathbf{j}_2'$ and spins at the same rate of rotation as the ball balancer. This allows the relative ball location from that of the eccentric mass to be computed. Figures 50a and b indeed show that the ball has not begun its rotation around the ball balancer; it is clear that the ball motion lags the ball balancer motion. This is shown in Figures 50b, where the location of the eccentric mass is situated at 0 rad. The dotted lines in Figure 50b do not represent the actual motion of the ball, only the change in angular location since the ball balancer is circular. The transition out of zone one signifies the rotational speed at which the ball is picked up by the ball balancer and begins its rotation,

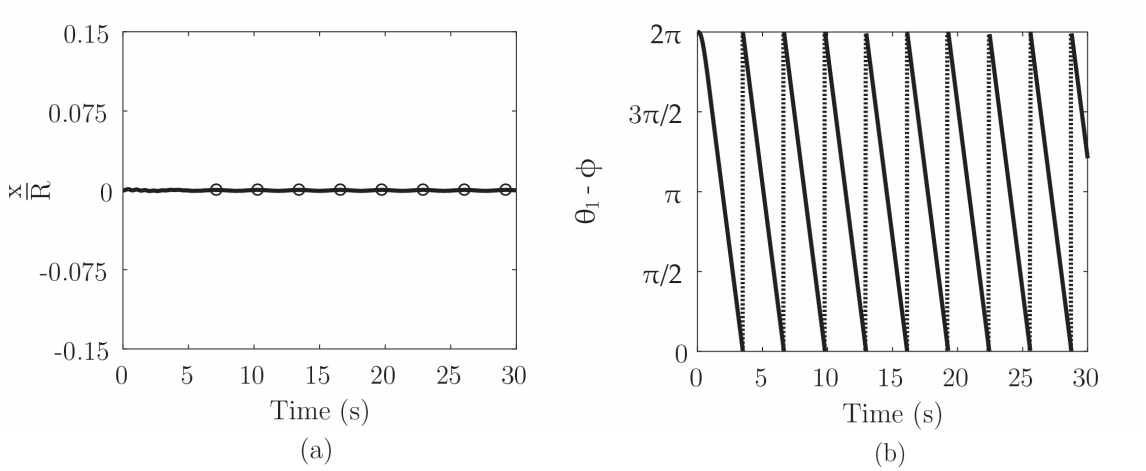

FIGURE 50 – Horizontal Ball Balancer and Ball Motion for Ball Balancer Velocity Located in Zone One

2. Zone Two - $0.34\omega_n \leq \dot{\phi} < 0.75\omega_n$

The second zone encompasses where the ball balancer is spinning fast enough such that the drag forces become of the same magnitude as the gravitational force acting on the ball, such that the ball finally begins rolling around the ball balancer. Additionally, the ball balancer velocity is still below the translational resonant frequency of the system ($0.34\omega_n < \dot{\phi} < 0.75\omega_n$), so the motion of the ball balancer continues to increase throughout this zone. Interestingly, there seem to be several sub-harmonics in this region; more investigation needs to be completed to understand what is causing these to develop. The horizontal motion of the ball balancer and the ball displacement are shown in Figures 51a and b, respectively, for a ball balancer velocity of $0.5\omega_n$. The Poincaré samples used to develop the bifurcation plot at this velocity are shown by circles in Figure 51a. Additionally in Figure 51b, a rotating reference frame is placed at point F'

that spins at the same rate of rotation as the ball balancer, this allows the relative ball location from that of the eccentric mass to be computed. Figure 51a and b indeed show that the ball is beginning its rotation around the ball balancer, but is still constantly lagging the motion of the ball balancer.

Unlike zone one, the Poincaré samples do not occur at the same relative location on each period of the horizontal motion response plot, even though the samples are in fact being taken at the correct sampling frequency. The reason for this drift in value is because the ball balancer motion frequency is slightly different from that of the ball balancer rotational frequency. This is caused by the presence of the ball and its interaction with the eccentric mass. Figure 51b shows that the ball is constantly lagging, which results in the ball adding to or offsetting the eccentric mass. The in-and-out phasing of the ball causes the ball balancer motion response frequency to deviate from the forcing frequency. In Figure 51b, the eccentric mass is located at 0 rad. Again, the dotted lines do not represent the actual motion of the ball, only the change in angular location since the ball balancer is circular. The transition out of zone two signifies the approach to the resonant frequency of the system,

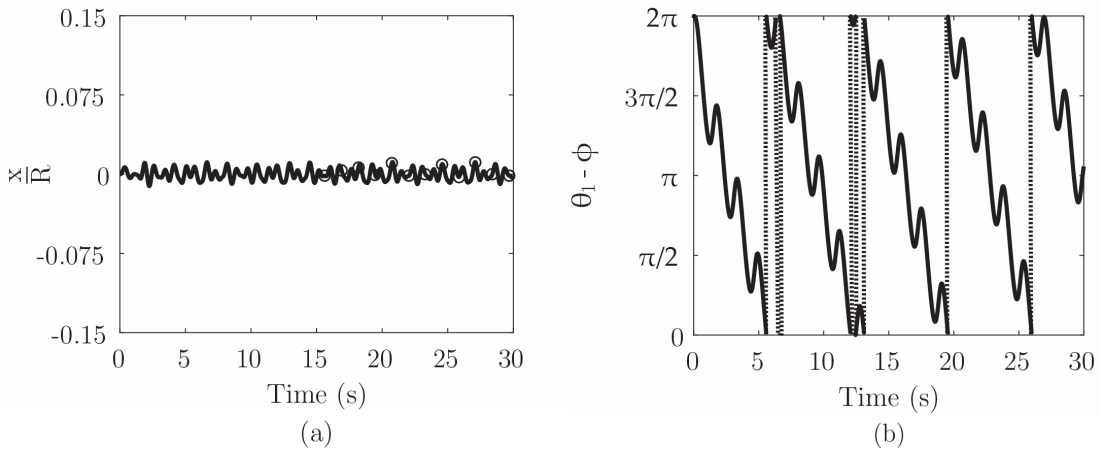

FIGURE 51 – Horizontal Ball Balancer and Ball Motion for Ball Balancer Velocity Located in Zone Two

3. Zone Three - $0.75\omega_n \leq \dot{\phi} < 1.11\omega_n$

The third zone represents the response of the ball balancer as the resonant frequency is approached and passed ($0.75\omega_n < \dot{\phi} < 1.11\omega_n$). The horizontal motion of the ball balancer and the ball displacement are shown in Figures 52a and b, respectively, for a ball balancer velocity of $1.0\omega_n$. In Figure 52b, a rotating reference frame is placed at point F' that spins at the same rate of rotation as the ball balancer, this allows the relative ball location from that of the eccentric mass to be computed. Similar to the second zone, the ball continues to lag the motion of the ball

balancer. However, as the rotational velocity continues to increase, the lagging motion continues to diminish, since the ball is beginning to find its settling position. Also since the ball balancer is passing through the resonant frequency of the system, the amplitude of the motion increases as the ball balancer velocity increases. Figures 52a and b indeed show both of these facts, the horizontal motion of the ball balancer is larger than that of zone two, and the ball is rotating around the ball balancer, but is constantly lagging the motion of the eccentric mass. Similar to zone two, the Poincaré samples do not occur at the same relative location on each period of the response plot, however the samples are in fact being taken at the correct sampling frequency. The reason for this drift in value is because of the motion of the ball relative to the eccentric mass. The same in-and-out phasing seen in zone two is also seen in zone three. In Figure 52b, the eccentric mass is located at 0 rad. The dotted lines do not represent the actual motion of the ball, only the change in angular location since the ball balancer is circular. The transition out of zone three signifies the rotational speed at which the ball begins to find its stable settling position; where there is no relative motion between the ball and the ball balancer,

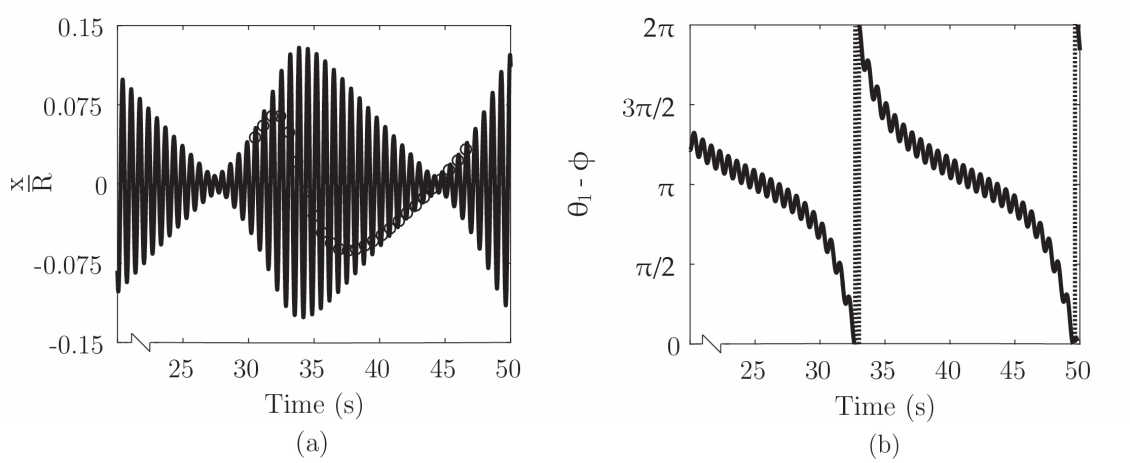

FIGURE 52 – Horizontal Ball Balancer and Ball Motion for Ball Balancer Velocity Located in Zone Three

4. Zone Four - $\dot{\phi} \geq 1.11\omega_n$

The fourth and final zone ($\dot{\phi} > 1.11\omega_n$) indicates where the ball balancer is spinning fast enough such that the ball achieves a stable settling position. This corresponds to a near zero amplitude on the bifurcation plot since the motion of the ball balancer is now in phase with the motion of the eccentric mass, as well as the fact that the ball is now offsetting the eccentric mass. This is the zone of operation where the ball balancer becomes effective at offsetting an eccentric mass. The horizontal motion of the ball balancer and the ball displacement are shown in Figures 53a and b, respectively, for a ball balancer velocity of $1.5\omega_n$. The Poincaré

samples used to develop the bifurcation plot at this velocity are shown by circles in Figure 53a. Additionally in Figure 53b, a rotating reference frame is placed at point F' that spins at the same rate of rotation as the ball balancer, this allows the relative ball location from that of the eccentric mass to be computed. Figures 53a and b indeed show that the ball has found its stable position within the ball balancer and is now moving in phase with the eccentric mass at an angular location that is opposite the eccentric mass. Similar to zone one, the Poincaré samples occur at the same relative location on each period of the response plot. Since the ball has found a stable settling location, there is no drift in Poincaré samples as seen in the second and third zones. In Figure 53b, the eccentric mass is located at 0 rad. The ideal settling location of the ball is located at π rad,

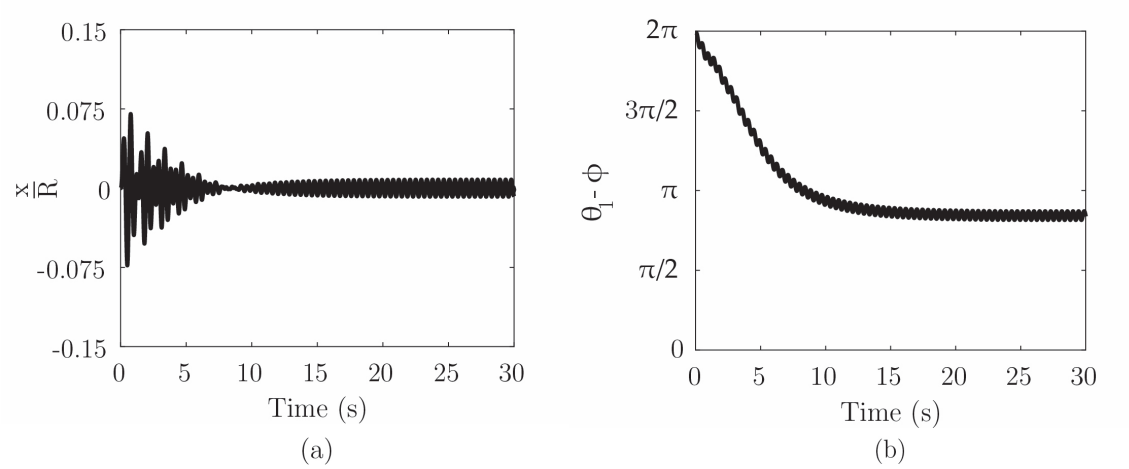

FIGURE 53 – Horizontal Ball Balancer and Ball Motion for Ball Balancer Velocity Located in Zone Four

As seen through the breakdown of the bifurcation plots, there are many interesting characteristics within each zone that could be studied. Each zone has a unique ball behavior that contributes to the total ball balancer motion in the region. Despite this, concentration will be placed on the transition between the third zone and into the fourth zone. This is the transition when the ball balancer finally becomes effective at offsetting the eccentric mass and when the ball finds a stable settling position. A desirable design parameter, the lower the rotational speed that this transition occurs, the more effective a ball balancer will be at offsetting an eccentricity. The following analysis will investigate how the maximum motion amplitude of the ball balancer changes with variable system parameters as this critical bifurcation point is crossed and exceeded.

C. Ball Balancer Maximum Motion Analysis

The next study will investigate the effect that the eccentric mass and ball interactions have on total ball balancer motion. As said before, the study will focus on the transition from the third zone and into the fourth zone, which defines the critical balancing bifurcation point. This bifurcation point will also be referred to as the "critical transition". This is when the maximum ball balancer motion begins to decrease due to the very presence of the balls. From a design standpoint, this transition is important; it reveals the rotational velocity/eccentric mass combination at which the ball balancer becomes effective at offsetting the eccentric mass. It is important to note that the speeds below the translational resonant frequency (zone one through three) are normally ramped through during normal operating behavior. This is because there are many steady state behaviors that are undesirable from a spin performance standpoint. Since speeds below the resonant frequency are ramped through, these regions are inherently transient in nature. For this reason, focus will only be placed on rotational velocities greater than the translational resonant frequency of the system, since the steady state behavior below the translational natural frequency is somewhat irrelevant. The analyses that follows will observe the motion of the ball balancer at three different rotational speeds, 140.8 RPM, 187.7 RPM and 234.6 RPM, which correspond to $1.5\omega_n$, $2.0\omega_n$ and $2.5\omega_n$, all of which are above the translational resonant frequency of the system. The effect that the eccentric mass and ball interactions have on the maximum ball balancer motion will be studied at these velocities. The amount of eccentric mass was varied between 0.000 lbs to 0.300 lbs and several test cases were run to determine the impact that ball count, presence/absence of collisions and ball size had on the motion behavior of a ball balancer.

1. Effect of Eccentric Mass on Ball Balancer Motion with PM Assumption

The bifurcation point that describes the critical transition is an important event that occurs in the operation of the ball balancer. The whole intent of the addition of the ball balancer is that the motion of the system is reduced when the balls finally find a stable settling position above the translational resonant frequency of the system. It is very interesting to determine the reduction in motion a ball balancer can achieve given a set of parameters before and after the critical transition. Instead of studying the steady state bifurcation plots further which were presented earlier, the amount of eccentric mass can be compared to maximum ball balancer motion amplitude to determine the relationship between the eccentric mass and ball balancer motion. The following study will begin by neglecting collisions, which has been the typical assumption of other ball balancer models. Figure 54 shows the maximum displacement amplitude of the ball balancer in the horizontal direction when zero, one and two balls are

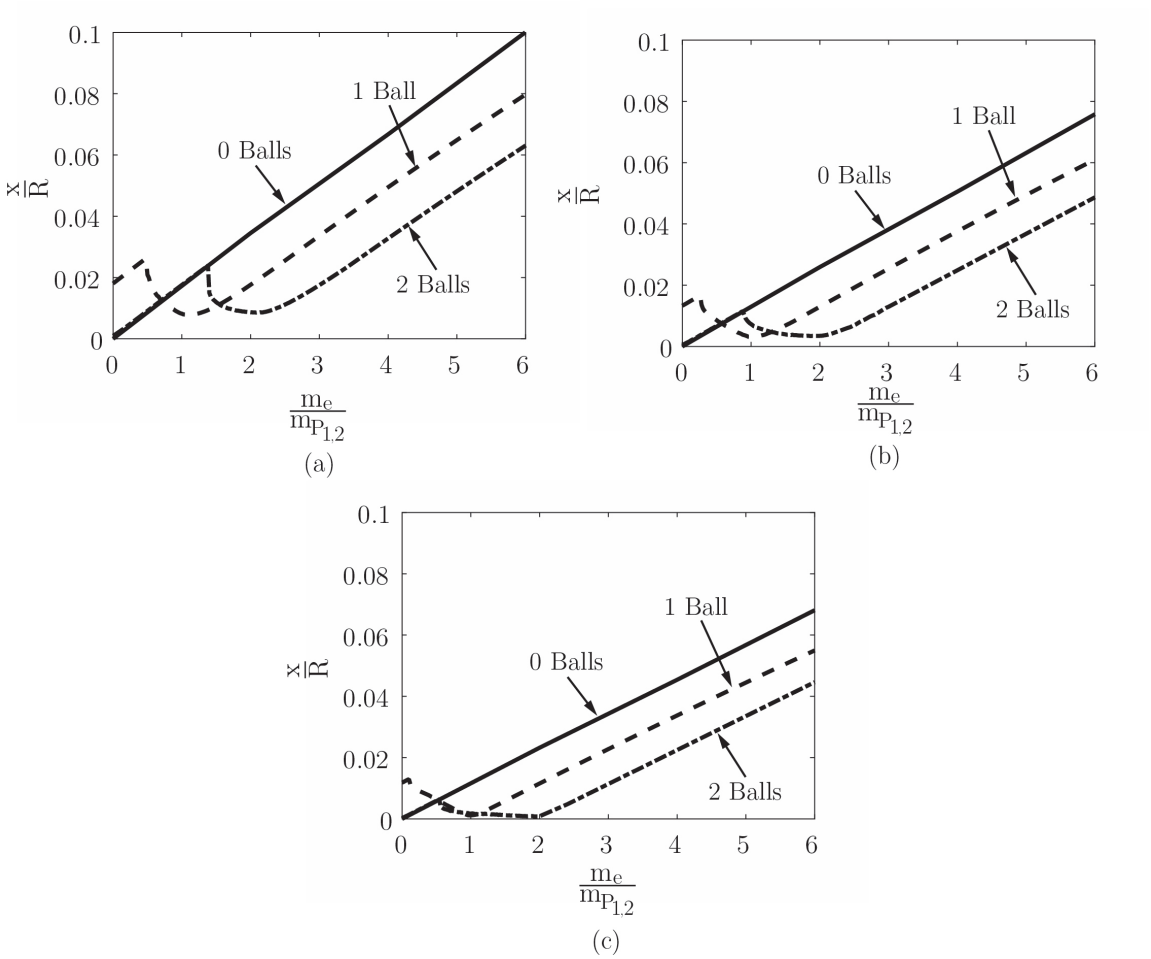

FIGURE 54 – The Maximum Horizontal Ball Balancer Motion as a Function of Eccentric Mass for Ball Balancer Rotational Velocities of $1.5\omega_n$ (a), $2.0\omega_n$ (b) and $2.5\omega_n$ (c) using the PM assumption

present and a point mass (PM) assumption is applied to the balls.

From the zero ball data in Figure 54, it can be seen that the horizontal displacement of the ball balancer increases linearly with eccentric mass. As the amount of eccentric mass increases, the offset of the center of gravity from the spin axis increases, thus the maximum whirling motion of the ball balancer increases. The zero ball data will serve as a baseline for the remaining test cases. This result is expected since there are no balls present to balance, or add to the eccentric mass.

The one ball test case finally shows the effectiveness of the ball balancer. The motion amplitude is eventually reduced, but at a price. In the $1.5\omega_n$ test case, it can be seen that the horizontal ball balancer motion begins at a higher amplitude than any other ball count. This is because the ball is either offsetting or adding to the eccentric mass; the maximum ball balancer motion occurs when the balls is adding to the eccentric mass. Since there is only one ball in the system, there is no balancing effect of the single ball due to the motion of a different

ball. Nonetheless, it can be seen that the amplitude of the motion increases linearly until a discontinuity occurs when $\frac{m_e}{m_{P_1}} = 0.48$. This discontinuity is the critical transition. At the critical transition, the ball finally becomes effective at balancing the eccentric mass because the ball stops lagging and begins moving in-phase with the eccentric mass. The ball also remains opposite the eccentric mass, where the eccentric mass is located at 0 rad. Figures 55a and b show how the ball stops moving when this bifurcation point is reached,

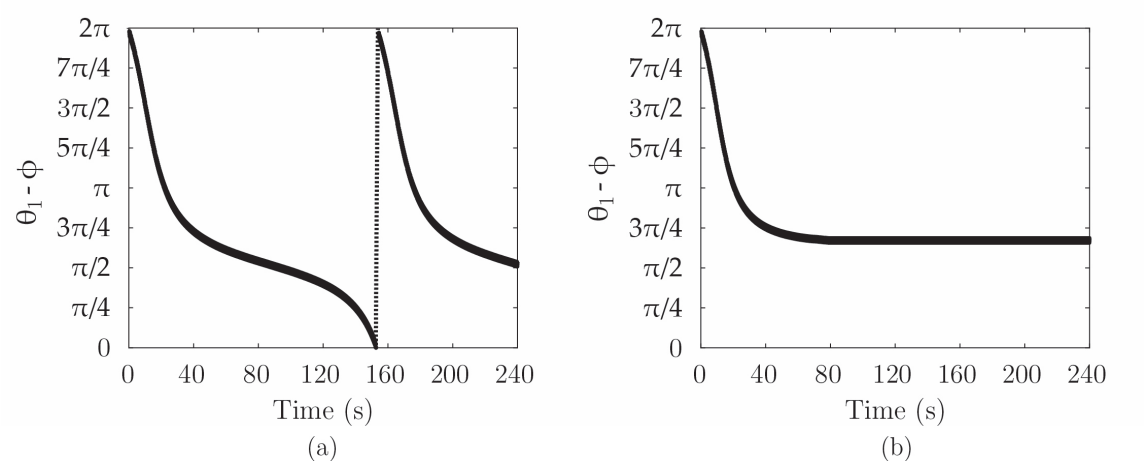

FIGURE 55 – The One Ball Motion Before (a) and After (b) the Critical Transition is Reached with a Ball Balancer Rotational Velocity of $2.0\omega_n$

After the critical transition is reached, the maximum ball balancer motion continues to decrease, until near $\frac{m_e}{m_{P_i}} = 1.12$, after which the motion begins to increase linearly again. This low point ($\frac{x}{R} = 0.0079$) is the "saturation point" of the ball balancer which means the ball balancer can no longer offset any more eccentric mass. The entire ball mass is being used to offset the eccentric mass. Increasing the ball balancer rotation speed, a similar trend is seen in the $2.0\omega_n$ case, but there are two significant differences. The first difference is the value of the eccentric mass at the critical transition ($\frac{m_e}{m_{P_i}} = 0.26$). As the velocity of the ball balancer increases, the onset of balancing occurs at a lower eccentric mass ratio. This is because the rotational forces acting on the ball are higher due to higher rotational velocity of the ball balancer. The onset of balancing is thus dependent on eccentric mass, as well as rotational velocity. The other difference is the magnitude of the ball balancer motion amplitude at the point of saturation ($\frac{x}{R} = 0.0032$). As the velocity of the ball balancer increases, the ball is able to more effectively offset the eccentric mass. The phase angle between the motion of the ball balancer and the forcing function approaches 180 degrees. Only when the phase angle is exactly 180 degrees will the ball be exactly opposite the eccentric mass. Although in equilibrium, the ball does not reside exactly opposite the eccentric mass at a rotational velocity equal to $1.5\omega_n$ and $2.0\omega_n$. Lastly, a similar trend is seen in the $2.5\omega_n$ case. The differences with this case

are that the critical transition occurs at an eccentric mass that is even lower than the previous two cases ($\frac{m_e}{m_{P_i}} = 0.10$) and the maximum amplitude at the saturation point is closer to zero ($\frac{x}{R} = 0.0010$), which is less than the previous two cases.

Figure 56a, b and c below show how the ball moves to offset the eccentric mass as the ball balancer velocity is increased from $1.5\omega_n$ to $2.5\omega_n$, where the eccentric mass is located at 0 rad,

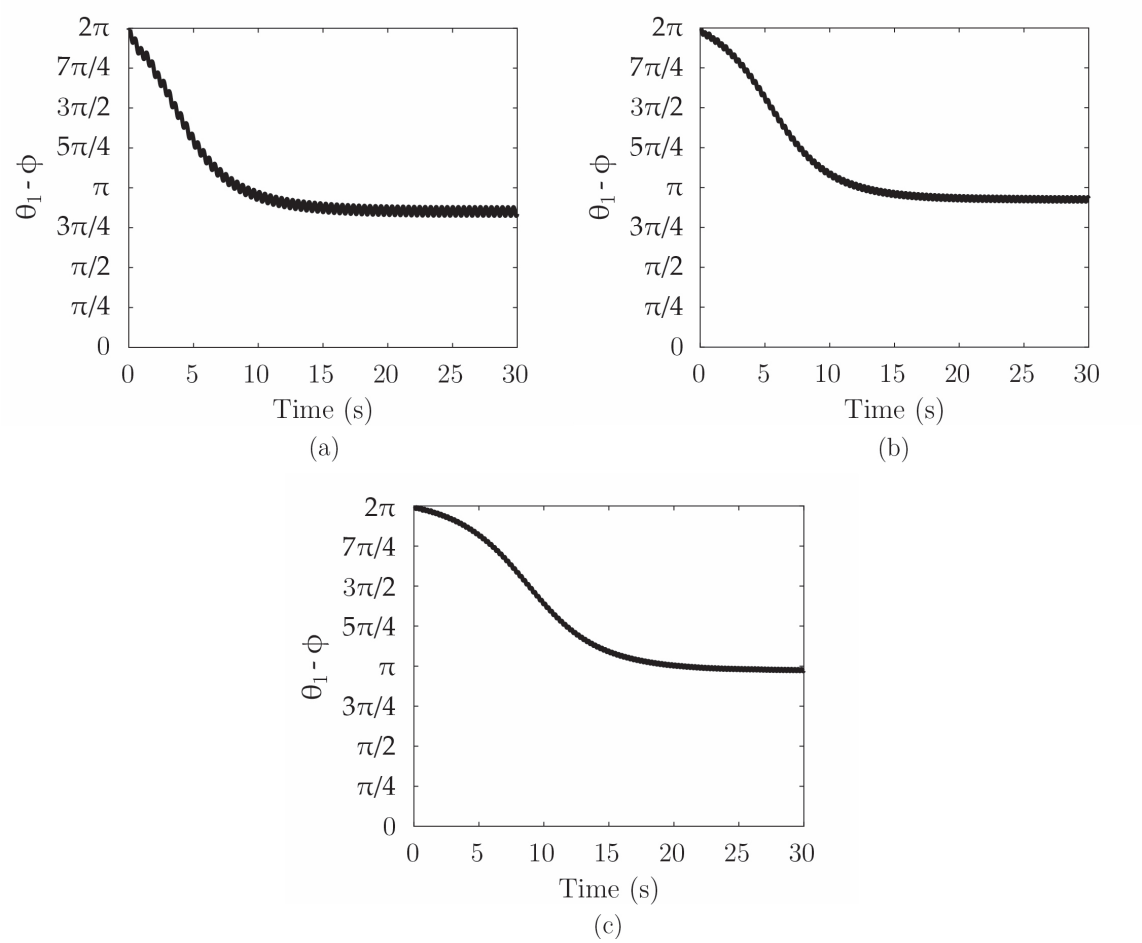

FIGURE 56 – The One Ball Motion with a Ball Balancer Rotational Velocity of $1.5\omega_n$ (a), $2.0\omega_n$ (b) and $2.5\omega_n$ (c)

The two ball test case is where more interesting motion begins to develop. As was seen in the one ball case, the motion of the ball balancer first begins to increase linearly as the eccentric mass is increased. However unlike the one ball case, the motion of the ball balancer is near zero when the eccentric mass is equal to zero. This is because the two balls work to balance each other, thus the eccentric mass is the sole unbalanced mass in the system. This is seen in Figure 57 which shows the ball balancer horizontal motion and the ball displacement. It can be seen that the balls are directly opposite one another, thus the net unbalanced mass is solely from the eccentric mass.

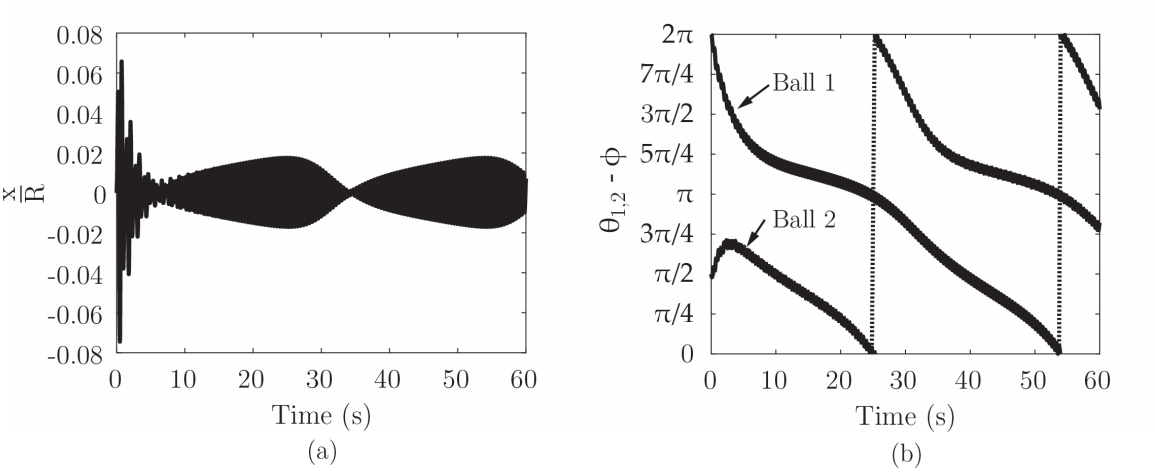

FIGURE 57 – The Two Ball Motion with a Ball Balancer Rotational Velocity of $1.5\omega_n$ with an Eccentric Mass Below the Critical Transition

In the $1.5\omega_n$ case, the motion of the ball balancer increases linearly as the eccentric mass is increased. The critical transition is reached when the eccentric mass equals $\frac{m_e}{m_{P_i}} = 1.38$, which represents the bifurcation point that determines when the two balls stop lagging the eccentric mass and settle to a stationary position. As the eccentric mass is increased further, the motion of the ball balancer continues to decrease. Figures 58a and b show how the balls find a stationary position to offset the eccentric mass once the critical transition has been reached, where the eccentric mass is located at 0 rad,

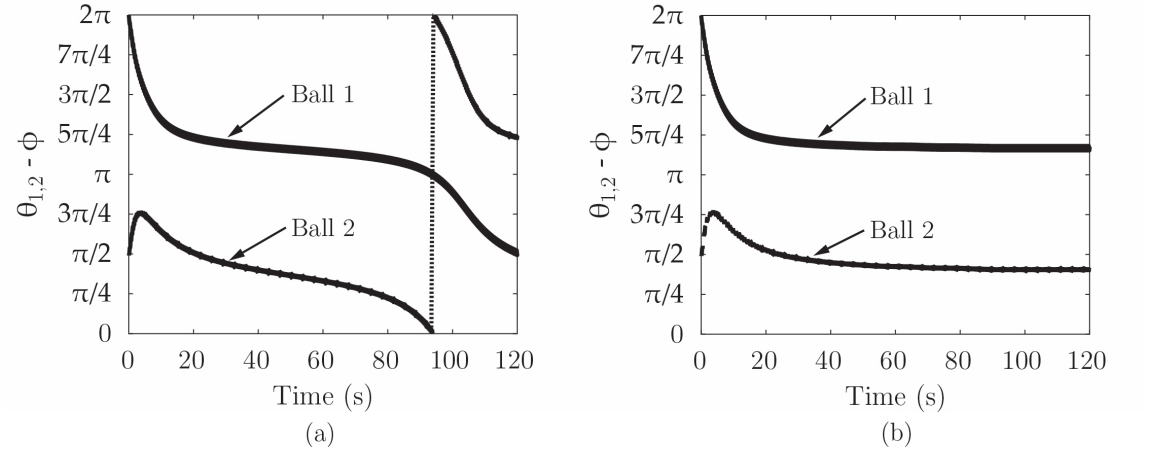

FIGURE 58 – The Two Ball Motion Before (a) and After (b) the Critical Transition is Reached with a Ball Balancer Rotational Velocity of $2.0\omega_n$

The reduction in ball balancer motion continues to decrease until approximately $\frac{m_e}{m_{P_i}} = 2.20$ after which the ball balancer motion begins to increase linearly. This low point ($\frac{x}{R} = 0.0087$) is when the ball balancer is saturated and can no longer completely offset any additional eccentric mass. Since there are two balls, the ball balancer has twice as much balancing capacity as the

single ball case. A similar trend is seen in the $2.0\omega_n$ case, but there are two significant differences. The first difference is the value of the eccentric mass at the critical transition. The eccentric mass at the critical transition is lower than before ($\frac{m_e}{m_{P_i}} = 0.88$). As the velocity of the ball balancer increases, the onset of balancing occurs at a lower eccentric mass since the rotational forces acting on the ball are larger. The other difference is the magnitude of the ball balancer motion at saturation ($\frac{x}{R} = 0.0035$). The ball balancer motion at saturation decreases with increasing rotational velocity. In the $2.5\omega_n$ case, the critical eccentric mass is even lower than the previous two cases ($\frac{m_e}{m_{P_i}} = 0.54$) and the maximum amplitude at saturation is close to zero ($\frac{x}{R} = 0.0047$), somewhat higher than the $2.0\omega_n$ case, but still lower than the $1.5\omega_n$ case. Another interesting behavior occurs as the rotational velocity is increased in the two ball case. Between the critical transition and the point of saturation, the motion amplitude of the ball balancer remains near zero and even decreases slightly as the eccentric mass is increased (seen more prominently in the $2.5\omega_n$ case). As the eccentric mass increases beyond the critical transition point, the balls move to an equilibrium position that attempts to completely offset the eccentric mass. As the rotational velocity and eccentric mass are increased, the forces that act on the balls that induce ball motion also increase. This increase in force tends to move the balls closer to the optimal balancing position. For this reason, the ball balancer motion amplitude decreases with increasing rotational velocity and increasing eccentric mass, until the saturation point is reached. Figure 59a, b and c show how the ball moves to a more optimal position that more effectively offsets the eccentric mass as the ball balancer velocity is increased, where the eccentric mass is located at 0 rad.

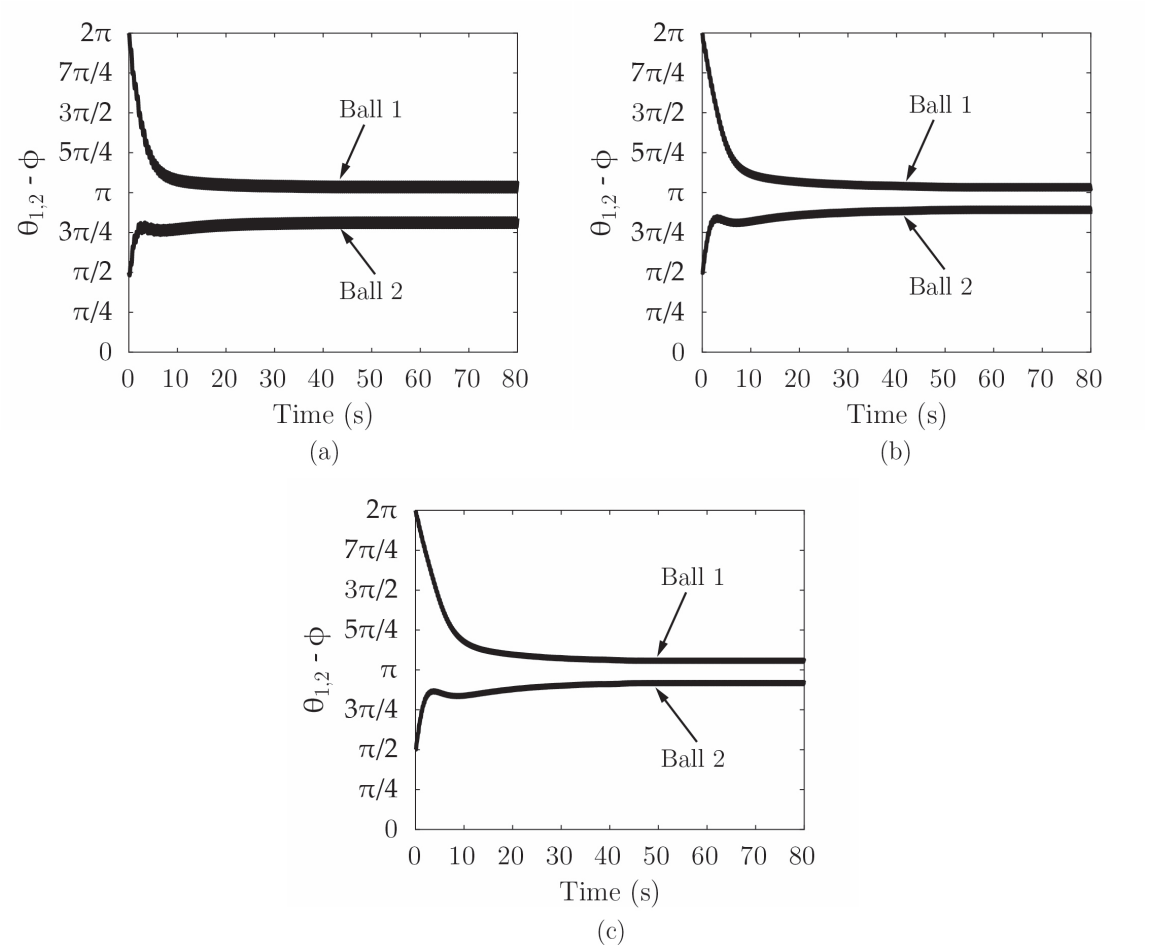

FIGURE 59 – The Two Ball Motion with a Ball Balancer Rotational Velocity of $1.5\omega_n$ (a), $2.0\omega_n$ (b) and $2.5\omega_n$ (c)

2. Effect of Eccentric Mass on Ball Balancer Motion with FR Assumption

It was seen from the previous study that the amount of eccentric mass and rotational velocity do have an effect on the motion amplitude of the ball balancer and ball motion. There is a critical transition (which is a function of eccentric mass and rotational velocity) that is reached, after which the motion amplitude of the ball balancer begins to decrease until a point of saturation. After the point of saturation, the motion amplitude increases linearly again. This next study will observe the change in ball balancer behavior when collisions and ball interactions are considered; the method discussed in Chapter III will be utilized. The next investigation studies the performance trade-off between the horizontal ball balancer motion and the amount of eccentric mass when zero, one and two balls are present in the ball balancer. Note that the algorithm will only apply to the two ball case. The main difference is that when in equilibrium, the balls cannot occupy the same space, instead they will have some relative angle that separates them. This offset will affect the final settling position of the two ball case if the two balls are touching. Figure 60 shows the steady state ball balancer motion when a finite radius assumption

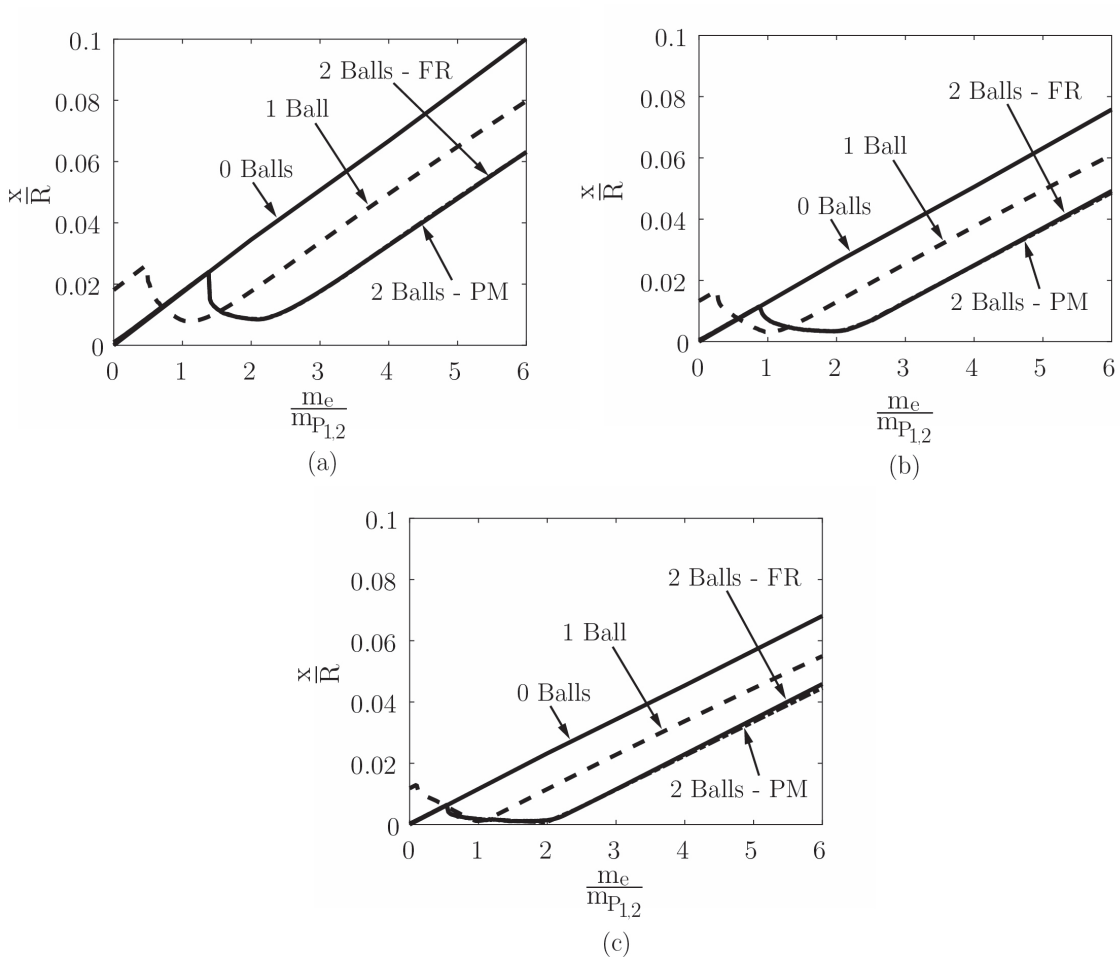

FIGURE 60 – The Maximum Horizontal Ball Balancer Motion as a Function of Eccentric Mass for Ball Balancer Rotational Velocities of $1.5\omega_n$ (a), $2.0\omega_n$ (b) and $2.5\omega_n$ (c) using the FR assumption

(FR) is used for two balls.

There is no difference in the zero and one ball behavior presented in Figure 60 since there is no difference when the PM assumption or FR assumption is used for these ball counts. The FR assumption only applies to the two ball case. Despite this, similar trends are seen with the two ball case when using the FR assumption as was seen with the PM assumption. It is clear that the ball balancer motion linearly increases as the eccentric mass is increased before the critical transition is reached. Once the critical transition is reached in the $1.5\omega_n$ case, the ball balancer motion begins to decrease and remains constant until the point of saturation is reached. At the point of saturation, the balls are now touching each other. For this reason the point of saturation occurs at a lesser eccentric mass ($\frac{m_e}{m_{P_i}} = 2.14$) than was seen with the PM assumption ($\frac{m_e}{m_{P_i}} = 2.20$). This makes sense since the balls are not able to occupy the same space, thus there is some angle that remains between them. The main difference between the PM assumption and the FR assumption occurs when the balls have finally arrived at the onset of

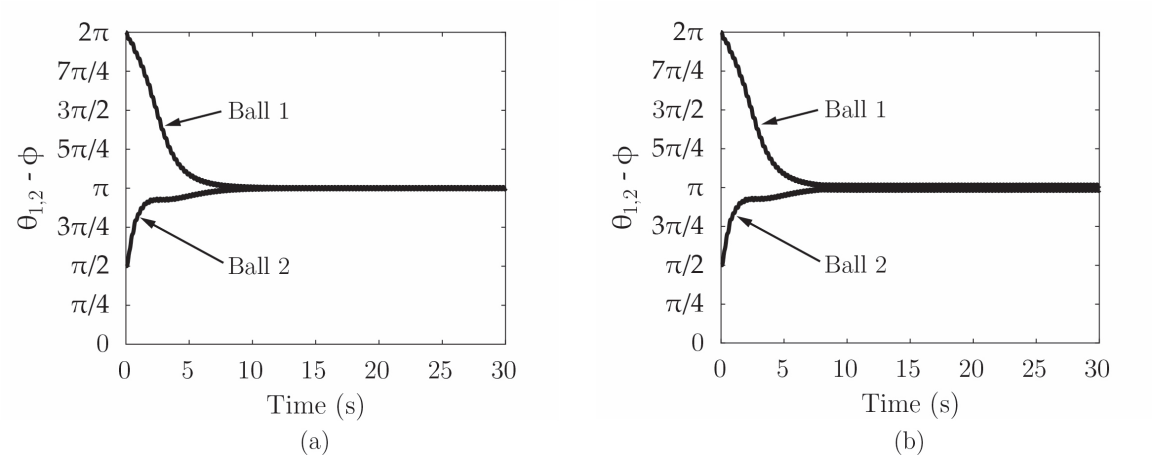

FIGURE 61 – The Angle that Separates the Balls in the Two Ball Case when the PM Assumption is Used (a) and when the FR Assumption is Used (b) with a Ball Balancer Rotational Velocity of $2.5\omega_n$ and $\frac{m_e}{m_{P_i}} = 4$

contact. As the eccentric mass is increased beyond the point of saturation, there is a small offset in the ball balancer motion between the two ball data when using the PM assumption versus the FR assumption. The center of gravity of the two ball system lies at some location closer to the geometric center of the ball balancer, thus the balls have a reduced balancing capacity. Regarding the two ball case, Figure 61a shows the location of the two balls when $\frac{m_e}{m_{P_i}} = 4$ at a rotational velocity equal to $2.5\omega_n$ when the PM assumption is used. Figure 61b shows the location of the balls when $\frac{m_e}{m_{P_i}} = 4$ at a rotational velocity equal to $2.5\omega_n$ when the FR assumption is used. It can be seen that there is a small offset between the two contacting balls.

It can be seen that the PM assumption allows the balls to occupy the same space, whereas the FR assumption causes the balls to remain some angular displacement apart from each other. This residual separation angle causes a very small increase in total ball balancer motion. For this particular test case, the ratio of ball radii to ball balancer radii was approximately 0.042. A ball radii to ball balancer radii of 0.042 increased the ball balancer motion by 0.025%. As this radii ratio is increased, one would expect the ball balancer motion to increase as well. Thus, the next study will investigate increasing the ball radii to something a bit larger and viewing the output of the ball balancer motion.

3. Effect of Eccentric Mass on Ball Balancer Motion with Different Ball Radii

A more interesting investigation singles out the two ball data and directly compares the two ball data using the PM assumption and the FR assumption when different ball radii are used. In the following investigation, three different ball radii are studied: $\frac{r}{R} = 0$, 0.042 and 0.167. Figure 62 shows the effect that the eccentric mass has on the total ball balancer horizontal motion when different radii of balls are present in the ball balancer. Note that only

a ball balancer rotational velocity of $2.5\omega_n$ is considered. This is because the balls have the highest chance of touching at this velocity since the angular forces acting on the balls are the highest. This will better illustrate the effect of the FR assumption,

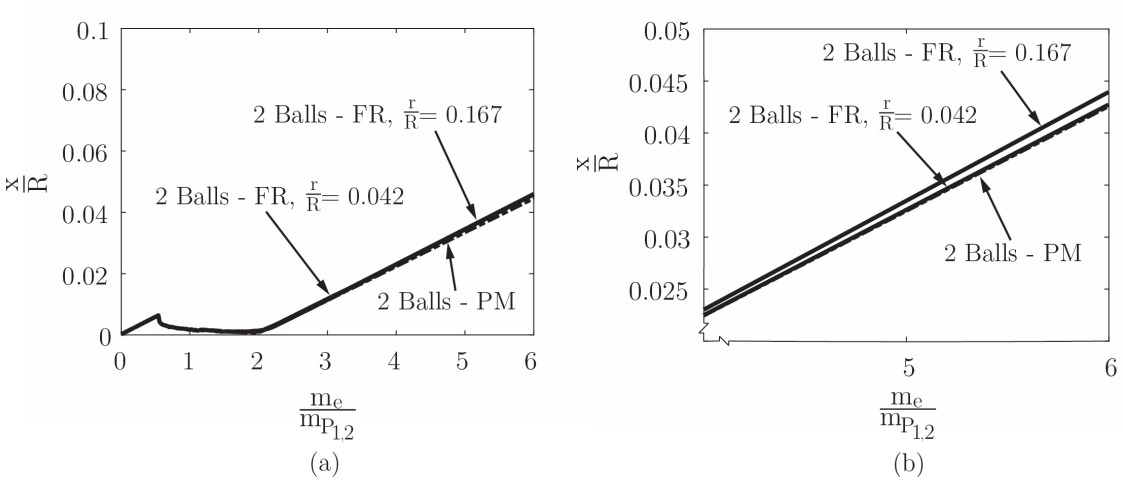

FIGURE 62 – The Maximum Ball Balancer Motion as a Function of Eccentric Mass for a Ball Balancer Rotational Velocity of $2.5\omega_n$ using the FR assumption (a). A Zoomed In View of the Maximum Ball Balance Motion for the Three Cases (b)

It can be seen that the effect of ball radii has no effect on ball balancer motion until the balls finally contact one another. The critical transition is the same for all three ball radii cases. However, the saturation point for the largest ball radii occurs at $\frac{m_e}{m_{P_i}} = 1.86$ with a ball balancer magnitude of $\frac{x}{R} = 0.0011$. The saturation point for the middle ball radii occurs at $\frac{m_e}{m_{P_i}} = 2.14$ with a ball balancer magnitude of $\frac{x}{R} = 0.0012$. The saturation point for the smallest radii (PM assumption) occurs at $\frac{m_e}{m_{P_i}} = 2.20$ with a ball balancer magnitude of $\frac{x}{R} = 0.0047$. The saturation point occurs at a smaller eccentric mass with a larger ball radii. This makes sense since the angle that separates the two contacting balls is larger than the other two cases. The larger separation angle reduces the balancing capacity of the ball balancer since the balls cannot occupy the same space. At a radii ratio equal to 0.042, the inclusion of the ball interactions caused a minimal increase in motion over the PM assumption. At a radii ratio equal to 0.167, the inclusion of the ball interactions caused a maximum increase in motion of $\frac{x}{R} = 0.0003$ over the PM assumption. In all, a maximum displacement error of 0.025% resulted from the case where the ball radii ratio was equal to 0.042. A maximum displacement error of 0.31% resulted from the case where the ball radii ratio was equal to 0.167. This shows that the size of the balls do in fact have an effect on the ball balancer motion at steady state, although somewhat small. As the sweep angle that defines a train of balls increases, the center of gravity of the train moves closer to the spin axis of the ball balancer. This reduces the effective balancing capacity of the system which in turn increases the system motion.

X. CONCLUSIONS

In conclusion, it was seen that the presence of a balancing device does in fact reduce the motion of a rotational system once that system has surpassed its translational resonant frequency. It was seen that the steady state behavior of a ball balancer displayed very interesting characteristics and could be split up into four zones. The first zone ($\dot{\phi} < 0.34\omega_n$) was characterized by small ball balancer displacements and a continually lagging ball motion. The viscous drag forces acting on the ball were not yet large enough to overcome the gravitational force acting on the ball. In the second zone ($0.34 \leq \dot{\phi} < 0.75\omega_n$), the viscous forces acting on the ball were large enough such that the ball began rotating around the ball balancer. The ball added to or offset the eccentric mass, such that the displacement of the ball balancer exhibited a phasing behavior. When the ball was near the eccentric mass, the ball balancer displacement was large. When the ball was opposite the eccentric mass, the ball balancer displacement was small. In the third zone ($0.75 \leq \dot{\phi} < 1.11\omega_n$), the rotational velocity of the ball balancer approached and surpassed the resonant frequency of the system. The ball balancer displacement increased as the resonant frequency was approached. Although the ball showed the phasing behavior as seen in zone two, the ball also showed the behavior of being on the verge of becoming stationary with respect to the eccentric mass. In the fourth zone ($\dot{\phi} \geq 1.11\omega_n$), the ball settled into a stationary position oriented opposite the eccentric mass. This reduced the overall motion of the ball balancer. This critical bifurcation point illustrated the benefit of using a ball balancer in rotational applications.

To narrow the focus of the analysis, the transition from the third zone into the fourth zone was studied. Two critical events were observed in the analysis. These two points were the "critical transition" and the "saturation point". The critical transition marked when the ball(s) stopped moving relative to the eccentric mass and settled into a position opposite the eccentric mass. After this transition, the ball balancer motion began to decrease. The saturation point marked when the full mass of the ball(s) could no longer offset the eccentric mass. After this point, the ball balancer motion began to increase again. In the first study, the PM assumption was used to understand the effect that eccentric mass and ball count had on ball balancer displacement. As was seen in the zero ball case, the ball balancer motion increased linearly with an increase in eccentric mass. With no balancing device present, the ball balancer motion was directly dependent on the amount of eccentric mass.

The single ball case had an undesirable effect before the critical transition was reached. The motion of the ball balancer was larger than that of the zero ball case since the ball directly added to the eccentric mass. In this case, the total unbalanced mass in the system was the sum of the eccentric mass and the ball. However, as the critical transition was surpassed, the single ball settled into a position that offset the eccentric mass. The ball balancer motion decreased below that of the zero ball case. The ball balancer motion continued to decrease until a saturation point was reached. After the saturation point, the ball balancer motion increased linearly again, but at an offset that was a reduction in motion compared to that of the zero ball case. These trends were also seen when the rotational velocity of the ball balancer was increased. When the rotational velocity was increased, the critical transition occurred with a smaller eccentric mass, and the amplitude of ball balancer motion at the saturation point was lower.

When two balls were placed in the ball balancer, the ball balancer motion did not exhibit the initial offset in motion below the critical transition like the one ball case. The two balls were shown to offset each other below the critical transition, thus the eccentricity was only a function of the eccentric mass. The two ball case showed similar behavior as compared to the one ball case. The differences being that the saturation point occurred at a larger eccentric mass since the combined balancing mass of the two ball case was double the one ball case. The other difference being that the offset in motion above the saturation point was further reduced. In all, the total motion of the ball balancer was reduced more when two balls were used. The same trends existed in the two ball case when the ball balancer rotational velocity increased. The key differences being that the critical transition occurred at a smaller eccentric mass and that the magnitude of ball balancer motion at the saturation point was reduced.

When the FR assumption was used in the two ball case, there was no change in ball balancer motion until the saturation point was reached. At the saturation point, the two balls came in contact with one another; this left some separation angle between the center of gravities of the two balls. The separation angle altered the equilibrium position for each ball, such that the center of gravity of the train was slightly closer to the spin axis of the system. This lead to a larger steady state ball balancer motion. The increase in motion only occurred when the balls were touching, which was more likely when the eccentric mass and the rotational velocity were larger. As the size of the balls increased, so did the angle that separated them, leading to a larger steady state ball balancer motion.

In all, there are many capabilities that are integrated into this ball balancer model. Although all these capabilities were not exercised in this paper, the data presented gives a glimpse into the power of this numerical tool and how the individual ball behavior can affect total ball balancer motion.

XI. RECOMMENDATIONS

The work completed in this paper indeed shows that the physical characteristics of the balls do make a difference. These differences may be small, but depending on the parameters of the system, the effect may not be negligible. Although all the data presented here involves the ball balancer rotating at steady state, due to the practical nature of ball balancers, the transient behavior should be just as interesting. Rotational speeds below the translational resonant frequency of the system are typically ramped through. However, these velocities must be traversed in order to reach higher velocities when the ball balancer is effective. For this reason, more work needs to be done to understand the transient effect that collisions and train formation have on steady state ball balancer motion. Although not seen in the analysis presented in this paper, the transient effect of collisions may have an effect on the end settling position of balls, as well as the amount of time it takes for a ball to find its equilibrium position. This research will help to develop the understanding of the transient region at speeds below the resonant frequency of the system so the total ball balancer motion can be reduced even at low speeds.

Although this paper only investigated the use of one and two balls, the next work should be focused on the use of more balls in the ball balancer, such that three, four or more balls are used. With more balls in the ball balancer, not only will collisions be more likely, but the sweep angle of a train of balls becomes larger. This larger sweep angle alters the net center of gravity of the train of balls and will possibly lead to larger deviations in motion compared to motion seen using the PM assumption. This will be especially important at high rotational velocities above the translational resonant frequency of the system when the balls tend to collect together and form a train. In addition, the PM assumption seems appropriate for two balls when the ratio between the ball radius to ball balancer radius is low and the system is at a rotational velocity above the resonant frequency of the system. However, care must be taken to consider the spatial characteristics of the balls as the ratio of the ball radius to ball balancer radius is increased or the sweep angle is increased.

The model that was presented in this paper is a powerful tool with many capabilities that were not totally utilized. However this model can be used to understand not only the total ball balancer behavior, but also the individual ball behaviors that contribute to the ball balancer motion. Further work using the FM assumption should be focused on this fact: how the ball-to-ball interactions affect the total ball balancer motion.

REFERENCES

Blanco-Ortega, A. et al. 2008. Active disk for automatic balancing of rotor-bearing systems. *2008 American Control Conference*, 3024–3028.

Bykov, B.G. 2013. Auto-balancing of a rotor with an orthotropic elastic shaft. *Journal of Applied Mathematics and Mechanics* 77, 369–379.

Chan, T.C., C.K. Sung, and Paul C.P. Chao. 2012. Friction effect on ball positioning of an automatic balancer in optical disk drives. *Microsystem Technologies* 18, 1343–1351.

— . 2011. Non-linear suspension of an automatic ball balancer. *International Journal of Non-Linear Mechanics* 46, 415–424.

Chao, Paul C.P., Yaw-Der Huang, and Cheng-Kuo Sung. 2003. Non-planar dynamic modeling for the optical disk drive spindles equipped with an automatic balancer. *Mechanism and Machine Theory* 38, 1289–1305.

Chung, J. 1999. Dynamic analysis of an automatic dynamic balancer for rotating mechanisms. *Journal of Sound and Vibration* 228-5, 1035–1056.

— . 2004. Effect of gravity and angular velocity on an automatic ball balancer. *Journal of Mechanical Engineering Science* 219,C, 43–51.

Dedow, G. and Dr. K. Murphy. 2016. Numerical computation of impact and separation events. *N/A* N/A, N/A.

Ehyaei, J. and Majid M. Moghaddam. 2009. Dynamic response and stability analysis of an unbalanced flexible rotating shaft equipped with n automatic ball-balancers. *Journal of Sound and Vibration* 321, 554–571.

Gorbenko, A.N. 2003. On the stability of self-balancing of a rotor with the help of balls. *Strength of Materials* 35-3, 305–312.

Green, K., A.R. Champneys, and M.I. Friswell. 2006. Analysis of the transient response of an automatic dynamic balancer for eccentric rotors. *International Journal of Mechanical Sciences* 48, 274–293.

Green, K., A.R. Champneys, and N.J. Lieven. 2006. Bifurcation analysis of an automatic dynamic balancing mechanism for eccentric rotors. *Journal of Sound and Vibration* 291, 861–881.

Green, K. et al. 2008. Investigation of a multi-ball, automatic dynamic balancing mechanism for eccentric rotors. *Philosophical Transactions of the Royal Society, A* 366, 705–728.

Henon, M. 1982. On the numerical computation of Poincaré maps. *Physica D* 5, 412–414.

Huang, Chun-Lung. 2008. Design and simulation of a sliding mode controller for reducing radial vibration of an eccentric rotor equipped with an automatic dynamic balancer. *IEEE Computer Society*, 23–28.

Huang, W.Y. and C.P. Chao. 2002. The application of ball-type balancers for radial vibration reduction of high-speed optic disk drives. *Journal of Sound and Vibration* 250-3, 415–430.

Hwang, Cheol-Ho and Jintai Chung. 1999. Dynamic analysis of an automatic ball balancer with double races. *JSME Series C* 42, 265–272.

Kim, Taekil and Sungsoo Na. 2013. New automatic ball balancer design to reduce transient-response in rotor system. *Mechanical Systems and Signal Processing* 37, 265–275.

Kim, W. and J. Chung. 2002. Performance of automatic ball balancers on optical disc drives. *Journal of Mechanical Engineering Science* 216-C, 1071–1080.

Kim, Wonsuk, Dong-Jin Lee, and Jintai Chung. 2005. Three-dimensional modeling and dynamic analysis of an automatic ball balancer in an optical disk drive. *Journal of Sound and Vibration* 285, 547–569.

Lu, Chung-Jen and Meng-Hsuan Tien. 2012. Pure-rotary periodic motions of a planar two-ball auto-balancer system. *Mechanical Systems and Signal Processing* 32, 251–268.

Lu, Chung-Jen and Ming-Cheng Wang. 2011. Stability analysis of a ball-rod-spring automatic balancer. *International Journal of Mechanical Sciences* 53, 846–854.

Rajalingham, C. and R.B. Bhat. 2006. Complete balancing of a disk mounted on a vertical cantilever shaft using a two ball automatic balancer. *Journal of Sound and Vibration* 290, 169–191.

Rajalingham, C., R.B. Bhat, and S. Rakheja. 1998. Automatic balancing of flexible vertical rotors using a guided ball. *International Journal of Mechanical Sciences* 40-9, 825–834.

Rajalingham, C. and S. Rakheja. 1998. Whirl suppression in hand-held power tool rotors using guided rolling balancers. *Journal of Sound and Vibration* 217-3, 453–466.

Rodrigues, D.J. et al. 2008. Automatic two-plane balancing for rigid rotors. *International Journal of Non-Linear Mechanics* 43, 527–541.

— . 2011a. Experimental investigation of a single plane automatic balancing mechanism for a rigid rotor. *Journal of Sound and Vibration* 330, 385–403.

— . 2011b. Two-plane automatic balancing: a symmetry breaking analysis. *International Journal of Non-Linear Mechanics* 46, 1139–1154.

Sohn, Jin-Seung et al. 2007. Dynamic analysis of a pendulum dynamic automatic balancer. *Shock and Vibration* 14, 151–167.

Sperling, L. et al. 2002. Simulation of two-plane automatic balancing of a rigid rotor. *Mathematics and Computers in Simulation* 58, 351–365.

Sung, C.K. et al. 2013. Influence of external excitations on ball positioning of an automatic balancer. *Mechanism and Machine Theory* 69, 115–126.

Thearle, E.L. 1961. Automatic dynamic balancers part 2 - ring, pendulum, ball balancers. *Naval Research Logistics Quarterly* 8, 175–191.

Tucker, W. 2002. Computing accurate Poincaré maps. *Physica D* 171, 127–137.

Yang, Quangang et al. 2005. Study on the influence of friction in an automatic ball balancing system. *Journal of Sound and Vibration* 285, 73–99.

Zhou, Shiyu and Jianjun Shi. 2001. Active balancing and vibration control of rotating machinery: a survey. *The Shock and Vibration Digest* 33-4, 361–371.

APPENDIX - NOMENCLATURE

A	Constant, varies
B	Constant, varies
C	Constant, varies
COR	Coefficient of restitution coefficient, unitless
D	Constant, varies
$E_{TOT,0}$	The initial amount of energy in the system, lbs-ft
E_{TOT}	The total amount of energy in the system, lbs-ft
F	Defines the geometric center of the ball balancer in an undeformed state
F'	Defines the geometric center of the ball balancer in a deformed state
FR	Abbreviation for Finite Radius
F_C	Collision force acting in the normal coordinate direction between the two colliding balls, lbs
F_I^*	Non-dimensional interaction force between the ith mass and the $(i+1)th$ mass, unitless
F_c	Force due to damper that acts on the system, lbs
F_k	Force due to spring that acts on the system, lbs
F_{AMP}	Amplitude of external forcing function acting on the system, lbs
F_{DEFORM}	Deforming force when two bodies collide with one another, lbs
F_{EXT}	External forcing function acting on the system, lbs
F_{EXT}^N	External force acting on the ball balancer in the normal coordinate direction, lbs
F_{EXT}^T	External force acting on the ball balancer in the tangential coordinate direction, lbs
F_{EXT}^x	External force acting on the ball balancer in the horizontal coordinate direction, lbs
F_{EXT}^y	External force acting on the ball balancer in the vertical coordinate direction, lbs
F_{I_i}	Normal interaction force between the ith ball and the $(i+1)th$ ball or the ith ball and the $(i-1)th$ ball, lbs
$F_{I_i}^N$	Interaction force acting between two contacting balls in a train in the normal coordinate direction, lbs
$F_{I_i}^T$	Interaction force acting between two contacting balls in a train in the tangential

	coordinate direction, lbs
F_{N_i}	Normal force acting on the ith ball in the radial coordinate direction, lbs
$F_{RESTORE}$	Restoring force when two bodies collide with one another, lbs
$F_{R_i,NET}$	Net radial force acting on the ith ball, lbs
F_{R_i}	Rolling friction force acting on the ith ball in the angular coordinate direction, lbs
$F_{\theta_i,NET}$	Net angular force acting on the ith ball, lbs
I	Mass moment of inertia of a body, slugs-ft^2
I_{BB}	Mass moment of inertia of the ball balancer, slugs-ft^2
I_{P_i}	Mass moment of inertia of the ith ball, slugs-ft^2
L	Lagrangian expression, lbs-ft
$N-T$	The normal-tangential reference frame oriented according to the radial-angular direction at an angle halfway between the two contacting balls
O	Defines the center of gravity of the ball balancer in an undeformed state
O'	Defines the center of gravity of the ball balancer in a deformed state
PM	Abbreviation for Point Mass
P_1	Defines the center of gravity of the first (global) ball in the ball balancer
P_S	Value of function evaluated at Poincaré sectioning plane S
P_j	Defines the center of gravity of the jth ball in the ball balancer
$P_{S'}$	Value of function evaluated at Poincaré sectioning plane S'
Q_{NC}	Non-conservative forces, lbs
R	Distance from the geometric center of the ball balancer to the center of gravity of the ith ball, ft
$R-\theta$	The radial-angular coordinate system located at the center of each ball
R_i	Radial force acting on the ith ball,lbs
S	Poincaré sectioning plane
S'	Poincaré sectioning plane
T_{BB}	Kinetic energy of the ball balancer, lbs-ft
T_{P_i}	Kinetic energy of the ith ball, lbs-ft
$T_{R_{BB}}$	Torque acting on ball balancer during a collision, lbs-ft
T_{TOT}	Total kinetic energy of the system, lbs-ft
$V_{BB}^{'N}$	Absolute velocity of the ball balancer in the normal coordinate direction after the collision, ft/s
$V_{SURR}^{'N}$	Absolute velocity of the surroundings in the normal coordinate direction after a collision, ft/s
$V_{BB}^{'T}$	Absolute velocity of the ball balancer in the tangential coordinate direction after

	the collision, ft/s
$V_{SURR}^{'T}$	Absolute velocity of the surroundings in the tangential coordinate direction after a collision, ft/s
$V_{i,j}^{'\theta_{i,j}}$	Absolute velocity of the ith, jth ball in the ith, jth ball angular coordinate direction after the collision, ft/s
V_G	Total gravitational potential energy of the system, lbs-ft
V_{BB}	Gravitational potential energy of the ball balancer, lbs-ft
V_{BB}^N	Absolute velocity of the ball balancer in the normal coordinate direction before the collision, ft/s
V_{BB}^T	Absolute velocity of the ball balancer in the tangential coordinate direction before the collision, ft/s
V_{BB}^x	Absolute velocity of the ball balancer in the horizontal coordinate direction before the collision, ft/s
V_{BB}^y	Absolute velocity of the ball balancer in the vertical coordinate direction before the collision, ft/s
V_{P_i}	Gravitational potential energy of the ith ball, lbs-ft
V_{SURR}^N	Absolute velocity of the surroundings in the normal coordinate direction before a collision, ft/s
V_{SURR}^T	Absolute velocity of the surroundings in the tangential coordinate direction before a collision, ft/s
V_{TOT}	Total potential energy of the system, lbs-ft
$V_{i,j}^N$	Absolute velocity of the ith, jth ball in the normal coordinate direction before the collision, ft/s
$V_{i,j}^T$	Absolute velocity of the ith, jth ball in the tangential coordinate direction before the collision, ft/s
$V_{i,j}^{\theta_{i,j}}$	Absolute velocity of the ith, jth ball in the ith, jth ball angular coordinate direction before the collision, ft/s
V_i^{N0}	Absolute velocity of the ith ball at the point of maximum deformation during a collision, ft/s
V_{k_x}	Potential energy of the horizontally oriented spring, lbs-ft
V_{k_y}	Potential energy of the vertically oriented spring, lbs-ft
$\mathbf{\Delta p}$	Vector defining the change in linear momentum of a body
$\mathbf{\Delta q}$	Vector defining the change in angular momentum of a body
Δt	Size of time integration step, s
Δt_e	Time error, s

Δx	Size of displacement integration step, rad
α	Collision angle, angle that separates two contacting balls, rad
β_j	Relative angular displacement of the jth ball with respect to the $(j-1)th$ ball, rad
β_{j_0}	Initial relative angular displacement of the jth ball with respect to the $(j-1)th$ ball, rad
$\mathbf{\Omega}_i$	Velocity vector defining the rotation between reference frames $\psi_{4,5}$ and reference frame ψ_2
$\dddot{\beta}_j$	Relative angular jerk of the jth ball with respect to the $(j-1)th$ ball, rad/s^3
$\dddot{\phi}$	Angular jerk of the center of gravity of the ball balancer, rad/s^3
$\dddot{\theta}_i$	Angular jerk of the ith ball with respect to the ball balancer, rad/s^3
$\dddot{x}$	Jerk of ball balancer in the horizontal coordinate direction, ft/s^3
$\dddot{y}$	Jerk of ball balancer in the vertical coordinate direction, ft/s^3
$\ddot{\beta}_j$	Relative angular acceleration of the jth ball with respect to the $(j-1)th$ ball, rad/s^2
$\ddot{\phi}$	Angular acceleration of the center of gravity of the ball balancer, rad/s^2
$\ddot{\theta}_i$	Angular acceleration of the ith ball with respect to the ball balancer, rad/s^2
$\ddot{x}$	Acceleration of the ball balancer in the horizontal coordinate direction, ft/s^2
$\ddot{y}$	Acceleration of the ball balancer in the vertical coordinate direction, ft/s^2
$\dot{F}_{N_i}$	Time derivative of the normal force acting on the ith ball in the radial coordinate direction, lbs/s
$\dot{F}_{N_{CCW}}$	Time derivative of the radial normal force acting on the ith ball from the ball that is directly counterclockwise, lbs/s
$\dot{F}_{N_{CW}}$	Time derivative of the radial normal force acting on the ith ball from the ball that is directly clockwise, lbs/s
$\dot{F}_{R_i}$	Time derivative of the rolling friction force acting on the ith ball in the angular coordinate direction, lbs/s
$\dot{\beta}_i$	Relative velocity between the ith ball and the $(i-1)th$ ball, rad/s
$\dot{\beta}_j$	Relative angular velocity of the jth ball with respect to the $(j-1)th$ ball, rad/s
$\dot{\beta}_{j_0}$	Initial relative angular velocity of the jth ball with respect to the $(j-1)th$ ball, rad/s
$\dot{\boldsymbol{\phi}}$	Velocity vector defining the rotational motion of the ball balancer
$\dot{\nu}_0$	Initial angular velocity of the swinging pendulum, rad/s
$\dot{\nu}_1$	Angular velocity of the swinging pendulum, rad/s
$\dot{\nu}_2$	Angular acceleration of the swinging pendulum, rad/s^2
$\dot{\phi}$	Angular velocity of the center of gravity of the ball balancer, rad/s

$\dot{\mathbf{x}}$	Vector of first derivatives of system
$\dot{\theta}_i$	Angular velocity of the ith ball with respect to the ball balancer, rad/s
$\dot{\theta}_{i_0}$	Initial angular velocity of the ith ball with respect to the ball balancer, rad/s
$\dot{u}_1$	Velocity of first mass in the horizontal coordinate direction, ft/s
$\dot{u}_2$	Acceleration of first mass in the horizontal coordinate direction, ft/s^2
$\dot{u}_3$	Jerk of first mass in the horizontal coordinate direction, ft/s^3
$\dot{u}_3$	Velocity of gap in the horizontal coordinate direction, ft/s
$\dot{u}_4$	Acceleration of gap in the horizontal coordinate direction, ft/s^2
$\dot{u}_4$	Time differentiated interaction force between the first and second mass in the horizontal coordinate direction, lbs/s
$\dot{v}_1$	Angular velocity of the first ball in a train with respect to the ball balancer, rad/s
$\dot{v}_2$	Angular acceleration of the first ball in a train with respect to the ball balancer, rad/s^2
$\dot{v}_3$	Angular jerk of the first ball in a train with respect to the ball balancer, rad/s^3
$\dot{v}_i$	Angular jerk of the ith ball in a train with respect to the ball balancer, rad/s^3
$\dot{x}$	Velocity of ball balancer in the horizontal coordinate direction, ft/s
$\dot{x}_i$	Velocity of the ith mass in the horizontal coordinate direction, ft/s
$\dot{x}_i^*$	Non-dimensional velocity of the ith mass in the horizontal coordinate direction, unitless
$\dot{x}_0$	Initial velocity of the ball balancer in the horizontal coordinate direction, ft/s
$\dot{x}_N$	Time derivative of the state variable of interest, varies
$\dot{x}_{i_0}$	Initial velocity of the ith mass in the horizontal coordinate direction, ft/s
$\dot{y}$	Velocity of ball balancer in the vertical coordinate direction, ft/s
$\dot{y}_0$	Initial velocity of the ball balancer in the vertical coordinate direction, ft/s
$\dot{y}_1$	Velocity of the mass in the vertical coordinate direction, ft/s
$\dot{y}_2$	Acceleration of the mass in the vertical coordinate direction, ft/s^2
γ	Phase shift of external forcing function, rad
λ	Roots of system, rad/s
μ_R	Coefficient of rolling friction between all balls and the ball balancer
ν_0	Initial angular displacement of the swinging pendulum, rad
ν_1	Angular displacement of the swinging pendulum, rad
ν_2	Angular velocity of the swinging pendulum, rad/s
ω'_{BB}	Pure rotation of the ball balancer after a collision, rad/s
ω'_{P_i}	Pure rotation of the ith ball after a collision, rad/s
ω_d	Damped natural frequency of the system, rad/s

ω_f	Frequency of external forcing function, rad/s
ω_n	Natural frequency of the ball balancer system, rad/s
ω_{BB}	Pure rotation of the ball balancer before a collision, rad/s
ω_{P_i}	Pure rotation of the ith ball about its center of gravity, rad/s
$\omega_{n,AVG}$	Average natural frequency of the entire system, rad/s
ω_{n_i}	Natural frequency of the ith system, rad/s
ϕ	Angular displacement of the center of gravity of the ball balancer, rad
ψ_0	Parent reference frame that describes the motion of the geometric center of the ball balancer in an undeformed state
ψ_1	Child frame that describes the motion of the center of gravity of the ball balancer in an undeformed state
ψ_2	Child reference frame that describes the motion of the geometric center of the ball balancer in a deformed state
ψ_3	Child frame that describes the motion of the center of gravity of the ball balancer in a deformed state
ψ_4	Child frame that describes the motion of the global ball around the ball balancer
ψ_5	Child frame that describes the motion of the jth ball around the ball balancer
$\mathbf{A}$	Matrix of coefficients of system
$\mathbf{F}$	Vector defining the force that acts upon a body during an impulse
$\mathbf{F}_{I_i}$	Vector defining the interaction force between two contacting balls
$\mathbf{I}_k$	Coordinate system for reference frame ψ_0
$\mathbf{J}$	Vector defining the linear momentum of a body
$\mathbf{L}$	Vector defining the angular momentum of a body
$\mathbf{R}_i$	Displacement vector defining the location of the center of gravity of the ith ball from the geometric center of the ball balancer
$\mathbf{e}$	Displacement vector defining the location of the shifted ball balancer center of gravity due to an eccentricity
$\mathbf{e}_k$	Coordinate system for reference frame ψ_4
$\mathbf{i}'_k$	Coordinate system for reference frame ψ_3
$\mathbf{i}_k$	Coordinate system for reference frame ψ_1
$\mathbf{j}'_k$	Coordinate system for reference frame ψ_2
$\mathbf{q}_{P_i}$	Velocity vector defining the pure rotation of the ith ball about its center of gravity
$\mathbf{v}_O$	Velocity vector defining the motion of point O
$\mathbf{v}'_O$	Velocity vector defining the motion of point O'
$\mathbf{v}_{F'}$	Velocity vector defining the motion of point F'

$\mathbf{v}_{P_i}$	Velocity vector defining the motion of the ith ball
$\mathbf{x}$	Vector of zeroth derivatives of system, varies
θ_i	Angular displacement of the ith ball with respect to the ball balancer, rad
θ_{i_0}	Initial angular displacement of the ith ball with respect to the ball balancer, rad
$\tilde{N}$	Normal coordinate direction between two contacting balls
$\tilde{R}_i$	Radial coordinate direction for the ith ball
$\tilde{T}$	Tangential coordinate direction between two contacting balls
$\tilde{\theta}_i$	Angular coordinate direction for the ith ball
$\tilde{x}$	Orthogonal coordinate direction one
$\tilde{y}$	Orthogonal coordinate direction two
$\tilde{z}$	Orthogonal coordinate direction three
ζ_i	Damping coefficient of the ith system, unitless
a	Counter used to populate each ball clockwise from the colliding ball in the primary train
$a^R_{P_i}$	Absolute acceleration of the ith ball in the radial coordinate direction, ft/s^2
b	Counter used to populate each ball counterclockwise from the colliding ball in the secondary train
c_i	Value of viscous damping constant in the horizontal coordinate direction for the ith system, lbs-s/ft
c_x	Value of viscous damping constant in the horizontal coordinate direction, lbs-s/ft
c_y	Value of viscous damping constant in the vertical coordinate direction, lbs-s/ft
d	Viscous fluid drag coefficient of the fluid inside ball balancer, lbs-s/rad
e	Distance from center of rotation to eccentric mass, ft
f_N	Equation that corresponds to transformation variable
f_i	The ith equation in a set of arbitrary equations of motion
g	Acceleration due to gravity, ft/s^2
i	Counter used to designate all balls
j	Counter used to designate all balls after the global ball
k	Counter used to designate interior balls within a train of balls
k_i	Value of spring constant in the horizontal coordinate direction for the ith system, lbs/ft
k_x	Value of spring constant in the horizontal coordinate direction, lbs/ft
k_y	Value of spring constant in the vertical coordinate direction, lbs/ft
k_{wall}	Value of spring constant of the stationary wall, lbs/ft
l	Moment arm used in torque equations, ft

m_e	Mass of eccentric mass present in rotational system, slugs
m_i	Mass of the ith mass, slugs
m_{BB}	Mass of the ball balancer, slugs
m_{P_i}	Mass of the ith ball, slugs
m_{SURR}	Mass of surroundings, slugs
n	Total number of balls in the ball balancer or train
r_i	Radius of the ith ball, in or ft
t	Time, s
u_1'	Displacement differentiated time, s/ft
u_2'	Displacement differentiated velocity, 1/s
u_1	Displacement of first mass in the horizontal coordinate direction, ft
u_2	Velocity of first mass in the horizontal coordinate direction, ft/s
u_3	Acceleration of first mass in the horizontal coordinate direction, ft/s^2
u_3	Displacement of gap in the horizontal coordinate direction, ft
u_4	Interaction force between the first and second mass in the horizontal coordinate direction, lbs
u_4	Velocity of gap in the horizontal coordinate direction, ft/s
v_1	Angular displacement of the first ball in a train with respect to the ball balancer, rad
v_2	Angular velocity of the first ball in a train with respect to the ball balancer, rad/s
v_3	Angular acceleration of the first ball in a train with respect to the ball balancer, rad/s^2
$v_{P_i}^R$	Absolute velocity of the ith ball in the radial coordinate direction, ft/s
x	Displacement of ball balancer in the horizontal coordinate direction, ft
x_N	State variable of interest
x_S	Value of function in orthogonal coordinate direction one evaluated at S, varies
x_i	Displacement of the ith mass in the horizontal coordinate direction, ft
x_i^*	Non-dimensional displacement of the ith mass in the horizontal coordinate direction, unitless
x_0	Initial displacement of the ball balancer in the horizontal coordinate direction, ft
x_{i_0}	Initial displacement of the ith mass in the horizontal coordinate direction, ft
y	Displacement of the ball balancer in the vertical coordinate direction, ft
y_S	Value of function in orthogonal coordinate direction two evaluated at S, varies
y_0	Initial displacement of the ball balancer in the vertical coordinate direction, ft
y_1	Displacement of the mass in the vertical coordinate direction, ft

y_2	Velocity of the mass in the vertical coordinate direction, ft/s
z_S	Value of function in orthogonal coordinate direction three evaluated at S, varies

CURRICULUM VITA

NAME:	Gregory A. Dedow
CONTACT INFORMATION:	gadedow@gmail.com
DOB:	Flint, Michigan - January 22, 1990
EDUCATION:	B.S., Mechanical Engineering University of Michigan, Ann Arbor 2008-2012
	M.S., Mechanical Engineering University of Louisville 2013-2016
AREAS OF INTEREST:	Rotational dynamics and kinematic motion
EMPLOYMENT:	General Electric, 2013 - present